

**CONDITION MONITORING SYSTEMS FOR AXIAL PISTON PUMPS:
MOBILE APPLICATIONS**

by

Nathan J Keller

A Dissertation

Submitted to the Faculty of Purdue University

In Partial Fulfillment of the Requirements for the degree of

Doctor of Philosophy



Agricultural and Biological Engineering

West Lafayette, Indiana

May 2020

**THE PURDUE UNIVERSITY GRADUATE SCHOOL
STATEMENT OF COMMITTEE APPROVAL**

Dr. Andrea Vacca, Chair

School of Mechanical Engineering
Department of Agricultural and Biological Engineering

Dr. Dennis Buckmaster

Department of Agricultural and Biological Engineering

Dr. José Garcia

School of Engineering Technology

Dr. Gregory Shaver

School of Mechanical Engineering

Approved by:

Dr. Nathan Mosier

To my wife, Kelsey, my family, and friends who have all given me encouragement and support.

ACKNOWLEDGMENTS

I would like to thank my major professor and advisor, Andrea Vacca, who has been generous with his time, and who was kind enough to take me on as his student after the passing of my previous professor, Monika Ivantysynova. I would not be where I am today without the guidance, encouragement, and generosity of the late Monika Ivantysynova. I also acknowledge my PhD committee members: Professor Dennis Buckmaster, Professor Gregory Shaver, and Professor José Garcia. Finally, I want to thank David Johnson and Ben Bumgarner for helping with test-rig development, and all the members of the Maha family for making Maha a pleasant place to be, and one I will miss.

TABLE OF CONTENTS

LIST OF TABLES.....	9
LIST OF FIGURES.....	10
SYMBOLS.....	14
ABBREVIATIONS.....	15
ABSTRACT.....	16
CHAPTER 1. INTRODUCTION.....	18
1.1 Motivation.....	18
1.2 Research Objectives.....	20
1.3 Original Contributions.....	20
1.4 Organization.....	21
CHAPTER 2. STATE OF THE ART.....	22
2.1 Condition Monitoring Methods for Fluid Power Systems.....	22
2.1.1 Contamination Monitoring.....	22
2.1.2 Thermodynamic Monitoring.....	23
2.1.3 Spectral Analysis of Noise or Vibrations.....	25
2.1.4 Machine Learning (Artificial Intelligence).....	27
2.2 Problem Formulation and Solution.....	30
CHAPTER 3. FAULTY COMPONENT SELECTION.....	33
3.1 Reference Pump.....	33
3.2 Selection of Faulty Components.....	34
3.3 Six Different Levels of Valve Plate Health.....	38
3.3.1 Naturally Occurring Valve Plate Wear.....	39
3.3.2 Artificially Induced Valve Plate Damage.....	42
CHAPTER 4. STATIONARY TEST-RIG DEVELOPMENT.....	47
4.1 Test-Rig Purpose.....	47
4.2 Schematic, Hardware, and Data Acquisition.....	48
4.2.1 Hydraulic Schematic.....	48
4.2.2 Accelerometer Placement.....	51
4.2.3 Data Acquisition.....	52

4.3	Duty Cycles	57
4.3.1	Steady-State.....	57
4.3.2	Dynamic Cycle.....	58
4.4	Data Structure	59
4.5	Measurement Process.....	60
CHAPTER 5. MEASUREMENT OBSERVATIONS		62
5.1	Notable Repeatability Observations.....	62
5.1.1	Temperatures.....	62
5.1.2	Drain Flow and Pressure	64
5.1.3	Outlet Transient Pressure	65
5.2	Observable Wear/Damage	66
5.2.1	Temperatures.....	66
5.2.2	Drain Flow	68
5.2.3	Outlet Transient Pressure	69
5.2.4	Volumetric Efficiencies.....	71
5.3	Summary.....	73
CHAPTER 6. FEATURE SELECTION/SENSOR REDUCTION		75
6.1	Feature Selection Background.....	75
6.2	Accelerometer Location Comparison	77
6.3	Backward Feature Elimination Method Using a Fine Decision Tree	81
6.3.1	Correlation Study.....	81
6.3.2	Cost of Sensor	83
6.3.3	Increase Performance of Supervised Learning Algorithm	84
6.3.4	Backward Elimination Results.....	84
6.4	Summary.....	89
CHAPTER 7. ALGORITHM SELECTION		90
7.1	K-Nearest Neighbor (KNN), Supervised Learning.....	90
7.2	Decision Tree, Supervised Learning	91
7.3	Pattern Recognition Neural Network, Supervised Learning	93
7.4	Clustering Neural Network, Unsupervised Learning	93
7.5	Results Summary.....	97

CHAPTER 8. EXCAVATOR INSTRUMENTATION	100
8.1 Test-Rig Purpose	100
8.2 Schematic, Hardware, and Data Acquisition	100
8.2.1 Hydraulic Schematic	101
8.2.2 Sensors	102
8.2.3 Data Acquisition	104
8.3 Duty Cycles	104
8.3.1 Controlled	105
8.3.2 Digging	106
8.3.3 Different Operator	107
CHAPTER 9. EXCAVATOR MEASUREMENT OBSERVATIONS	108
9.1 Excavator Repeatability Observations	108
9.1.1 Cab Speed	108
9.1.2 Engine Speed	109
9.2 Pressure Ports	110
9.2.1 Drain Line Pressure	111
9.3 Observable Wear/Damage	112
9.3.1 Cab Speed	112
9.3.2 Engine Speed	113
9.3.3 Pressure Ports	114
9.3.4 Drain Pressure	115
CHAPTER 10. EXCAVATOR MACHINE LEARNING RESULTS	116
10.1 Feature Selection	116
10.1.1 Controlled Cycle	116
10.1.2 Digging Cycle	118
10.2 Algorithm Selection	119
10.2.1 Controlled Cycle	119
10.2.2 Digging Cycle	120
10.3 Trained Model Results	121
10.4 Summary	124
CHAPTER 11. CONCLUSION	126

CHAPTER 12. FUTURE WORK.....	129
REFERENCES	130
APPENDIX.....	137
PUBLICATIONS	139

LIST OF TABLES

Table 3.1: Parker P1 pump general specifications.	34
Table 4.1: Summary of sensor characteristics.	51
Table 4.2: Steady-state operating conditions	57
Table 4.3: Data structure example.	59
Table 6.1: Approximate cost of sensors.	84
Table 6.2: Results of the backward elimination feature selection method for OpCon_1.	86
Table 6.3: List of features with their corresponding abbreviations.	86
Table 6.4: Feature selection summary of each operating condition.	88
Table 7.1: General confusion matrix.	96
Table 7.2: Clustering network confusion matrices.	96
Table 7.3: Summary of results from classification algorithm comparison under the steady-state operating condition OpCon_2.	98
Table 7.4: Summary of results from classification algorithm comparisons under the dynamic operating condition.	99
Table 8.1: Sensors equipped on pump.	103
Table 10.1: Feature selection results of the controlled cycle using a fine decision tree algorithm.	117
Table 10.2: Feature selection results of the digging cycle using a fine decision tree algorithm.	118
Table 10.3: Trained Fine KNN model of controlled cycle using data from different operating conditions.	122
Table 10.4: Trained Fine KNN model of digging cycle using data from different operating conditions.	122

LIST OF FIGURES

Figure 2.1: Mass balance of pump with no external drain line.....	24
Figure 2.2: Mass balance of pump with external drain line.....	25
Figure 2.3: k-fold cross-validation method (Bishop, 2006).....	29
Figure 3.1: Swashplate type axial piston pump (Ye and Xu, 2018).....	34
Figure 3.2: Swashplate type axial piston pump component interactions.	36
Figure 3.3: Wear interfaces of Danfoss Series 90 axial piston pump.	37
Figure 3.4: Main lubricating interfacing on a swashplate type axial piston pump.....	38
Figure 3.5: Profilometer measurements of valve plate with no wear or damage.	40
Figure 3.6: Profilometer measurements of valve plate with minor wear.	41
Figure 3.7: Profilometer measurements of valve plate with moderate wear.	41
Figure 3.8: Profilometer measurements of valve plate with severe wear.	42
Figure 3.9: Profilometer measurements of valve plate with minor damage.	44
Figure 3.10: Profilometer measurements of valve plate with moderate damage.	44
Figure 3.11: Profilometer measurements of valve plate with severe damage.	45
Figure 3.12: Optical profilometer measurements of valve plate with extreme damage.....	46
Figure 4.1: Stationary Test-Rig	47
Figure 4.2: Hydraulic schematic of stationary test-rig with component and sensor legend.	50
Figure 4.3: Accelerometer placement.....	52
Figure 4.4: Data acquisition hardware setup.....	53
Figure 4.5: Kistler piezoelectric charge amplifier.	54
Figure 4.6: National Instruments (NI) data acquisition hardware.	54
Figure 4.7: Parker D1FP pump control valve.	55
Figure 4.8: Stationary test-rig wiring diagram.....	56
Figure 4.9: Viscosity – Temperature diagram for Shell Tellus S2 VX oil.	58
Figure 4.10: Dynamic duty cycle.....	59
Figure 4.11: Generalized data structure.	60
Figure 5.1: Steady-state repeatability measurements of health valve plate inlet temperatures.	63

Figure 5.2: Steady-state repeatability measurements of health valve plate drain temperatures. ...	63
Figure 5.3: Steady-state measurements of the difference between drain and ambient temperatures for healthy valve plate conditions.	64
Figure 5.4: Repeatability measurements of drain flow for healthy valve plate conditions.	64
Figure 5.5: Repeatability measurements of drain pressure for healthy valve plate conditions.	65
Figure 5.6: FFT of outlet transient pressure repeatability analysis.	65
Figure 5.7: FFT of outlet transient pressure zoomed to see 9 th harmonic.....	66
Figure 5.8: Drain temperature comparison between healthy and unhealthy valve plates operating under steady-state conditions.	67
Figure 5.9: Difference between ambient and drain temperatures for comparing healthy and unhealthy valve plates operating under steady-state conditions.	67
Figure 5.10: Difference between ambient and drain temperatures for comparing healthy and unhealthy valve plates operating under dynamic conditions.	68
Figure 5.11: Drain flow comparison between healthy and unhealthy valve plates, excluding extreme damage.	68
Figure 5.12: Drain flow comparison of healthy and unhealthy valve plates, including extreme damage.....	69
Figure 5.13: FFT of outlet transient pressure comparing faulty valve plates.	70
Figure 5.14: FFT of outlet pressure comparing faulty valve plates, zoomed between 260-320 Hz.	70
Figure 5.15: FFT of outlet pressure comparing faulty valve plates, zoomed at 9 th harmonic.	70
Figure 5.16: Outlet flow with respect to differential pressure at a fixed speed and displacement.	71
Figure 5.17: Outlet flow with respect to differential pressure at a fixed speed and displacement, including Extreme Damage.....	71
Figure 5.18: Volumetric efficiency comparison between healthy and unhealthy valve plates.	72
Figure 5.19: Volumetric efficiency comparison between healthy and unhealthy valve plates, including Extreme Damage.....	73
Figure 6.1: Accelerometer FFT location comparison of drain port, roller bearings, end case, and swashplate pivot.....	77
Figure 6.2: Accelerometer backstrum location comparison of drain port, roller bearings, end case, and swashplate pivot.....	78
Figure 6.3: Accelerometer FFT location comparison of roller bearings, inlet port, outlet port, and the end case near the shaft.....	79

Figure 6.4: Accelerometer backstrum location comparison of roller bearings, inlet port, outlet port, and the end case near the shaft.....	79
Figure 6.5: Accelerometer FFT location comparison of roller bearings, nameplate, and control port.....	80
Figure 6.6: Accelerometer backstrum location comparison of roller bearings, nameplate, and control port.....	81
Figure 6.7: Correlation between differential pressure and outlet pressure.	83
Figure 7.1: K-Nearest Neighbor (KNN) example (Keller <i>et al.</i> , 2019).	91
Figure 7.2: Simple or coarse decision tree (Webb, 2002).	92
Figure 7.3: Neural pattern recognition network structure.	93
Figure 7.4: Clustering neural network structure	94
Figure 7.5: Sample hits from clustering algorithm.	95
Figure 8.1: Maha Bobcat 435 DC prototype mini excavator.	100
Figure 8.2: Hydraulic schematic of excavator (Busquets, 2016).....	102
Figure 8.3: Measured parameters on excavator.	103
Figure 8.4: Folding crane (Atlas GMBH, 2020).....	105
Figure 8.5: Controlled duty cycle illustration.	106
Figure 8.6: Cabin speed for the controlled duty cycle.	106
Figure 8.7: Digging cycle illustration.....	107
Figure 9.1: Excavator cab rotation speed of repeatability analysis of the controlled cycle.	109
Figure 9.2: Zoomed view of cab speed rotation repeatability.	109
Figure 9.3: Engine speed of repeatability analysis of the controlled cycle.	110
Figure 9.4: Port A pressure of repeatability analysis of the controlled cycle.	110
Figure 9.5: Port B pressure of repeatability analysis of the controlled cycle.	111
Figure 9.6: Drain port pressure of repeatability analysis of the controlled cycle.	112
Figure 9.7: Comparison of cab speed between healthy and unhealthy pump states.	113
Figure 9.8: Comparison of engine speed between healthy and unhealthy pump states.	113
Figure 9.9: Comparison of pA between healthy and unhealthy pump states.....	114
Figure 9.10: Comparison of pB between healthy and unhealthy pump states.	115
Figure 9.11: Comparison of drain pressures between healthy and unhealthy pump states.	115
Figure 10.1: Algorithm selection summary for controlled cycle.....	120

Figure 10.2: Algorithm selection summary for digging cycle.....121

Figure 10.3: Breakdown of each valve plate condition under the digging operation using a trained Fine KNN model of the controlled cycle.124

Figure 14.1: Algorithm selection results of controlled cycle using a 25% hold-out validation with the following features: *(a)* pD only, *(b)* pB and pD, *(c)* pD and N, *(d)* pB, pD, and N, *(e)* pD and Beta.137

Figure 14.2: Algorithm selection results of digging cycle using a 25% hold-out validation with the following features: *(a)* pD only, *(b)* pB and pD, *(c)* pD and N, *(d)* pB, pD, and N, *(e)* pD and Beta, *(f)* pB, pD, Beta, *(g)* pA, pB, pD, Beta, N.....138

SYMBOLS

Symbol	Description	Units
β	Swashplate angle	[–]
f_s	Sample frequency	[Hz]
h	Enthalpy	[J/kg]
h'	Enthalpy for isentropic change of state	[J/kg]
k	Number of nearest neighbors	[–]
\dot{m}	Mass flow rate	[kg/s]
M_e	Effective torque	[Nm]
M_{th}	Theoretical torque	[Nm]
N	Rotational speed	[rpm]
η_{hm}	Hydro-mechanical efficiency	[–]
η_{tot}	Total overall efficiency	[–]
η_v	Volumetric efficiency	[–]
p	Pressure	[bar]
Q_e	Effective flow rate	[L/min]
Q_s	Flow loss	[L/min]
Q_{th}	Theoretical flow rate	[L/min]
s	Entropy	[J/(K · kg)]
T	Temperature	[°C]
t	Time	[s]
t_s	Sample time	[s]
w	Specific work	[J/kg]

ABBREVIATIONS

Symbol	Description
AI	Artificial Intelligence
ANN	Artificial Neural Network
DC	Displacement Control
DFT	Discrete Fourier Transform
ED	Extreme Damage
FFT	Fast Fourier Transform
FN	False Negative
FMEA	Failure Modes and Effects Analysis
FP	False Positive
IEPE	Integrated Electronics Piezoelectric
IOT	Internet of Things
KNN	K-Nearest Neighbor
LDA	Linear Discriminate Analysis
MinW_ModD	Minor Wear, Moderate Damage
MinW_SD	Minor Wear, Severe Damage
ModW_MinD	Moderate Wear, Minor Damage
NI	National Instruments
OEM	Original Equipment Manufacturer
PCA	Principal Component Analysis
RUL	Remaining Useful Life
SOM	Self-Organizing Map
SW_ND	Severe Wear, No Damage
TN	True Negative
TP	True Positive

ABSTRACT

Condition monitoring of hydraulic systems has become more available and inexpensive to implement. However, much of the research on this topic has been done on stationary hydraulic systems without the jump to mobile machines. This lack of research on condition monitoring of hydraulic systems on mobile equipment is addressed in this work. The objective of this work is to develop a novel process of implementing an affordable condition monitoring system for axial piston pumps on a mobile machine, a mini excavator in this work. The intent was to find a minimum number of sensors required to accurately predict a faulty pump. First, an expert understanding of the different components on an axial piston pump and how those components interact with one another was discussed. The valve plate was selected as a case study for condition monitoring because valve plates are a critical component that are known for a high percentage of failures in axial piston pumps. Several valve plates with various degrees of natural wear and artificially generated damage were obtained, and an optical profilometer was used to quantify the level of wear and damage. A stationary test-rig was developed to determine if the faulty pumps could be detected under a controlled environment, to test several different machine learning algorithms, and to perform a sensor reduction to find the minimum number of required sensors necessary to detect the faulty pumps. The results from this investigation showed that only the pump outlet pressure, drain pressure, speed, and displacement are sufficient to detect the faulty pump conditions, and the K-Nearest Neighbor (KNN) machine learning algorithms proved to be the least computationally expensive and most accurate algorithms that were investigated. Fault detectability accuracies of 100% were achievable. Next, instrumentation of a mini excavator was shown to begin the next phase of the research, which is to implement a similar process that was done on the stationary test-rig but on a mobile machine. Three duty cycle were developed for the excavator: controlled, digging, and different operator. The controlled duty cycle eliminated the need of an operator and the variability inherent in mobile machines. The digging cycle was a realistic cycle where an operator dug into a loose pile of soil. The different operator cycle is the same as the digging cycle but with another operator. The sensors found to be the most useful were the same as those determined on the stationary test-rig, and the best algorithm was the Fine KNN for both the controlled and digging cycles. The controlled cycle could see fault detectability accuracies of 100%, while the digging cycle only saw accuracies of 93.6%. Finally, a cross-compatibility

between a model trained under one cycle and using data from another cycle as an input into the model. This study showed that a model trained under the controlled duty cycle does not give reliable and accurate fault detectability for data run in a digging cycle, below 60% accuracies. This work concluded by recommending a diagnostic function for mobile machines to perform a preprogrammed operation to reliably and accurately detect pump faults.

CHAPTER 1. INTRODUCTION

1.1 Motivation

Fluid power systems are central to the operation of numerous industries with mobile equipment, such as aerospace, mining, construction, agriculture, forestry, automotive, and others. The drive to increase reliability, reduce machine downtime, and to increase the understanding of hydraulic failures brings condition monitoring to the cutting edge of mobile hydraulic systems. Common components in hydraulic systems include valves, cylinders, accumulators, motors, and pumps. The hydraulic pump is the heart of the hydraulic system. If the pump fails, the entire hydraulic system is rendered inoperable. Therefore, it is critical to ensure the axial piston pump operates as desired without failure.

Pump failure is often attributed to wear. Wear can be defined as the removal of material by mechanical and/or chemical interactions (Silva Gabriel, 1990). Approximately 80% to 90% of machine breakdowns are attributed to wear (Drozdor, 1985). Several different types of wear exist, but the most prevalent type of wear will be discussed in this work.

Abrasion, the asperity contact between two materials of different hardness, accounts for 50% of failures in industrial machines (Eyre, 1976), and Feicht found that up to 70% of hydraulic failures are caused by contamination, which is a result and can cause abrasive wear (Feicht, 1976). This wear occurs in the lubricating interfaces of the hydraulic system, such as the valve plate/cylinder block interface of an axial piston pump. Therefore, it can be stated that abrasion occurs under lubricated conditions from asperity contact of the two lubricating surfaces or from the asperity caused by loose particles in the fluid (Silva Gabriel, 1990). Wear from contamination accounts for about 10% of damage found in hydraulic pumps (Feicht, 1976).

Since failure caused by wear is so prevalent in hydraulic systems, then maintenance strategies must be implemented to ensure the machine remains operating as reliably as possible. Three main maintenance strategies exist, and they are breakdown maintenance, preventative or predictive maintenance, and condition monitoring.

Breakdown maintenance is considered the most archaic maintenance method that is possibly too most expensive and dangerous. Breakdown maintenance is a “fix when broken” approach that replaces a component after failure has already occurred. This strategy results in unplanned downtime of the equipment, requires time for technicians to search and repair the faulty component, and can compromise the safety of personnel near the machine when failure occurs. Additionally, failure of a component in a fluid power system can send debris throughout the system, which can cause further damage to other components.

Predictive maintenance is a significant improvement to breakdown maintenance. A predetermined maintenance schedule is developed from manufacturer data and experience to replace components. This method reduces the downtime of the equipment and maintenance is scheduled in advance. However, this method causes components to be replaced even if they are considered healthy.

The final maintenance strategy is condition monitoring and is considered the best maintenance strategy. This strategy continuously monitors the condition of the system using a data acquisition system and a decision maker to determine the state of the system being monitored. This method improves the understanding of how the machine operates, in addition to increasing the machine availability and reducing the inventory of required spare parts. However, condition monitoring requires sensors, some sort of signal processing, and maintenance staff must be trained in instrumentation and calibration (Watton, 2007).

Condition monitoring of hydraulic systems in mobile equipment has been an area of increasing interest for Original Equipment Manufacturers (OEMs), operators, and researchers. Condition monitoring is more readily available and easier to implement on industrial or stationary machinery. However, the implementation of a condition monitoring method on mobile machines is more difficult because of the various operating conditions of the machines and the limited space on the machine. The amount of readily available computing software with machine learning packages makes condition monitoring a more affordable and realistic maintenance strategy to implement on mobile machinery than in previous years. Therefore, the motivation of this work is to bring an affordable condition monitoring system to mobile machinery, specifically to axial piston pumps on mobile equipment.

1.2 Research Objectives

The research objectives are to develop a process for implementing a condition monitoring system for a swashplate type axial piston pump on mobile machinery that will determine if the pump is healthy or unhealthy using a machine learning algorithm. The aim is not for the machine learning algorithm to determine which component of the pump is failing or to predict the Remaining Useful Life (RUL) of the pump. Instead the aim is to determine the binary state of the pump, healthy or unhealthy. The research will include:

- A study on which component to investigate for pump failure.
- Determining whether the varying degrees of wear and damage on valve plates are detectable under controlled conditions.
- Resolve the minimum number of sensors required for the successful detection of pump damage.
- Selecting a machine learning algorithm that accurately classifies the pump as healthy or unhealthy, while requiring the least amount of computational power.
- Demonstrating this process on a stationary test-rig under steady-state and dynamic operating conditions.
- Instrument a mini excavator for condition monitoring purposes.
- Demonstrate the same process that was performed on the stationary test-rig but on the mini excavator under controlled and digging duty cycles.
- Investigate the effects of using different operators on a condition monitoring system trained with one operator during the digging cycle.

1.3 Original Contributions

This work provides novel contributions to the field of fluid power and condition monitoring research.

1. The implementation of valve plates with quantifiable damage and wear for the use of condition monitoring on axial piston pumps.

2. The investigation of existing condition monitoring methods for the implementation on axial piston pumps on a stationary test-rig using physically damaged valve plates under dynamic operating conditions.
3. Determine the minimum number of sensors required to detect valve plate wear on an axial piston pump in a stationary test-rig setting.
4. Demonstrate a process for producing a condition monitoring process for axial piston pumps with physically damaged valve plates on a mini excavator using machine learning algorithms.
5. Determine the minimum number of sensors required on a mini excavator to detect pump failure.
6. Investigate how actual duty cycles of a mini excavator and operator variability influence the ability to detect pump failure.

1.4 Organization

A review of relevant literature is discussed in Chapter CHAPTER 2 that shows the state-of-the-art in condition monitoring of axial piston pumps, and the different methods used. Chapter CHAPTER 3 explains which component is selected to produce a faulty pump and shows the varying degrees of wear and damage on the component. The experimental stationary test-rig is shown in Chapter CHAPTER 4, which also includes the data acquisition system and data structure. Chapter CHAPTER 5 discusses the observations on pump performance characteristics between the different states of pump health. The process of feature selection, dimensionality reduction, or sensor reduction is shown in Chapter CHAPTER 6. Machine learning algorithm selection is shown in Chapter CHAPTER 7. The instrumentation of the mobile mini excavator is described in Chapter CHAPTER 8. The observations of the excavator's measurements, and the machine learning results are discussed in Chapter CHAPTER 9 and Chapter CHAPTER 10, respectively. The conclusion is found in Chapter CHAPTER 11. Finally, a brief discussion of possible future work is found in Chapter CHAPTER 12.

CHAPTER 2. STATE OF THE ART

The purpose of this chapter is to show previous research that has been conducted in the area of condition monitoring of hydraulic pumps. Additionally, this chapter will expose areas where research is lacking with respect to condition monitoring of hydraulic pumps on mobile equipment.

2.1 Condition Monitoring Methods for Fluid Power Systems

Several methods of condition monitoring have been implemented on fluid power systems. Some methods require more expert knowledge than others. A common method to monitor the condition of the fluid power system as a whole is through monitoring the oil condition, or contamination. Another method is a highly analytical technique that calculates the pump efficiency based on the first law of thermodynamics. The next method that is commonly used is to perform a spectral analysis of the vibrations of the pump. Finally, quite possibly the fastest growing and easiest to implement is the machine learning or artificial intelligence method. This method is more of a black box approach that is typically used with purely experimental data. The machine learning method shows significant promise, especially since computational power is becoming more affordable and readily available.

2.1.1 Contamination Monitoring

Monitoring the contamination and condition of the hydraulic oil is one of several methods that is used to monitor the health of the hydraulic system. Oil contamination monitoring is an excellent method at observing the condition of the hydraulic system. However, it is not necessarily effective on determining the state of health on a component level.

Contamination in hydraulic systems is caused by the ingress of particles into the oil through seals, such as a hydraulic cylinder seal or pump shaft seal. In fact, approximately 50-60% of particles enters the system from cylinder seal, and this percentage would only increase as the seals wear (Stecki, 1998). Contamination is also caused by the wear of components within the hydraulic system. In addition to solid particles, liquid contamination from the presence of water in the hydraulic oil can cause corrosion and failures. Monitoring the contamination of the oil can monitor

the age and its remaining useful life, but it can also carry information about the state of the hydraulic system based on the debris particles entrained in the oil (Opperman, 2007).

Failures related to contamination in hydraulic systems did not exist before 1975, but serious consideration and research into oil contamination began in 1973 (Edlund, 1979). An off-line particle counter was used to help determine the condition of the oil. In 1985, Hunt was capable of analyzing the oil condition for automobile and motorcycle oils by using a portable contamination meter measuring the pressure drop across a filter (Hunt, 1985).

In the above-mentioned work, Hunt presented his results from the portable contamination meter, Neale discussed condition monitoring methods used in other industries. Neale observed that aircraft gas turbines condition monitoring had been successful implementing a magnetic plug to catch wear particles (Neale, 1985). The idea is that a magnetic plug is placed in the hydraulic oil in a location with high catch efficiency, and the rate at which the magnetic plug fills with magnetic debris indicates the condition of the system.

Many companies now produce products that are capable of determining the online condition of the oil by monitoring the temperature, relative humidity, relative permittivity, and the debris particles entrained in the oil (Argo-Hytos, 2019; Bosch-Rexroth, 2019; Hydac, 2019; MP Filtri, 2019).

2.1.2 Thermodynamic Monitoring

The efficiency of a hydraulic pump can be found by implementing temperature and flow measurements to the first law of thermodynamics. Monitoring a decrease in efficiency suggests a decrease in health for the pump. This is another tested method for monitoring the state of hydraulic pumps.

The idea that the efficiency of hydraulic turbines could be evaluated using a thermodynamic method began in 1920 (Babbillion and Poirson, 1920), but it wasn't until Witt in 1974 that thermodynamic measurements were used in the context of monitoring the efficiency in hydraulic systems (Witt, 1974). The overall efficiency of the pump is determined through the mass balance of the pump and fluid properties, but this method does not consider an external drain line, see

Figure 2.1. The pump efficiency is calculated for a steady-state process using Equation (2.1). The total efficiency is the specific work out divided by the specific work into the pump. The work terms can be found from dividing the change in enthalpy for an isentropic state by the change in enthalpy of the pump outlet minus the inlet.

$$\eta_{tot} = \frac{w_{t,out,s}}{w_{t,in}} = \frac{(h'_A - h_B)_s}{h_A - h_B} \quad (2.1)$$

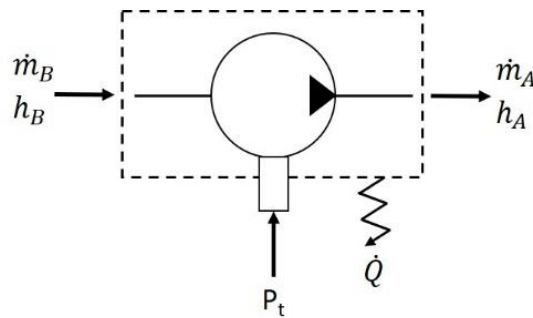


Figure 2.1: Mass balance of pump with no external drain line.

Kjølle applied the thermodynamic method to a hydrostatic transmission in 1993 (Kjølle, 1993). In 2001, Pomierski applied the thermodynamic approach to the propulsion system of a combine harvester to monitor hydraulic unit efficiency. This approach was tested under steady-state conditions but theorized for a dynamic operating condition (Pomierski, 2001). The thermodynamic method was successfully used on a gear-type pump in 2006 (Dalla Lana, Eduardo and De Negri, 2006).

Up to this point, the thermodynamic method to determine the efficiency of a hydraulic pump has neglected the drain line and has been used for an open-circuit pump. However, in 2007 Opperman showed a modification to the method developed by Witt by including an external drain line for both closed- and open-circuit pumps (Opperman, 2007). Pump efficiency including an external drain line can be calculated using Equation (2.2, see Figure 2.2 as a reference. This incorporates ratio of the mass drain flow to the mass outlet flow. Opperman utilized this concept on a mobile wheel loader with artificial volumetric pump losses.

$$\eta_{tot,oc} = \frac{w_{t,out,s}}{w_{t,in}} = \frac{(h'_A - h_B)_s}{(h_A - h_B) + \frac{\dot{m}_L}{\dot{m}_A} \cdot (h_L - h_B)} \quad (2.2)$$

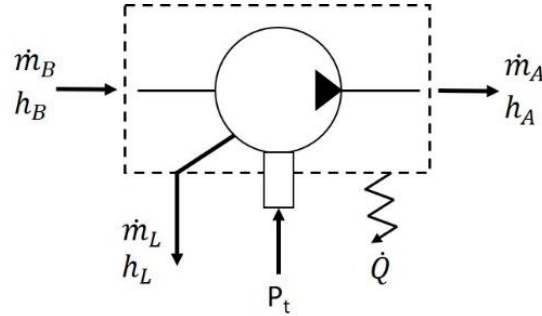


Figure 2.2: Mass balance of pump with external drain line.

More recent work in 2018 utilizes the external drain line when calculating the pump efficiency. However, this work makes the important point that each of the thermodynamic methods require a torque meter and flow meters to measure the outlet flow of the pump. These sensors are not cost effective for condition monitoring purposes on mobile machines and are difficult to install (Casoli, Campanini, *et al.*, 2018).

Casoli *et. al.* proposes the concept of measuring the differential pressure across a known orifice in the drain line to calculate drain flow. From this information, the effective, or outlet, flow can be estimated by subtracting the calculated drain flow from the ideal pump flow. This concept would eliminate the need for costly torque and flow meters.

2.1.3 Spectral Analysis of Noise or Vibrations

A third method for monitoring the condition of a pump is to perform a spectral analysis of the noise or vibrations from the pump. Often, accelerometers are mounted on the case of the pump to monitor vibrations at different locations. The change in frequency content can suggest a deterioration of pump performance and health.

Spectral analysis is the study of the frequency content of a signal in the time domain. The time domain is converted into the frequency domain by taking the Discrete Fourier Transform (DFT) of the signal or by using the less computationally expensive Fast Fourier Transform (FFT) developed in 1965 (Cooley and Tukey, 1965).

Ramdén et al implemented a spectral analysis study on axial piston pumps as a method that introduced the least amount of interference to the hydraulic system as possible and was sensitive to variations in the signals by installing accelerometers on the outside casing of the pump (Ramden, Weddfelt and Palmberg, 1993; Ramden, 1998). Ramdén implemented the accelerometers to detect differences in faulty pump bearings.

This work included the use of the FFT to observe the frequency content of the accelerometer signals. Another method to observe the accelerometer signals was used, and it is called the backstrum. The backstrum is a variation of the cepstrum, which has been used in condition monitoring of axial piston pumps (Backe and Schwarz, 1989) and can be seen below. A variation of the cepstrum used by Ramdén is shown in Equation (2.3 and was originally develop in 1963 (Bogert, 1963).

$$\text{Cepstrum: } C(q) = |F\{^{-1}\log[F\{u(t)\}]\}|^2 \quad (2.3)$$

The backstrum is slightly easier to calculate, since it does not contain the logarithm function. The backstrum can be calculated as seen below. The cepstrum and backstrum are not part of the frequency domain, but rather part of the time domain called quefreny. The quefreny is the inverse of the distance between successive lines in a Fourier transform and is measured in seconds. This work compares accelerometer locations by observing the different signals by taking the magnitude of the fast Fourier transform and the backstrum of the accelerometer signals.

$$\text{Backstrum: } B(q) = |F\{F\{u(t)\}\}|^2 \quad (2.4)$$

A more recent study on fault detection of axial piston pumps implementing a spectral analysis study was conducted in 2018 and was able to detect slipper damage from vibrational data collected

by accelerometers (Casoli, Bedotti, *et al.*, 2018). These studies were conducted under steady-state conditions.

2.1.4 Machine Learning (Artificial Intelligence)

The final condition monitoring method for pumps to be discussed in this work is the machine learning or Artificial Intelligence (AI) method. Machine learning algorithms, AI, can find corollaries between data that are too complex for the human to comprehend. Machine learning algorithms can handle highly nonlinear data, which is beneficial considering the nonlinearity of hydraulic systems. This approach is more like a black box approach, where one does not necessarily require an expert knowledge of the system being monitored. Areas such as regression, classification, clustering, and neural networks are each a branch in the machine learning tree. This work will discuss classification and clustering, but neural networks will also be discussed and can fall within both areas.

Machine learning algorithms require training and testing, or validation, to develop a connection from the input data set to the outputs. Once the training and validation is completed, then a model is generated with the appropriate settings to map input data to the trained outputs. The training depends on what main category the machine learning algorithm falls under, supervised or unsupervised learning.

Supervised learning algorithms take a set of input data and create a mapping to corresponding target outputs provided by the supervisor (Bishop, 2006; Alpaydin, 2010). This means the machine learning algorithm knows what the outcomes are supposed to be and can find connections from the input data to the output. A sub-type of supervised machine learning is classification.

A classifier takes input data then assigns the input of a set to discrete output classes. The objective of the classification algorithm is to learn the mapping of the input to the output. Practically, this means a model or rule is developed that allows the machine learning algorithm to make future predictions based on past data. Classification helps designers and operators extract more information about the system. The more information known about the system, then the better it can be designed to become more reliable and productive for the consumer. In addition to predicting

future behavior and extracting more information about the system, learning systems perform a compression (Alpaydin, 2010). A compression is done by creating a rule or model from the data explaining the behavior of the system simpler than the data itself.

Unsupervised learning algorithms take the input data and group the data into clusters of similar characteristics. These algorithms do not have a priori knowledge of what to look for or how to group the data. They do not know the “true” target outputs but try to find regularities within the input data (Alpaydin, 2010).

Once the algorithm has been trained, its performance should be evaluated in making predictions on new datasets (MathWorks, 2019b). This means the model should be validated with data that is not used in the training set. The validation data can protect the model from overfitting the data, therefore, making a more generalized model. Hold-out and k-fold validation are the two main methods for validating the model generated by the machine learning algorithm.

The hold-out method divides the dataset into training and testing groups. For example, a common hold-out percentage is 25%, where 25% of the dataset is reserved for validation or testing, while the remaining 75% of the data is used for training. Hold-out validation is an effective method with large datasets, like the data used in this work.

K-fold cross-validation is a proven effective and statistically justified validation method for smaller datasets (Foster, Koprowski and Skufca, 2014). This method partitions that dataset into k randomly chosen groups, also known as folds, that are roughly equal in size. One group is used to validate while the remaining groups are used for training. This process is repeated until each group is used to validate the model.

An example of k-fold cross-validation can be found in Figure 2.3, which is taken from (Bishop, 2006). This example has $k = 4$ folds. The dataset is divided into roughly four equal sized groups, with the first group being the validation set and the remaining 3 groups belonging to the training set. In run 2 the second group is now the validation set, and the first, third and fourth groups are used for training. This process is repeated until each group is used for validation.

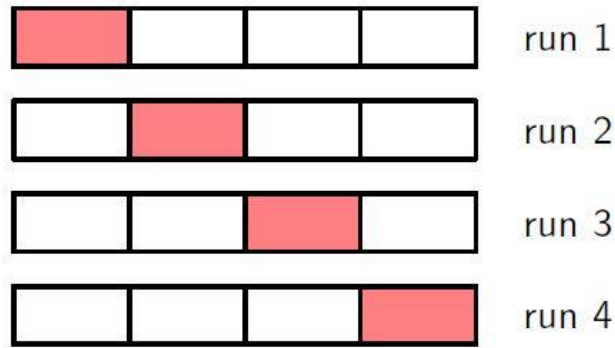


Figure 2.3: k-fold cross-validation method (Bishop, 2006).

(Lu, Burton and Schoenau, 1994, 1995) trained an artificial neural network (ANN) to detect piston/cylinder faults on an axial piston pump using purely experimental data. The pistons had varying degrees of wear and were each tested. The inlet and outlet pressures were measured and fed into an ANN to be trained with the known faults, supervised learning.

(Ramdén, Krus and Palmberg, 1995) trained an ANN, Self-Organizing Map (SOM) type of ANN, to detect faulty valves in a hydraulic system using data obtained from simulation results. (Crowther *et al.*, 1998) determined that ANNs trained on experimental data were more accurate than those trained using simulation data by comparing the fault detection of cylinder actuators trained using either simulation or experimental data. This is likely because the simulations contain assumptions and inherently do not capture the complete understanding of the system (Schoenau, Stecki and Burton, 2000).

(Ramdén, Krus and J. Palmberg, 1995) showed the detection of worn-out bearings and a valve plate using an ANN that was trained on purely experimental data. These tests were conducted under a single operating condition running at steady state.

(Li, 2005) used various condition monitoring algorithms to detect faulty pistons in an axial piston pump. The faulty piston/cylinder interface was artificially induced to simulate the leakage of a worn piston/cylinder interface. This was done by implementing a pressure control servo valve that diverted flow from the pump outlet to the drain with a waveform simulating different degrees of piston wear.

(Krogerus *et al.*, 2007) developed a SOM neural networks that was able to detect a faulty cylinder and proportional valve on a water hydraulic forklift. The faults on the proportional valve were obtained by damaging the seals, or O-rings, to induce leakage and a difference in performance. A bleed valve connected either side of the cylinder to artificially induce a fault caused by a faulty seal in the cylinder. Only the pressures were used for fault detection.

An ANN trained to detect the valve plate and slipper/swashplate wear was implemented in 2011. This work was interesting as it implemented neural networks in conjunction with chaos theory (Lu, Ma and Wang, 2011). The actual condition of the valve plate and slipper/swashplate were not quantified to show the degree of wear.

(Du, Wang and Zhang, 2013) used a layered clustering algorithm to detect multiple faults on an aerospace axial piston pump by measuring drain flow, outlet pressure, radial vibrations, and axial vibrations.

(Lan *et al.*, 2018) developed implemented a pattern recognition ANN in conjunction with spectral analyzes of pump vibrations and outlet flow to detect slipper wear on an axial piston pump. The results were comparable to other machine learning algorithms used.

With the exception of (Krogerus *et al.*, 2007), each of the previously mentioned work concerning machine learning algorithms has been completed under steady-state conditions in stationary test-rigs. They also do not give a detailed account of the degree of damage on the components, if faults were not artificially generated by using some modification to the hydraulic system or by simulation.

2.2 Problem Formulation and Solution

The work that has been presented in this chapter does not consider monitoring the condition of axial piston pumps with physically damaged components on mobile equipment. Most of the work includes the use of artificially generated faults and running tests under steady-state conditions. Additionally, the focus of the previous works has not been to reduce the number of sensors required to accurately monitor the health or state of the pump. This thesis work will address the lack of

research performed on condition monitoring of axial piston pumps for mobile machines under dynamic operating conditions with physically faulty components.

The following steps show the steps to achieve the goal of creating a condition monitoring algorithm for a mobile hydraulic machine.

1. Selection of Faulty Component

- a. An application of expert knowledge and FMEA type principles is to be used to understand all the different components in an axial piston pump and how they interact with one another.
- b. An extensive literature review will be conducted to determine the critical components of a swashplate type axial piston pump.
- c. Obtaining selected components that have varying degrees of wear.
- d. Document the degree of wear and damage using an optical profilometer.

2. Experimental Stationary Test-Rig

- a. Perform fault detectability under the following conditions:
 - i. Various steady-state conditions.
 - ii. Controlled dynamic duty cycle.
- b. Test for repeatability to ensure experiments are valid and repeatable.
- c. Perform a sensor/dimensionality reduction to reduce the cost and complexity required for future implementation on mobile machine.
 - i. Implement backward elimination feature selection.
- d. Select a machine learning algorithm that accurately detects a faulty pump condition that also requires minimal computational power.
 - i. Compare various machine learning algorithms.

3. Experimental Mini excavator Test-Rig

- a. Develop repeatable duty cycles.
- b. Perform fault detectability using repeatable machine cycle.
- c. Test for repeatability.

- d. Perform a sensor/dimensionality reduction.
 - i. Ideally using less sensors than the stationary test-rig because of the results obtained from performing a dimensionality reduction on the stationary test-rig.
- e. Select a machine learning algorithm that accurately detect the faulty pump but is computationally inexpensive.
- f. Further test condition monitoring model with different operators and various operating cycles.

CHAPTER 3. FAULTY COMPONENT SELECTION

This chapter briefly introduces axial piston pumps and reveals the reference pump and its general specifications for this work. A detailed description of how each of the components in an axial piston pump interact with one another is then discussed. The wear interfaces of the pump are then discussed and limited to three main wear interfaces: piston/cylinder, valve plate/cylinder block, and slipper/swashplate interfaces. The scope of the work is narrowed to only include the valve plate/cylinder block wear interface. Finally, physical wear and damage on the valve plates are shown in detail with the use of an optical profilometer.

3.1 Reference Pump

An axial piston pump is known as a positive displacement machine. This means that the pump displaces a fixed amount of fluid each rotation. Essentially, this means the pump outputs the same amount of flow regardless of pressure, neglecting small amounts of leakages between pump interfaces (Esposito, 2009). Positive displacement machines are flow sources and do not supply pressure to the hydraulic system. The swashplate type axial piston pump is a variable displacement pump that allows for the pump outlet flow to vary by changing the swashplate angle, see Figure 3.1. This type of pump is what has been selected for this work.

Fluid is displaced by the reciprocating action of the pistons. The amount of fluid displaced by this type of pump is dependent on the swashplate angle and shaft speed. A larger swashplate angle results in larger displacement chambers of the piston, therefore greater quantities of fluid are displaced each rotation. The shaft speed determines how quickly the pistons reciprocate, so increasing the shaft speed increases the flow rate of the pump.

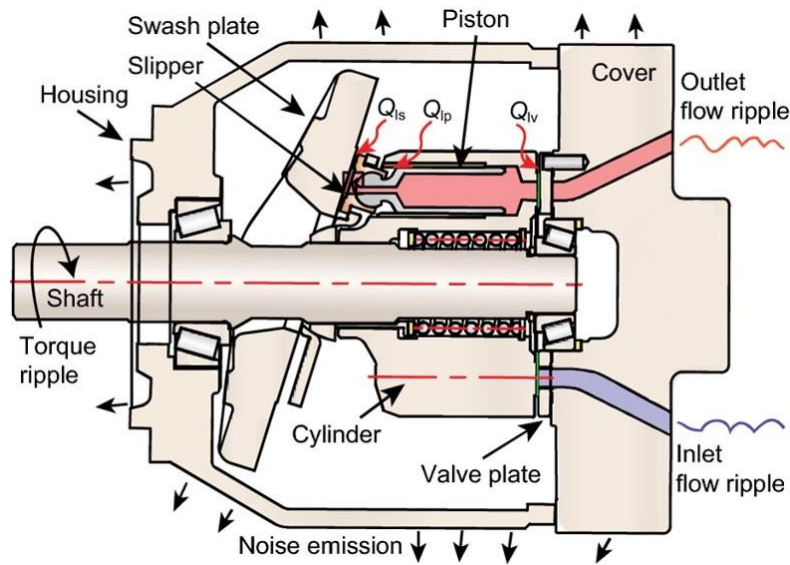


Figure 3.1: Swashplate type axial piston pump (Ye and Xu, 2018).

The selected reference pump for this work is an 18 cc/rev Parker P1 swashplate type axial piston pump. This pump is chosen because of its availability to the researcher, and the readily availability of several components for this pump. This Parker P1 pump is a closed-circuit pump that can control the swashplate to the over-center position, meaning flow can be reversed without changing the direction of shaft rotation. It is rated for pressures up to 350 bar and rotational speeds up to 3600 rpm. Table 3.1 gives the general specifications for the Parker P1 pump selected for this work.

Table 3.1: Parker P1 pump general specifications.

Max. Displacement	18 cc/rev
Pressure Range	0 to 350 bar
Speed Range	600 to 3600 rpm
Temperature Range	-40 to +95 °C
Rated Fluid Viscosity	6 to 160 cst
Pistons	9
Overcenter Capable	Yes
Closed-Circuit	Yes

3.2 Selection of Faulty Components

An extensive Failure Modes and Effects Analysis (FMEA) and literature review is required to determine which component or components should be included in this condition monitoring

investigation. FMEA requires expert knowledge of the operation of the pump and how the different pump components interact with one another.

Figure 3.2 is a diagram of the interactions for each of the components in a swashplate type axial piston pump. This diagram represents how reactionary forces, moments, and motions interact between each of the components of the axial piston pump. Simplified explanations will be given of the interaction between some of these components and how an axial piston pump function. The components are divided into four main groups: drive shaft subassembly (colored in grey), rotating group subassembly (colored in purple), control subassembly (colored in blue), and the hydraulic system (colored in green). Additional components, such as the charge pump, valve plate, and end case are considered.

The drive shaft subassembly, shown in grey in Figure 3.2, consists of the drive shaft, rear, and front bearings. The drive shaft is connected to a prime mover, electric motor or internal combustion engine, and transfers rotational speed (ω) to the bearings. The bearings, in turn, produce a resistive torque (M) on the shaft due to frictional losses.

The drive shaft also transfers rotational speed (ω) to the rotating group subassembly, which consists of the cylinder block, pistons, and slippers. The rotating group subassembly is colored purple in Figure 3.2. The rotational motion of the cylinder block (ω) and the linear motion of the pistons (\dot{x}) transfer flow to the hydraulic system, which feeds the pressure back to the pistons (p_{in}). The pressure in the piston chambers (p_{out}) and the reactional forces from the slipper/swashplate interaction produces a radial force (F_{radial}) on the cylinder block. This radial force causes a torque (M_z), which is transferred to the drive shaft. For more detailed description of the operation and the forces involved with the rotating group subassembly see (Ivantysyn and Ivantysynova, 2003).

The cylinder block receives flow from the inlet source (Q_{in}), which passes flow through the end case and valve plate porting to the cylinder block. A valve plate, in simple terms, determines the timing of the flow into and out of the piston chambers.

The control subassembly consists of the swashplate, swashplate bearings, control arm, feedback mechanism, unit control cylinder, unit control valve, the low-pressure setting relief valve, and the controller. The controller subassembly is colored blue in Figure 3.2. The purpose of the control subassembly is to control the outlet flow of the pump (Q_{out}) by varying the angle of the swashplate (β). The changing angle of the swashplate ($\dot{\beta}$) changes the piston stroke (x) in the rotating group, thus increasing the displacement of the pump. The charge pump and low-pressure relief valve provide the flow (Q_{charge}) and necessary pressure ($p_{control}$) to overcome the resistive torques transferred to the swashplate at the slipper/swashplate interface (M_x and M_y).

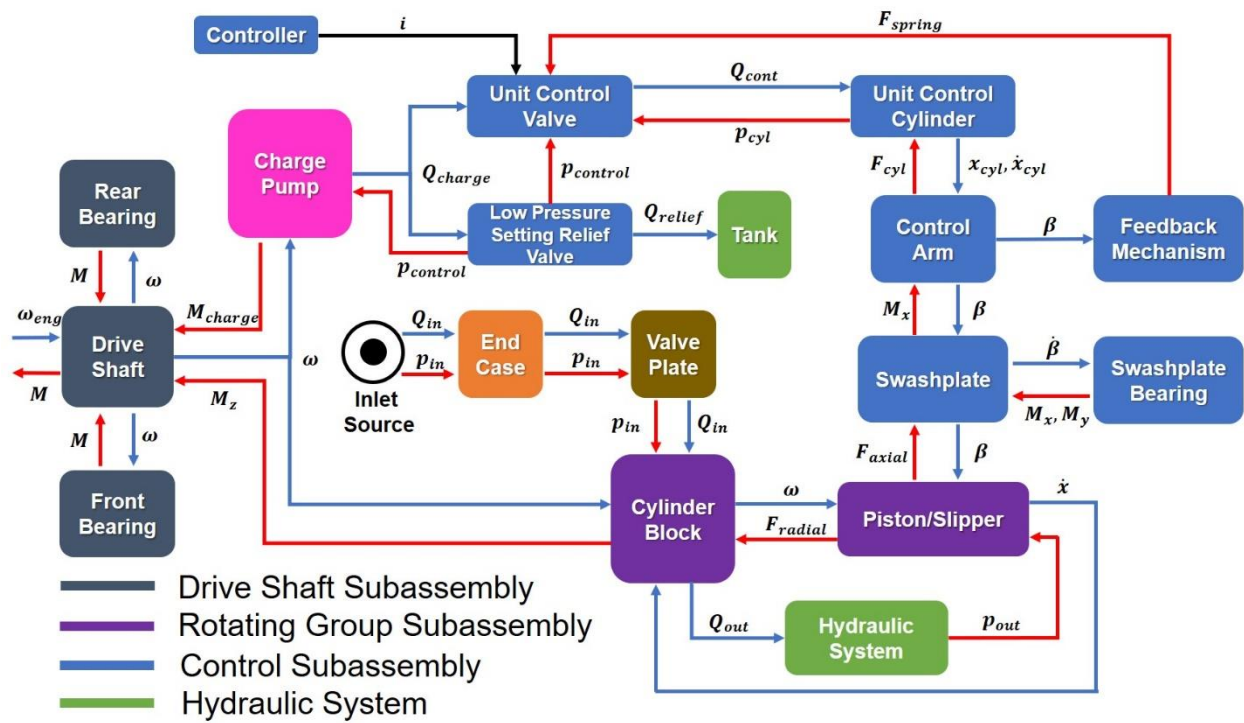


Figure 3.2: Swashplate type axial piston pump component interactions.

To narrow the scope of the investigation, only the wear interfaces on the pump are considered. The wear interfaces are where two components move relative to one another. Figure 3.3 shows a cross-section of a Danfoss Series 90 axial piston pump, and its wear interfaces. While this is not the reference pump for this work, the wear interfaces are shown clearly in the cross-section and can be applied to the reference Parker P1 pump. These interfaces are common among most variable displacement swashplate type axial piston pumps, even though pump architectures can vary.

Eight wear interfaces are shown in Figure 3.3 and include: roller bearings, swashplate bearings, piston/slipper, control piston/cylinder, rear bushing, valve plate/cylinder block, and the piston/cylinder interfaces. The roller bearings reduce radial loads on the shaft and are a major source of failure and wear on rotating machinery (Zhao-neng and Wang, 1989; Wang and Wang, 1993; Fey *et al.*, 2000; Lybeck, Marble and Morton, 2007; Huang *et al.*, 2010; Du, Wang and Zhang, 2013). The swashplate bearings support the axial loads placed on the swashplate from the rotating group and the control arm. The swashplate bearings also allow for reduced friction motion as the swashplate rotates about its axis. The slipper/swashplate interfaces is where the slippers move across the swashplate with a microscopic fluid film between the two surfaces to provide lubrication and load bearing capabilities (Ivantysyn and Ivantysynova, 2003), these type of interfaces are often known as a hydrodynamic or hydrostatic bearing (Rowe, 2012). Other hydrodynamic bearings that allows for relative motion between them are the piston and slipper, control piston and cylinder, piston and cylinder, valve plate and cylinder block, and the rear bushing.

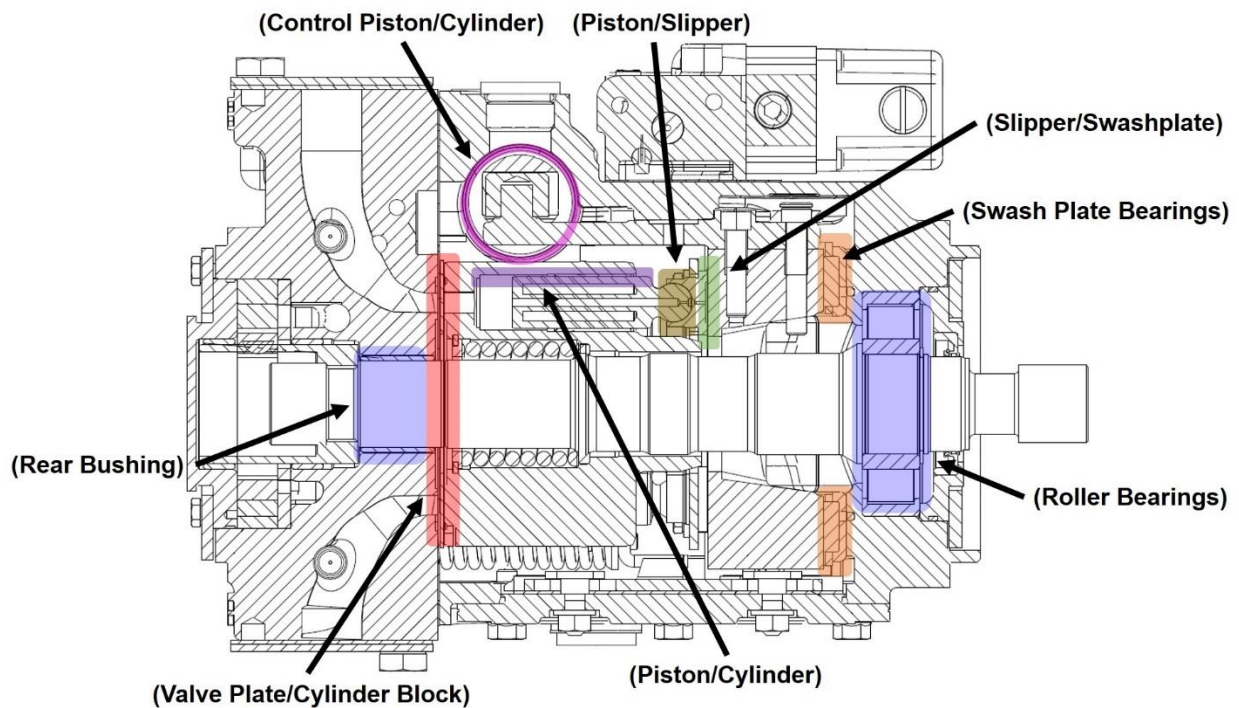


Figure 3.3: Wear interfaces of Danfoss Series 90 axial piston pump.

It is well known that the main sources of energy dissipation in swashplate type axial piston pumps occur at the slipper/swashplate, piston/cylinder, and valve plate/cylinder block interfaces (Zecchi, 2013; Busquets, 2018; Mizell, 2018). These three main lubricating interfaces can be seen in Figure 3.4. These interfaces are also the locations that exhibit the most wear on a pump, not including the roller bearings (Silva Gabriel, 1990; Hertz *et al.*, 1991; Yamaguchi and Matsuoka, 1992; Kazama and Yamaguchi, 1993, 1995; Li, 2005; Du, Wang and Zhang, 2013; Fatima *et al.*, 2013; Wang *et al.*, 2016).

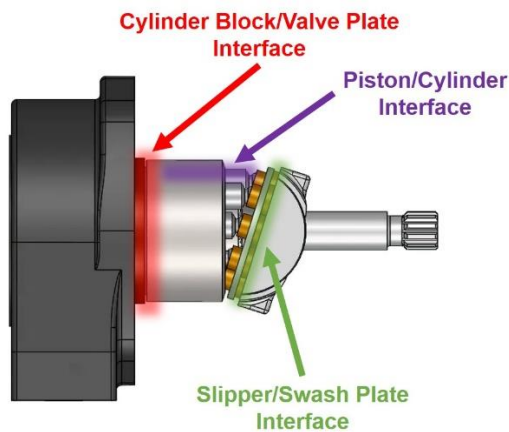


Figure 3.4: Main lubricating interfacing on a swashplate type axial piston pump.

The valve plate is a critical component that is one of the components that experiences the most wear and damage. Valve plates contribute to up to 38% of pump failures in some aerospace pumps (Du, Wang and Zhang, 2013). For these reasons, the valve plate is the component that is chosen to investigate condition monitoring of axial piston pumps for mobile applications in this work. Additionally, several valve plates are readily available with varying degrees of wear.

3.3 Six Different Levels of Valve Plate Health

Six valve plates of varying degrees of wear and damage have been obtained to perform the necessary experiments for a condition monitoring investigation. It is important to note that the effects on the performance of the pump with the various states of valve plate health cannot be exactly known and is difficult to predict because of the high nonlinearity of these interfaces (Wang *et al.*, 2016). The selected valve plates can be seen in the list below.

1. No Wear with No Damage (Healthy)
2. Severe Wear with No Damage (SW_ND)
3. Minor Wear with Moderate Damage (MinW_ModD)
4. Minor Wear with Severe Damage (MinW_SD)
5. Moderate Wear with Minor Damage (ModW_MinD)
6. Extreme Damage (ED)

3.3.1 Naturally Occurring Valve Plate Wear

The wear on the valve plate occurred naturally from being in a Bobcat 435 mini excavator. The wear was not artificially generated or induced. Four valve plates with varying degrees of wear have been obtained, and they include: no wear, minor wear, moderate wear, and severe wear. The wear profile on each of the valve plates is measured using a ZeGage® optical profilometer. This is done to observe and rank the severity of wear. The wear profile is measured at the same location for each of the valve plates.

No Wear

The valve plate that exhibited the least amount of wear can be seen in Figure 3.5. The film thickness of this lubricating interface is designed to be on the order of microns. Notice that the profile varies on the sub-micron level. Therefore, the wear could be considered negligible and is designated at the “healthy” valve plate.

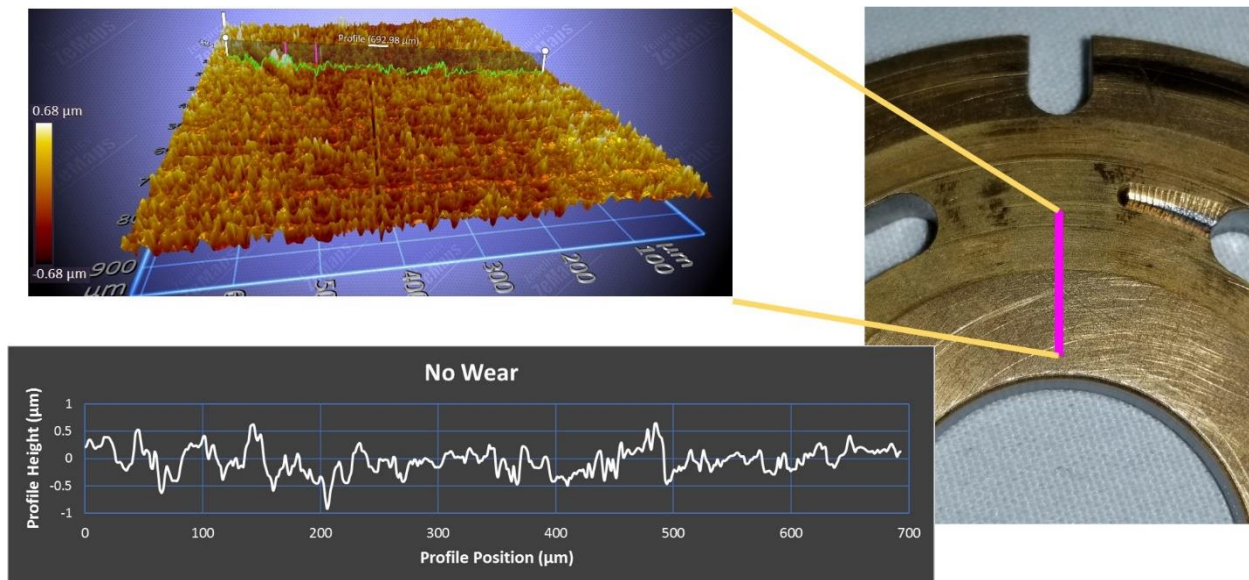


Figure 3.5: Profilometer measurements of valve plate with no wear or damage.

Minor Wear

The valve plate that is classified with minor wear can be seen in Figure 3.6. This valve plate has a wear profile of about four micrometers. This is not a significant amount of wear but is on the same order of magnitude that the film thickness is designed for, therefore some differences in performance are possible.

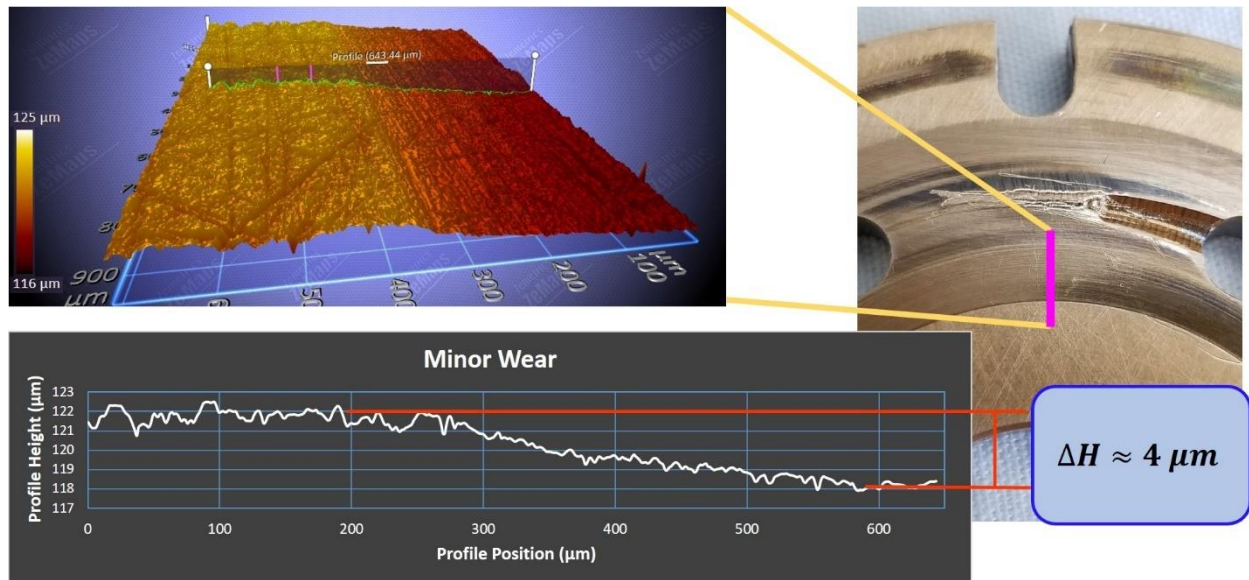


Figure 3.6: Profilometer measurements of valve plate with minor wear.

Moderate Wear

The severity of the wear begins to drastically increase with the valve plate classified as moderate wear. The variation in wear is approximately ten micrometers, see Figure 3.7. The wear profile is now an order of magnitude greater than the “healthy” valve plate. Performance is more likely to be affected by the amount of wear observed in Figure 3.7.

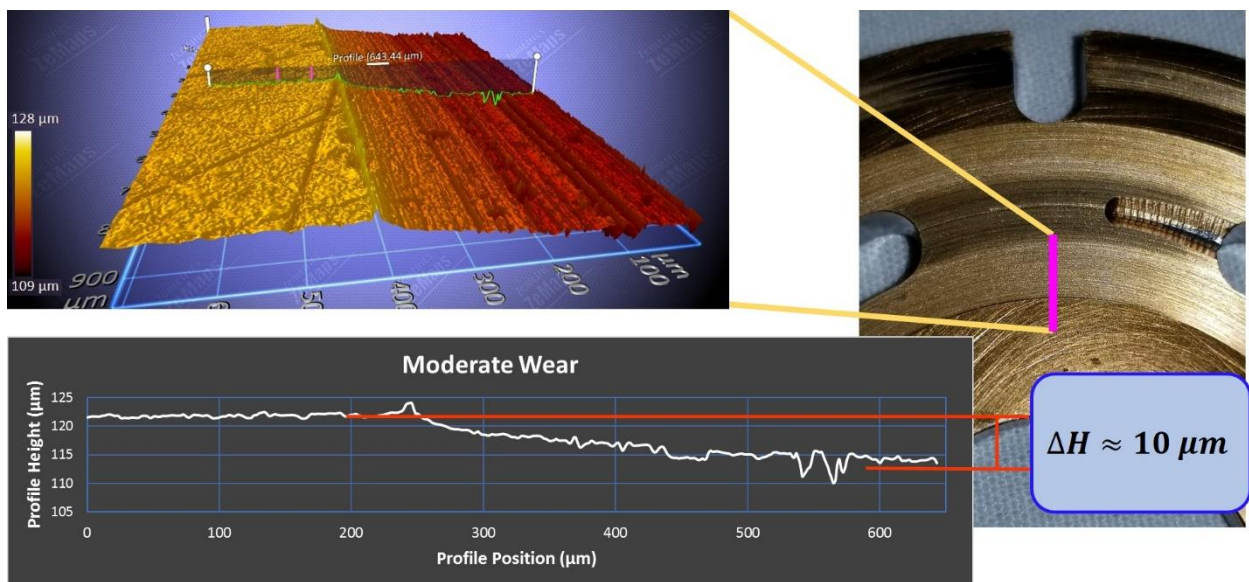


Figure 3.7: Profilometer measurements of valve plate with moderate wear.

Severe Wear

Severe wear on a valve plate can be observed in Figure 3.8. The variation in the wear profile is about 20 micrometers. An interesting phenomenon can be observed in Figure 3.8 where a ridge with a height of about 20 micrometers is present. This ridge is likely caused by the contact from the cylinder block and caused the soft brass-alloy material to deform into a ridge. This ridge is higher than the fluid film thickness. The distance from the top of the ridge to the bottom of the wear profile is approximately 40 micrometers, which is significant. Observable performance differences are more likely to be seen with the severely worn valve plate when compared to the healthy valve plate. A ridge of smaller height can be observed in the moderately worn valve plate in Figure 3.7, likely due to less wear.

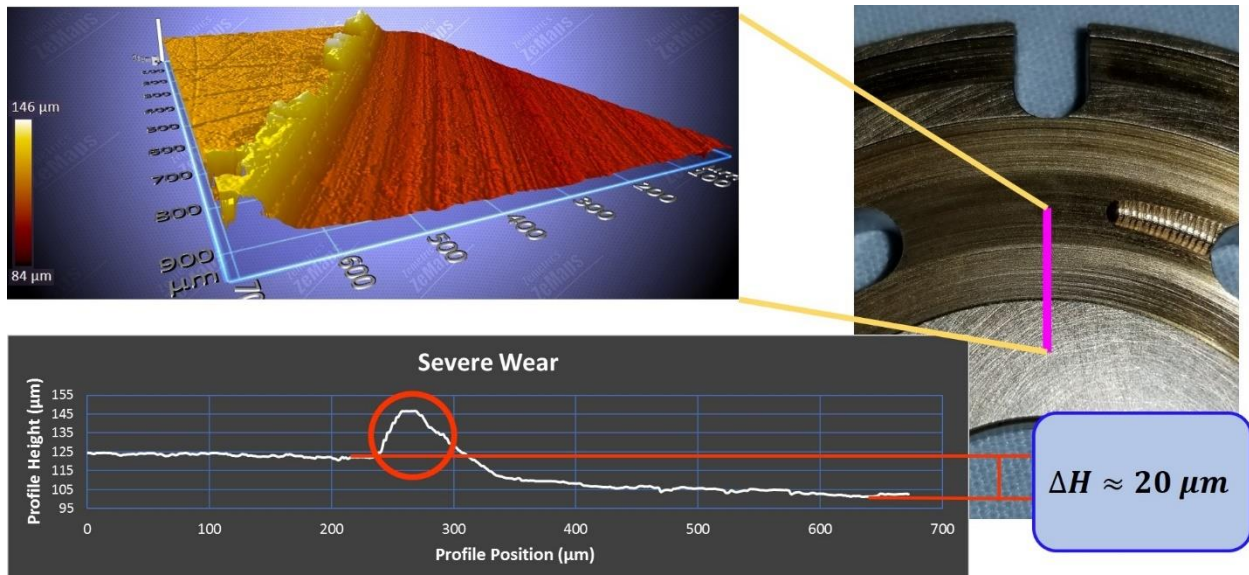


Figure 3.8: Profilometer measurements of valve plate with severe wear.

3.3.2 Artificially Induced Valve Plate Damage

To observe the effects that a damaged valve plate would have on the performance of the pump, some valve plates have been artificially damaged at the relief groove on the suction side of the valve plate. The artificial damage is used to approximate damage from debris particles gouging and removing material at the suction side of the pump. This debris could have come from another segment in the system or have been caused by cavitation.

The damage was caused by using a tungsten carbide tip scribe to manually scratch the surface of the valve plate. The scratches were placed in approximately the same location with varying degrees of depth and material removed. An optical profilometer, Zegage™, is used to observe the profile of the damage. Four levels of damage are performed and measured: No damage, minor damage, moderate damage, and severe damage.

No Damage

The healthy valve plate does not contain any artificial damage, as can be seen in Figure 3.5. This valve plate serves as a no wear and no damage case to determine the performance of a healthy pump. However, there is no damage on the valve plate with severe wear. This allows for a comparison of wear versus damage. The severe wear and healthy cases can be compared, and the minor wear and severe damage case can be compared to the healthy case to observe differences in performance. The extreme damage case is used to observe trends in the pump's volumetric performance.

Minor Damage

Figure 3.9 shows the minor damage that is induced on the suction relief groove on the valve plate. The scratch was placed in a radial pattern as to follow the motion of the cylinder block relative to the valve plate. The scratch is deep but narrow. It goes down approximately 30 micrometers but is less than 0.5 micrometers in width. This damage is classified as minor in comparison to the other selected valve plates.

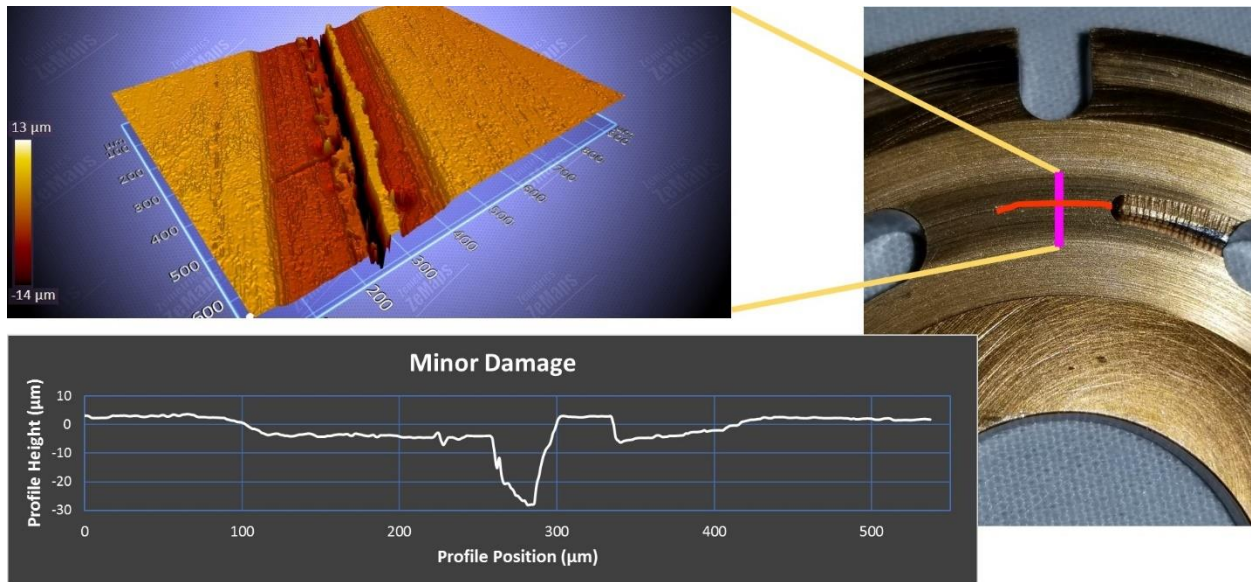


Figure 3.9: Profilometer measurements of valve plate with minor damage.

Moderate Damage

The moderate damage is in the same location as the minorly damaged valve plate, see Figure 3.10. This damage profile consists of several scratches around 15 micrometers in depth with each scratch spanning about 25 micrometers.

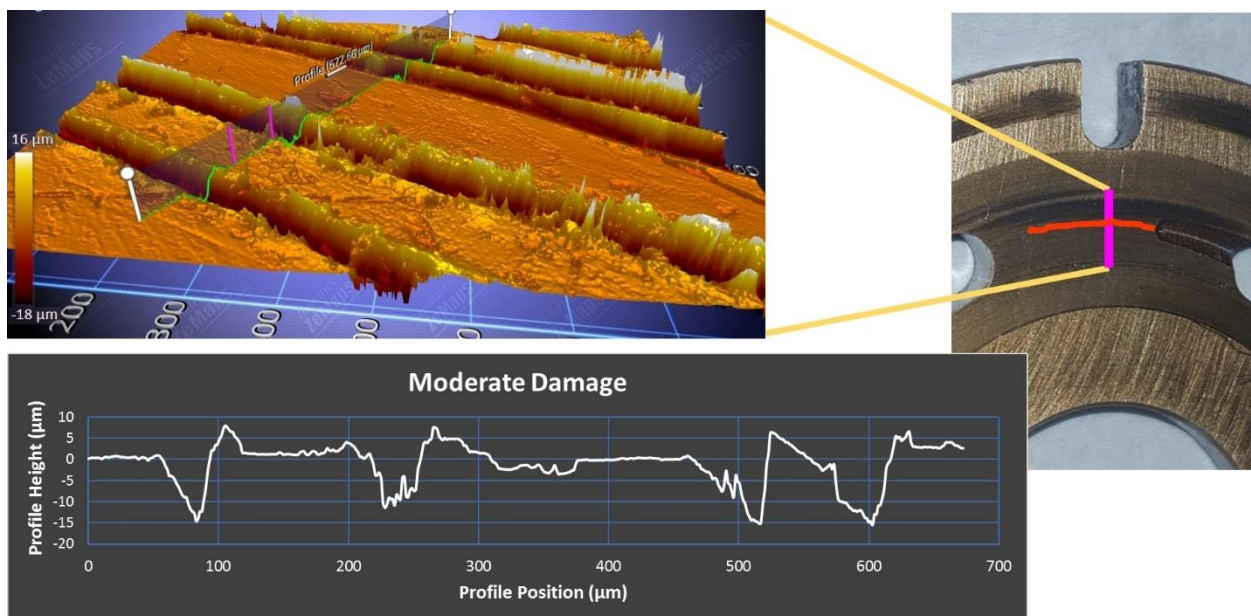


Figure 3.10: Profilometer measurements of valve plate with moderate damage.

Severe Damage

The damage done to the relief groove on the suction side of the valve plate is significantly more severe than the other damage on the previously discussed valve plates. Figure 3.11 shows the damage varies from 20 to 80 micrometers in depth while spanning almost 800 micrometers. Not measured but observable in the picture of the valve plate in Figure 3.11, a significant dent can be seen at the beginning of the relief groove. This dent is a result of a spring-loaded automatic steel center hole punch and was used to provide extra severity to the damage on the valve plate. This valve plate could simulate a severe case of cavitation and abrasion damage.

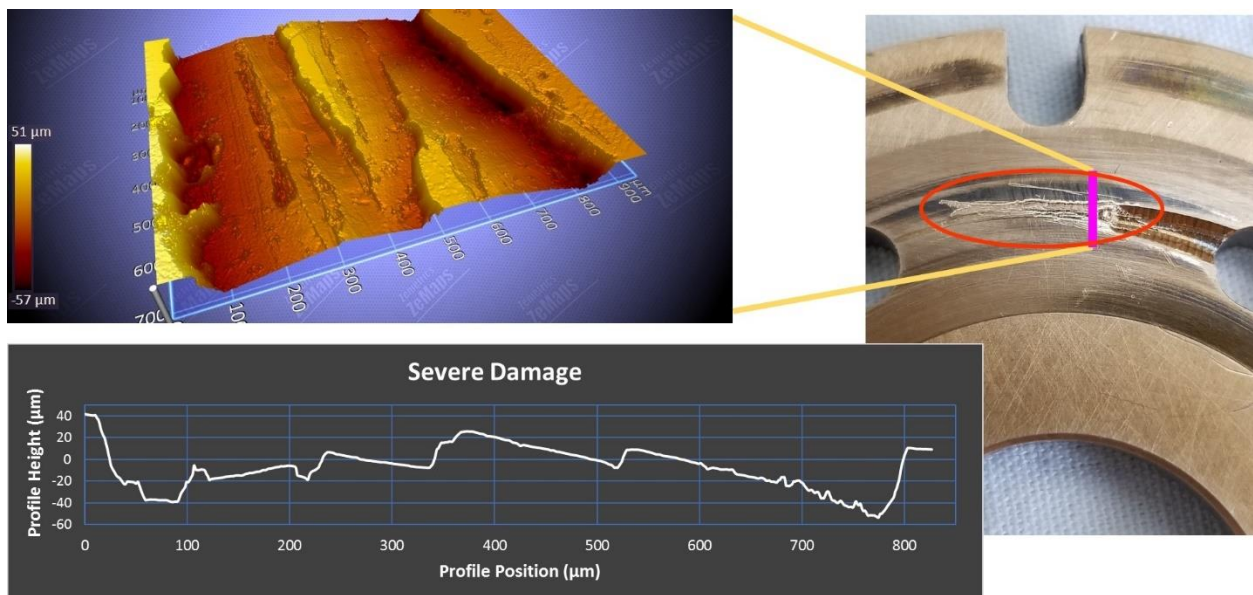


Figure 3.11: Profilometer measurements of valve plate with severe damage.

Extreme Damage

A valve plate with extreme damage is used to help ensure a difference can be observed and detected. Figure 3.12 shows measurements from a Bruker® optical profilometer of an extremely damaged valve plate. The Bruker® optical profilometer is used because the ZeGage® optical profilometer that was used to measure the wear and damage on the other valve plates is incapable of measuring the depth of damage that exists on the extreme damage valve plate.

This valve plate is artificially damaged to simulate a scenario where the sealing function of the valve plate is compromised. Figure 3.12 shows the extent of the damage induced on this valve plate. The width of the damage is approximately 2 mm while the depth of the damage groove is

about $350 \mu\text{m}$. This type and severity of damage would increase the leakage to the case of the pump, thus increasing case drain flow.

The extreme damage valve plate will only be used for observational purposes during procedures on the stationary test-rig. However, this valve plate will be included in machine learning algorithms on the mobile mini excavator.

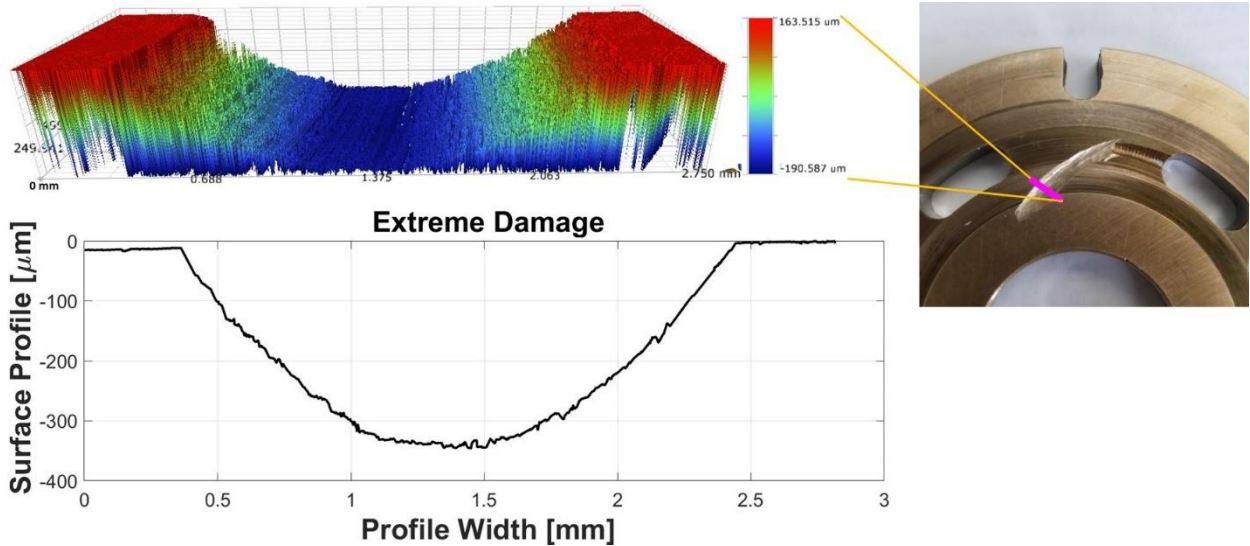


Figure 3.12: Optical profilometer measurements of valve plate with extreme damage.

CHAPTER 4. STATIONARY TEST-RIG DEVELOPMENT

The selection of a reference pump and faulty components now leads into the need for the development of a stationary test-rig to investigate fault detectability, machine learning algorithms, pump performance characteristic based on the various valve plates, and sensor/dimensionality reduction. This chapter will discuss the purpose of the stationary test-rig, show the schematics, hardware, and data acquisition system, the different duty cycles, how the data is structured, and the measurement process.

4.1 Test-Rig Purpose

Three main purposes exist for the stationary test-rig: perform fault detectability, sensor/dimensionality reduction, and machine learning algorithm development. The stationary test-rig can be seen in Figure 4.1. It is crucial to perform fault detectability on a stationary test-rig before the faulty pumps are instrumented on the mobile excavator. Fault detectability is the determination of whether the faulty component affects the performance of the pump in an observable or detectable manner. If the fault cannot be observed or detected on the stationary test-rig under controlled conditions, then the fault will not be able to be observed on the mobile machine where the operating conditions are not as controllable.



Figure 4.1: Stationary Test-Rig

Sensor or dimensionality reduction is the process of eliminating redundant or unnecessary signals. In machine learning, sensor/dimensionality reduction is also known as feature selection. The aim for reducing the dimensionality of machine learning algorithms is to decrease the chance of overfitting the data, decrease algorithm or model training time, and increase the prediction speed of the model. However, a main driver for dimensionality reduction in this work is to find the minimum number of sensors required to detect the faulty pump. Mobile equipment has limited space for extra components, such as flow meters or torque meters, and mobile equipment manufacturers do not want to increase the cost of the machine. Therefore, the decrease in the number of sensors is critical for implementation and performance of the condition monitoring system on mobile equipment. In coming chapters, more detail will be discussed on how dimensionality is performed.

The final main purpose of the stationary test-rig is to determine which machine learning algorithm is “best” for the case of faulty valve plates. The term “best” simply means the algorithm that successfully and accurately can detect the faulty pump with the minimum amount of training time, number of dimensions, and adequate prediction speed. More will be discussed on algorithm selection in a later chapter of this dissertation.

4.2 Schematic, Hardware, and Data Acquisition

The stationary test-rig consists of an electric motor, hydraulic pump, 24 sensors, signal conditioning boxes, National Instruments (NI) cDAQ chassis, several NI data acquisition cards, and a computer running LabVIEW. Many sensors have been included in this study to compare the effectiveness of the different sensors in detecting a pump in a faulty condition. It is not the intent to include these many sensors on a mobile machine.

4.2.1 Hydraulic Schematic

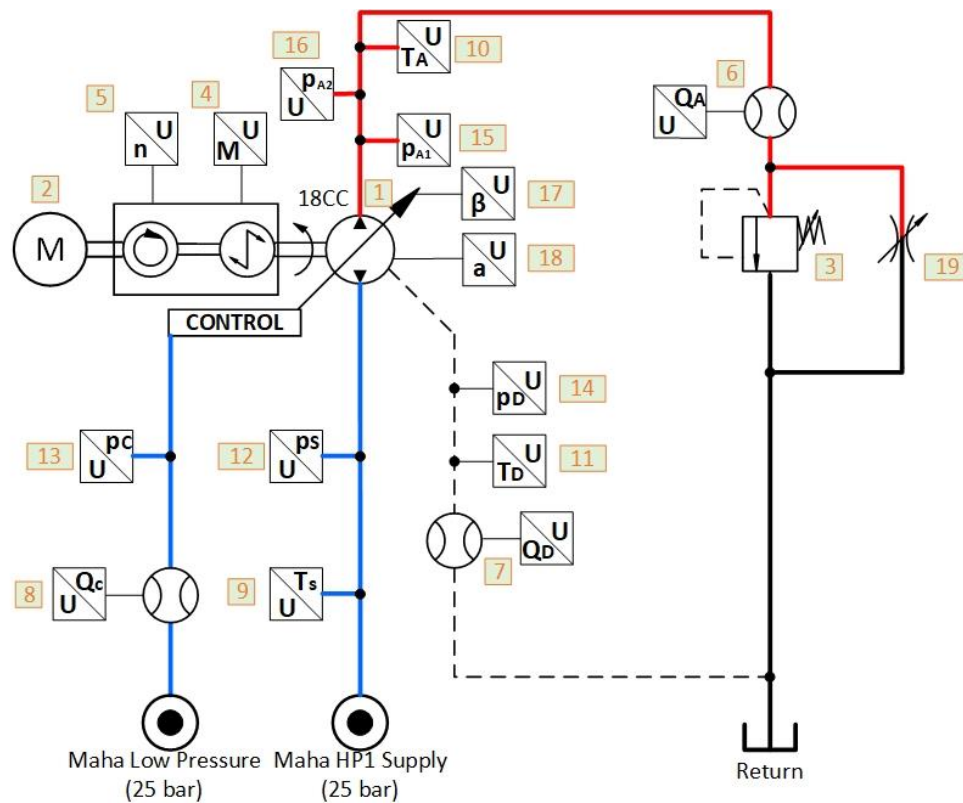
As mentioned previously, the chosen reference pump for this investigation is a Parker P1 18cc pump and is chosen because of the access to many faulty components. The 18cc pump (1) is driven by an electric motor (2), see Figure 4.2, and receives hydraulic fluid at 25 bar from the Maha power supply. The pump sends the flow through a gear-type flow meter (6) and, either, over a pressure

relief valve (3) or through a variable orifice (19). The variable orifice is closed, and the pressure relief valve is set to a predefined pressure during steady-state measurements. However, the pressure relief valve is set to the max pressure of the system, 350 bar, and the variable orifice is set to a predefined position during the dynamic duty cycle.

In addition to the flow meter that measures the outlet flow of the pump, two similar gear-type flow meters are measuring the flow in the drain (7) and control (8) lines, respectively. An accurate measurement of the volumetric losses can be obtained with the combination of these three flow meters. The flow loss is determined by subtracting the control flow from the drain flow, since the control flow drains to tank through the case drain of the pump.

Pressures are monitored and measured in the outlet (15 and 16), supply (12), control (13), and drain (14) lines. All the pressure sensors are piezoresistive, except for the additional pressure sensor on the pump outlet (15). Mounted directly on the pump outlet port fitting is a piezoelectric pressure transducer designed to measure the pressure transients of the fluid. This pressure sensor can measure the pressure ripple from the pump.

Four thermocouples are mounted on or near the test-rig to measure hydraulic oil and ambient air temperatures. The pump supply (9), outlet (10), and drain (11) temperatures are monitored with a thermocouple that is inserted in the center of fluid flow for accurate temperature readings. An additional thermocouple, not shown in Figure 4.2, is mounted outside the hydraulic test-rig near the pump to capture the ambient air temperature. The ambient air temperature is important to capture the difference between oil and air temperatures.



Components	
1. Parker P1 18cc Pump	10. Omega K Thermocouple [Outlet]
2. Electric Motor	11. Omega K Thermocouple [Drain]
3. Pres. Rlf.Valve [420 bar, 1500 L/min]	12. Hydac HDA 4400 Piezoresitive
4. Torque Meter	13. Keller Valueline Piezoresitive
5. Encoder	14. Keller PR-33x Piezoresitive
6. VSE 40L/Min Flow Meter [Outlet]	15. Kistler 603C Piezoelectric
7. VSE 18L/Min Flow Meter [Drain]	16. Hydac HDA 4400 Piezoresitive
8. VSE 18L/Min Flow Meter [Control]	17. Parker RS60 Hall Effect
9. Omega K Thermocouple [Supply]	18. PCB 356A16 & PCB 352C03 Accel.
	19. Needle Valve

Figure 4.2: Hydraulic schematic of stationary test-rig with component and sensor legend.

The shaft torque (4) and speed (5) are measured with a torque meter that contains an integrated speed sensor. The pump displacement is measured using a Hall effect sensor (17) that senses the relative position of the swashplate. Finally, nine single axis accelerometers (18) are mounted on the pump in various locations.

It can be noted there is an obvious lack of oil condition and contamination sensors on this test-rig. These sensors were considered but have been deliberately neglected for this study. The main

reason for not including these sensors is because the components were worn and damaged outside of the hydraulic system under investigation, and, therefore, the wear particulates are not circulating through the hydraulic system on the stationary test-rig. An additional reason to disregard oil condition and contamination sensors is because this stationary test-rig shares a hydraulic power supply with many other test-rigs in the Maha Fluid Power Laboratory. This would not guarantee that the wear particles are caused by the stationary test-rig where the condition monitoring investigation is taking place. The list of sensors and their corresponding accuracies can be seen in Table 4.1.

Table 4.1: Summary of sensor characteristics.

Company	Model	Type	Full Scale	Accuracy
Keller	Valueline	Diaphragm Strain Gauge	0 - 30 bar	$\pm 0.1\%$ FS
Keller	PR-33x	Diaphragm Strain Gauge	0 - 30 bar	$\pm 0.02\%$ FS
Hydac	HDA 4475-B-0150	Diaphragm Strain Gauge	0 - 400 bar	$\leq \pm 0.5\%$ BFSL
Omega	KMQSS-062G-6	Thermocouple	1-1250 °C	0.75% FS
Parker	RS60	Hall Effect	47°	1.4° FS
PCB Electronics	352C03	Piezoelectric Accelerometer	± 50 g	$\pm 1\%$ FS
Kistler	4503A	Torque Sensor	500 Nm	± 0.1 Nm
Kistler	4503A	Speed Encoder	8000 rpm	± 0.1 rpm
VSE	VS0.2	Gear Type Flow Meter	18 L/min	$\pm 0.3\%$ MV
VSE	VS0.4	Gear Type Flow Meter	40 L/min	$\pm 0.3\%$ MV
Kistler	603C	Piezoelectric Pressure Transducer	1000 bar	$\leq \pm 0.4$ bar FS

4.2.2 Accelerometer Placement

Nine accelerometers are mounted on the outside casing of the pump to measure the vibrations throughout the pump, see the location in Figure 4.3. The selected accelerometers measure the vibrations perpendicular to the mounting surface. Critical locations, such as at the pump inlet,

outlet and roller bearings are selected because of the presence of higher vibrations based on previous experience and literature review. However, other locations are considered to ensure adequate coverage over the pump.

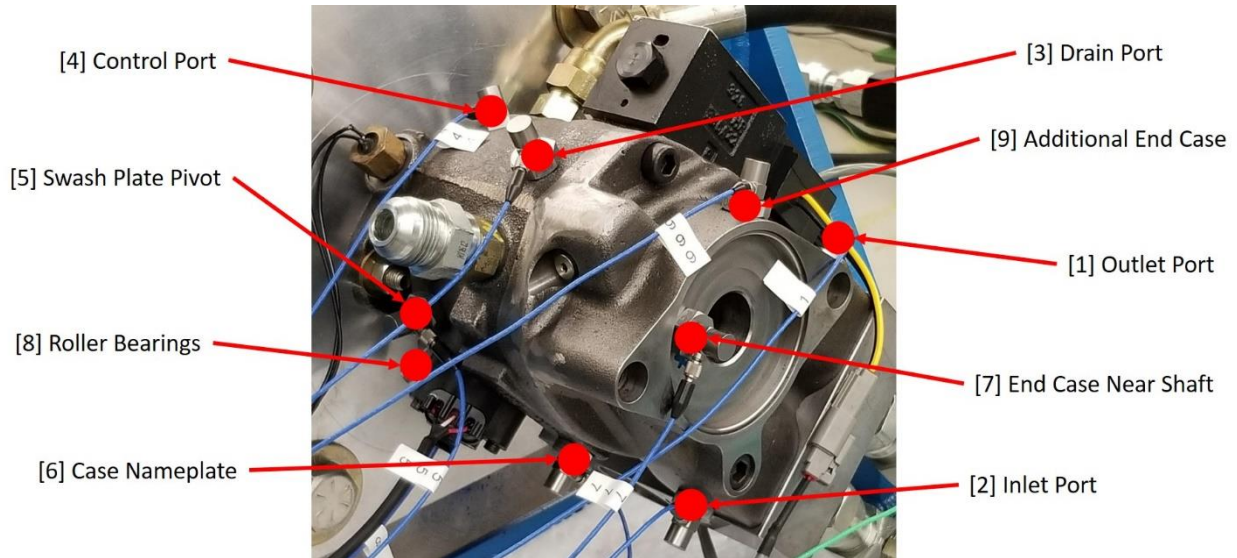


Figure 4.3: Accelerometer placement.

An accelerometer is mounted at each of the pump ports, as well as other locations that could see higher vibrations. The swashplate pivot is a location that can potentially experience high variations in vibrations due to the swashplate movement. Other locations on the pump have been instrumented with an accelerometer. Additional places such as the case nameplate, end case, and end case of the pump in the direction of the shaft axis.

4.2.3 Data Acquisition

Data acquisition includes sensors that measure an observable phenomenon, measurement hardware, and a computer running a programmable software, such as LabVIEW. The sensors have already been discussed, but this section discusses the hardware and software implemented on the stationary test-rig.

The sensors have been discussed in the previous section, but it is appropriate at this time to explain the sampling frequencies of the different sensors. The accelerometers and the piezoelectric

pressure transducer are sampled at a frequency rate, f_s , of 50 kHz, or a sample time, t_s , of $2 \cdot 10^{-5}$ seconds. The chosen accelerometers have a Nyquist frequency of 10kHz, so a sampling frequency five times greater than the Nyquist frequency is selected to prevent aliasing. The piezoelectric pressure transducer requires the same National Instruments (NI) data acquisition card as the accelerometers, so it is sampled at the same frequency as the accelerometers. Of course, it is possible to obtain cheaper accelerometers with reduced frequency characteristics, but these accelerometers are readily available and accurate for initial vibration investigations. All other signals are sampled at a frequency of 1,000 Hz, or 0.001 seconds.

Figure 4.4 shows the data acquisition system for the test-rig. The flow meter and torque/speed sensor signal conditioning boxes can be seen on the right in Figure 4.4. These signal conditioning boxes apply necessary filtering, amplifying, and additional conditioning to produce an analog voltage. Another crucial component to the DAQ system is the charge amplifier used to convert the charge produced by the piezoelectric pressure transducer into an analog voltage, see Figure 4.5. The piezoelectric accelerometers have an amplifier built into the sensor to convert from charge to voltage, therefore a conditioning box is unnecessary for the accelerometers.

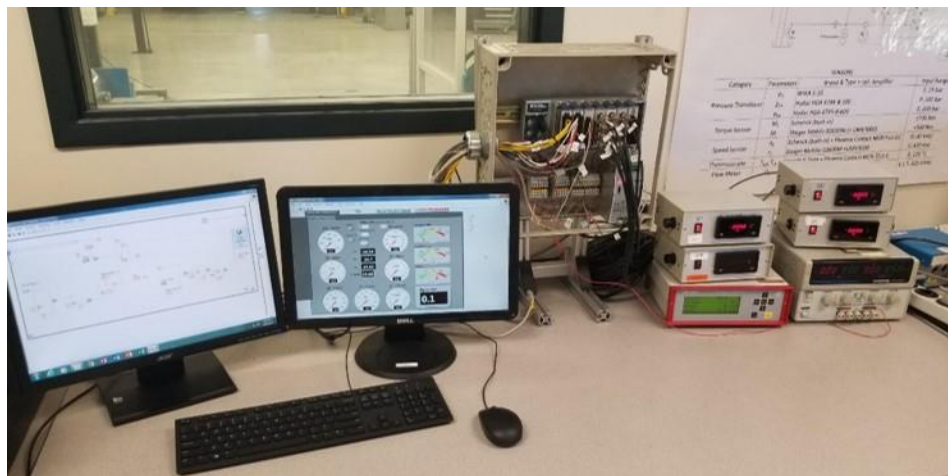


Figure 4.4: Data acquisition hardware setup.



Figure 4.5: Kistler piezoelectric charge amplifier.

Once the sensors have observed the phenomenon, and the necessary signals have been passed through signal conditioning boxes, then the signals are sent to the appropriate cards mounted in the NI cDAQ-9178 chassis, see Figure 4.6. The accelerometer and piezoelectric pressure transducer signals are sent to NI 9234 analog input Integrated Electronics Piezoelectric (IEPE) cards. The thermocouple signals are fed into a NI 9213 thermal couple card, while the remaining signals are sent to an NI 9205 analog input card.

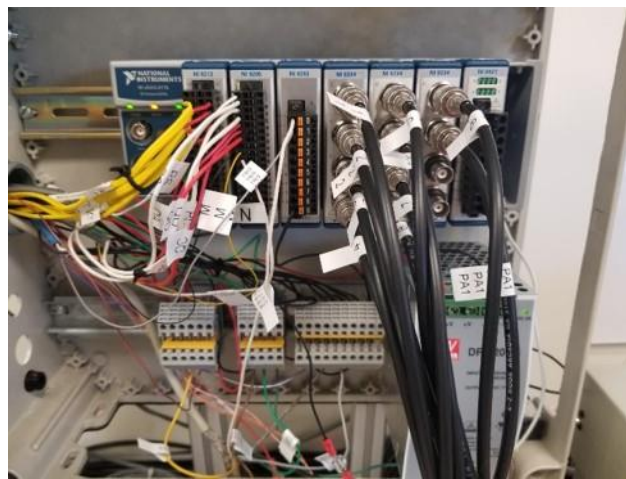


Figure 4.6: National Instruments (NI) data acquisition hardware.

The NI cDAQ communicates with LabVIEW, which is installed on the computer. In LabVIEW, the signals can be routed, sorted, modified, and saved to a designated location. LabVIEW is where the measurement recording process is initialized and carried through.

LabVIEW and NI DAQ systems do not only receive signals but can also send electrical signals to necessary components. The pump displacement is controlled by commanding a certain swashplate reference position, comparing the reference command to the measured swashplate position, and then sending that comparison through a PI controller in LabVIEW. The appropriate command is sent to the pump control valve, Figure 4.7, through an NI 9263 analog output card. The wiring diagram for the stationary test-rig can be found in Figure 4.8.



Figure 4.7: Parker D1FP pump control valve.

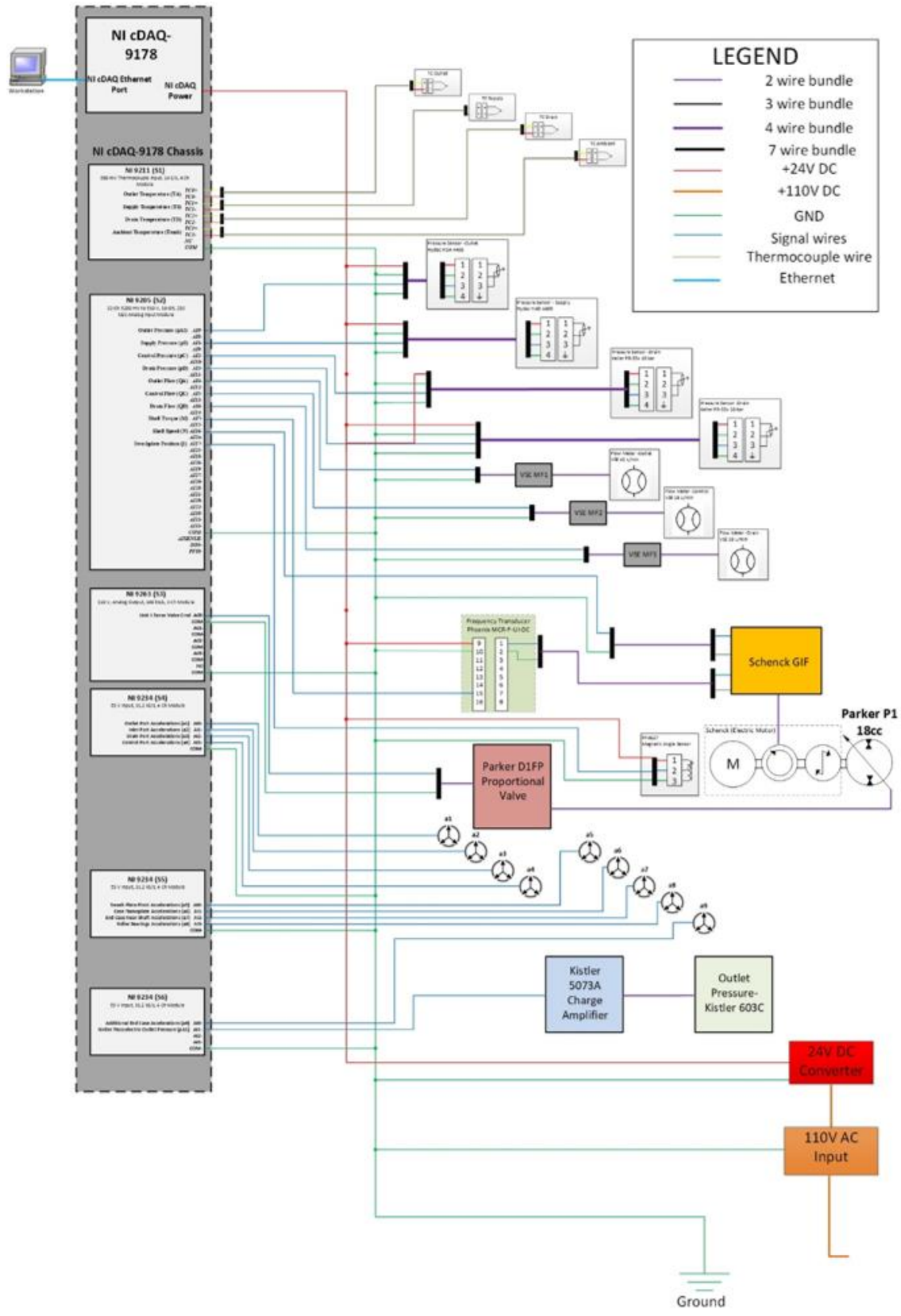


Figure 4.8: Stationary test-rig wiring diagram.

4.3 Duty Cycles

Another important aspect to the stationary test-rig that needs to be discussed is the duty cycles or operating conditions in which the measurements will be acquired. The purpose of the steady-state operating conditions is to see if the faulty pump valve plates can be detected in the most stable and controlled environment as possible. The next step before implementing the condition monitoring algorithm on the mobile excavator is to see if the same faults are detectable under a dynamic duty cycle performed in a controlled environment.

4.3.1 Steady-State

Table 4.2 lists the steady-state operating conditions under which measurements are taken. Measurements are taken at three different pressure differentials: 100 bar, 150 bar, and 200 bar. At each pressure range, measurements are taken at two different pump displacements. All measurements are taken at a constant shaft speed of 2000 RPM, and a pump inlet temperature of 52°C.

Table 4.2: Steady-state operating conditions

Operating Condition	N [RPM]	β [-]	T_{supply} [C]	Δp [bar]
OpCon_1	2000	1	52	100
OpCon_2				150
OpCon_3				200

An inlet, supply, temperature of approximately 52°C is chosen because the viscosity of the ISO 32 oil used in the tests is 10 centistokes (cSt), as can be seen in Figure 4.9. Additionally, the same viscosity of 10 cSt is obtained at a temperature of about 64°C in ISO 46 hydraulic oil, which is often used in mobile equipment.

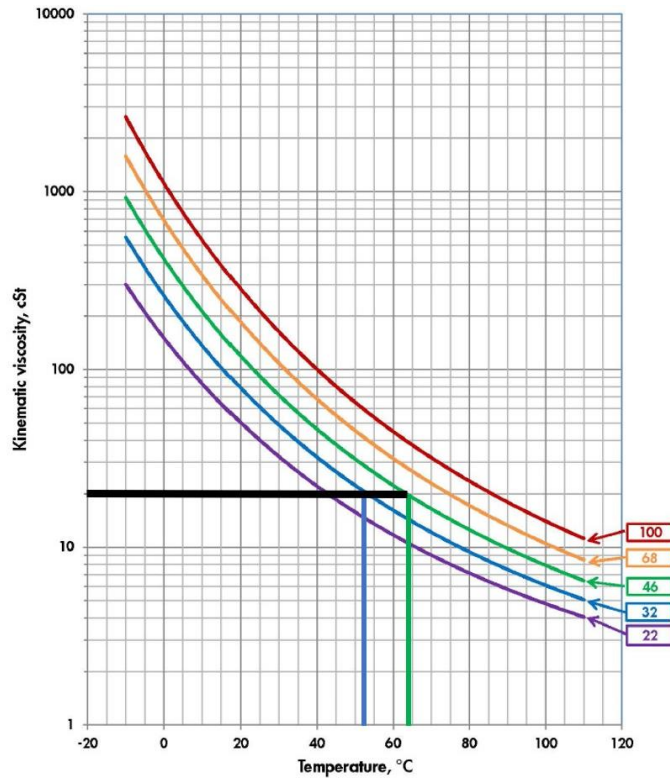


Figure 4.9: Viscosity – Temperature diagram for Shell Tellus S2 VX oil.

4.3.2 Dynamic Cycle

As mentioned previously, the dynamic cycle’s purpose is to see if faults are observable or detectable once they can be observed under steady-state conditions. A simple method for generating a repeatable dynamic cycle under controlled conditions is done by varying the outlet flow of the pump and sending that flow through a fixed orifice diameter. The pump displacement is commanded from a β of 0.5 to 1.0 and back to 0.5. This is repeated several times to capture the dynamic changes in the operating conditions. The pressure in the system is then determined by the flow through the fixed orifice, which can be seen in Equation (4.1). Figure 4.10 illustrates how the pressure is related to the displacement of the pump. It is to be noted that the speed of the unit is fixed at 2000 rpm.

$$Q = C_f \Omega \sqrt{\frac{2\Delta p}{\rho}} \quad (4.1)$$

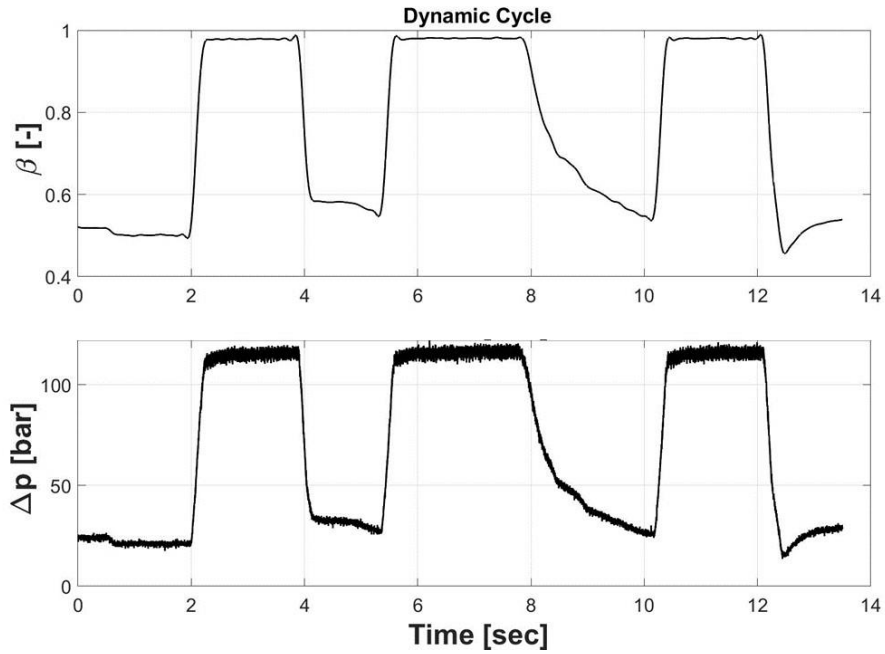


Figure 4.10: Dynamic duty cycle.

4.4 Data Structure

The data is structured in matrices to make data manipulation and postprocessing easier. Matrices are also the required format the data needs to be in to be entered the machine learning algorithms used in MATLAB. An example of the data structure can be seen in Table 4.3, where the rows of the matrix are each time step and the columns are the different sensor signals, or features in machine learning.

Table 4.3: Data structure example.

Time	TA	TS	TD	TAMB	pA2	pS	pD
0.001
0.002
0.003
0.004
0.005
0.006
0.007
0.008
0.009
0.01

A generalized matrix of the data can be seen below in Figure 4.11, where the rows represent time steps or measurement points, and the columns represent the measured sensor signals or feature. Each matrix represents the measurements taken during a specific operating condition and valve plate condition. These matrices can be combined to include data from healthy and all unhealthy, faulty, pumps for each operating condition.

$$\begin{bmatrix} F_{1,1} & \cdots & F_{1,n} \\ \vdots & \ddots & \vdots \\ F_{m,1} & \cdots & F_{m,n} \end{bmatrix}$$

Figure 4.11: Generalized data structure.

4.5 Measurement Process

Several operating conditions and faulty components can make the measurement process inconsistent and arduous if a measurement plan is not put in place before measurements begin. Below is the measurement process used for consistency and to maximize time efficiency.

1. Select Healthy valve plate
2. Install Healthy valve plate into pump
3. Heat oil to a pump inlet temperature of 52°C
4. Set displacement and pressures for OpCon_1
5. Wait for drain temperatures to stabilize
6. Take measurements for 10 seconds
7. Repeat steps 4-6 for Operating Conditions 2-3.
8. Run the dynamic operating condition
 - a. $\beta = 0.5$
 - b. Increase β to 1.0
 - c. Decrease β to 0.5
 - d. Repeat a-c four times
9. Shutdown test-rig
10. Allow oil to cool to ambient temperature (approximately 22°C)
11. Repeat steps 1-10 for the five other selected valve plates.

Additional measurements are taken to test the repeatability of the experiments. The experiments show good repeatability if the measurements exhibit similar characteristics between the different measurements. If good repeatability is achieved, then the experiments are valid, and the different fault cases can be successfully compared to one another. Repeatability measurements are taken only using the healthy valve plate, to reduce the amount of time and data storage. Steps 1-10 in the previously discussed measurement process are repeated until a total of five separate “healthy” measurements exist. These five measurements are compared to one another to assess the experiment’s repeatability. The results from the repeatability measurements will be discuss in the next chapter.

CHAPTER 5. MEASUREMENT OBSERVATIONS

While machine learning algorithms used in condition monitoring are often a black box method and determine whether the fault is detectable, it is valuable for a human to observe the differences in pump behavior between the different states of health on the pump. First, measurement repeatability will be introduced. Then observations between healthy and unhealthy valve plate measurements will be discussed.

5.1 Notable Repeatability Observations

As mentioned in the previous chapter, measurements that achieve good repeatability indicates that the measurements are valid and can be compared to other conditions. This section shows notable observations on the repeatability of the experiment. Five measurements are conducted using the healthy valve plate to establish repeatability results. The inlet and drain temperatures will first be discussed. Then, the drain flow, drain pressure, and the pump outlet transient pressure will then be shown. Not all parameters are shown in this document for repeatability purposes. However, it can be noted that the engine speed, pump displacement, and outlet pressure have incredibly repeatable measurements.

5.1.1 Temperatures

The repeatability results of the steady-state temperatures for the inlet and drain ports show results that could lead to misclassifications from a machine learning algorithm. Figure 5.1 and Figure 5.2 shows the inlet and drain temperatures of the five different healthy measurements taken under steady-state conditions, respectively. The inlet temperatures vary by about one degree. However, the drain temperatures have some measurements that vary by almost ten degrees. To ensure this drain temperature difference is not caused by a difference in ambient air temperature, the temperature difference between ambient and drain conditions can be seen in Figure 5.3. The temperatures still vary by about ten degrees.

Several factors may cause the inconsistencies in the temperatures. First, while the outlet pressures are very similar, they are slightly different. This would cause slight differences in drain

temperatures due to small variations in leakages. Second, the inlet temperatures vary by about a degree, which would influence the drain temperature. The inlet temperature is controlled by regulating an oil cooler on the Maha power supply. Lastly, the variations in temperature are likely caused by human error by not letting the system truly get to thermally stable conditions before measurements are taken. It is very difficult to have precise consistency in oil temperatures because of the many factors that influence temperatures.

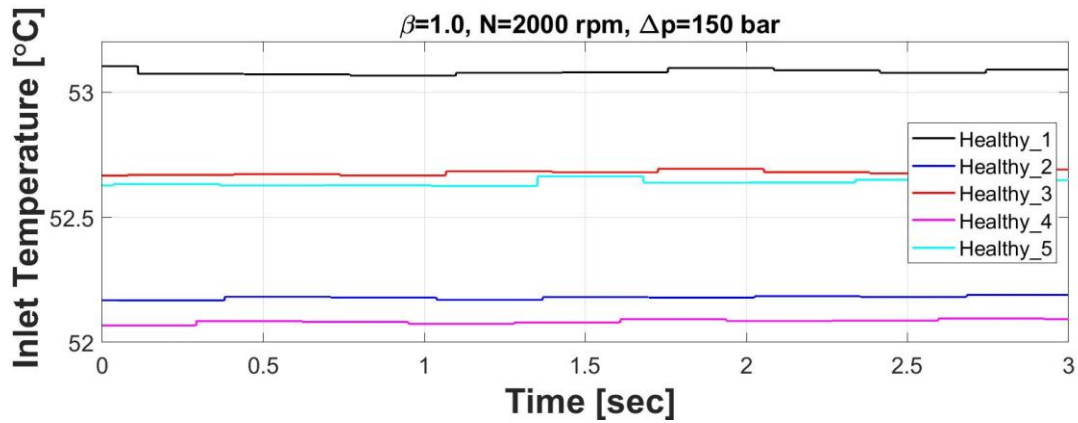


Figure 5.1: Steady-state repeatability measurements of health valve plate inlet temperatures.

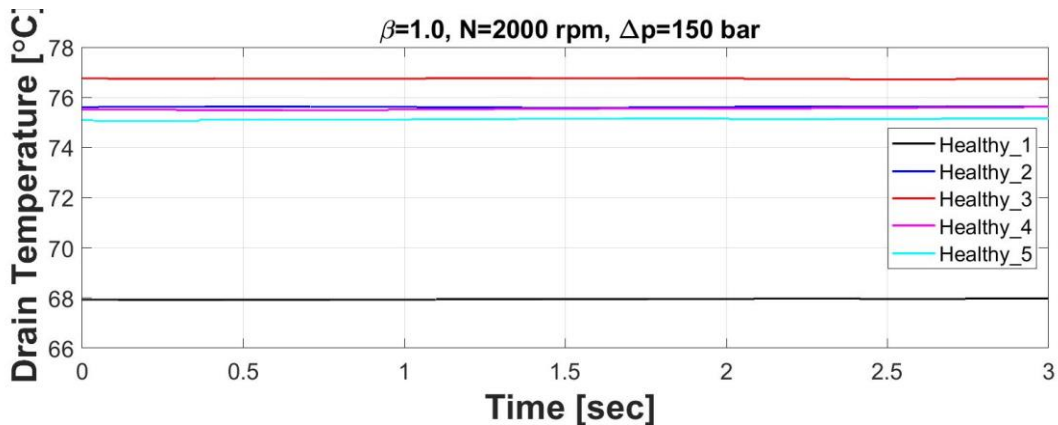


Figure 5.2: Steady-state repeatability measurements of health valve plate drain temperatures.

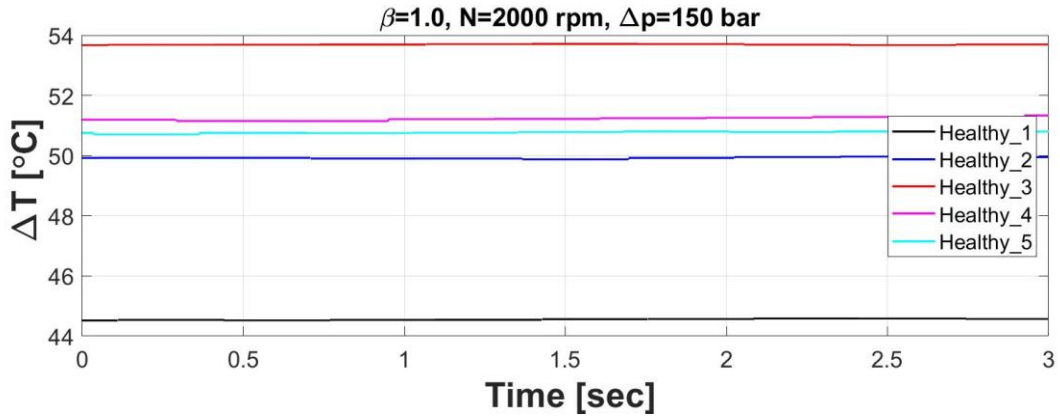


Figure 5.3: Steady-state measurements of the difference between drain and ambient temperatures for healthy valve plate conditions.

5.1.2 Drain Flow and Pressure

The next notable parameters to observe for repeatability are the drain flow and drain pressure. Figure 5.4 shows the drain flow of the five healthy measurements and demonstrates the repeatability. The drain flow is between 0.93-1.03 L/min . The drain pressure, Figure 5.5, has very repeatable measurements with pressures between 0.81-0.83 bar . The contrast between the healthy drain port conditions and those of the unhealthy will show drastic difference and will be discussed in the next section of this chapter.

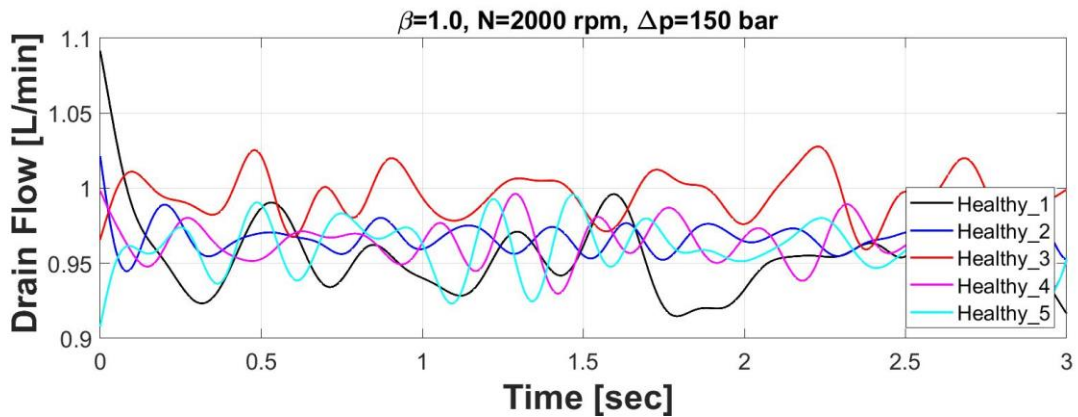


Figure 5.4: Repeatability measurements of drain flow for healthy valve plate conditions.

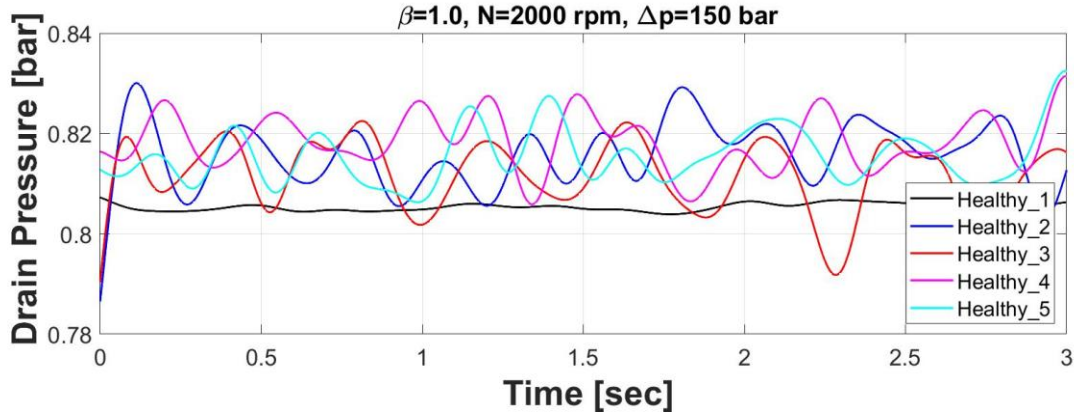


Figure 5.5: Repeatability measurements of drain pressure for healthy valve plate conditions.

5.1.3 Outlet Transient Pressure

The next method to observe repeatability is to check the frequency domain of the pressure transients at the pump outlet, Figure 5.6, which has characteristics at higher frequencies than the flow rate. The major spikes in pressure occur at the 9th, 18th, 36th, etc. harmonics. This is logical since the axial piston pump contains nine pistons, so the spikes in magnitude would be at harmonic multiples of nine. Taking a close look at the 9th harmonic in Figure 5.7 the measurements are exceptionally repeatable.

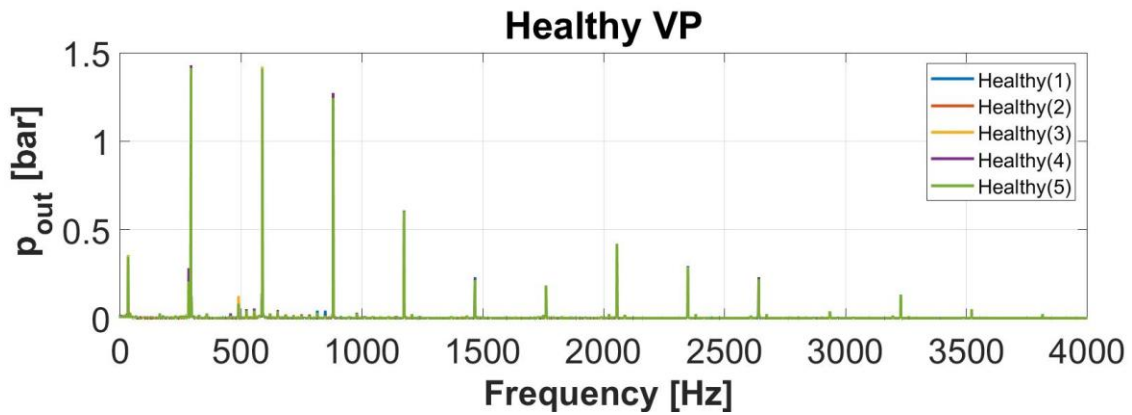


Figure 5.6: FFT of outlet transient pressure repeatability analysis.

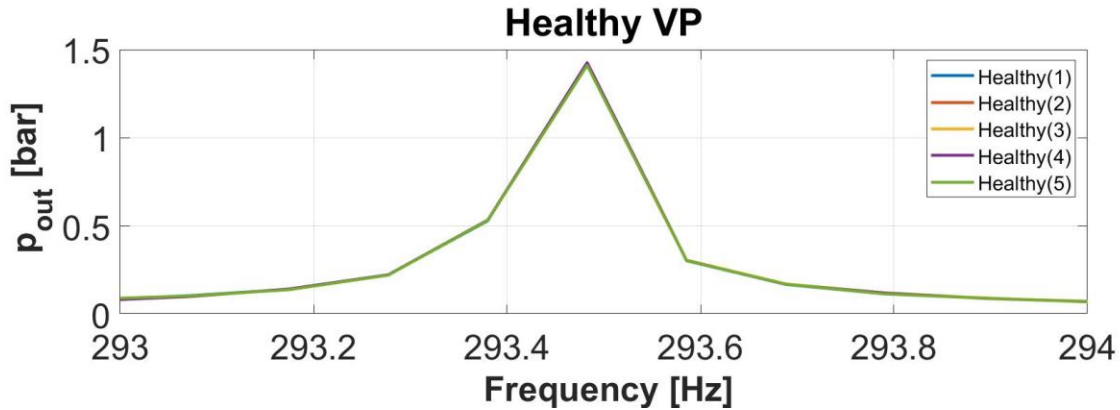


Figure 5.7: FFT of outlet transient pressure zoomed to see 9th harmonic.

5.2 Observable Wear/Damage

Now that repeatability has been shown, it is now necessary to observe the differences between the healthy pump and the unhealthy states. If a notable difference is observed, then it is likely a machine learning algorithm would be able to successfully detect valve plate fault. Several parameters will be observed to show comparison. Drain temperature, drain flow, outlet transient pressure, and volumetric efficiency are among those parameters to be observed.

5.2.1 Temperatures

The temperatures presented in this section show all the healthy valve plate measurements in black with the four faulty valve plate in color. Figure 5.8 shows the drain temperatures, and Figure 5.9 and Figure 5.10 show the temperature difference between drain oil and ambient conditions for steady-state and dynamic conditions, respectively.

The most important thing to be discussed at this time is the clear stratification of temperatures between all the different measurements, including the five healthy measurements. This stratification gives clear differences between the different measurements, and a machine learning algorithm trained with these temperature measurements would easily be able to classify the data with near 100% accuracy. However, the inconsistencies in the temperatures and the non-repeatable nature of them makes temperatures not ideal for a condition monitoring system on axial piston pumps with valve plate faults.

Another reason temperature may not be enough to use in a condition monitoring system like the one in this work is because of the slow response of the temperature. Figure 5.10 shows the difference between the drain and ambient temperatures during the dynamic duty cycle. Figure 4.10 shows the dynamic behavior of the pump displacement and outlet pressure throughout the cycle. These variable operating conditions result in a dynamic behavior of the pump. However, the oil temperature does not capture these transients. In fact, the oil temperature remains nearly constant. Additionally, oil temperature is often influenced by the many components within a hydraulic system and not necessarily the pump itself. For the reasons prescribed above, it is not recommended to use temperatures for detecting valve plate faults in axial piston pumps and is, therefore, eliminated from further investigation in this work.

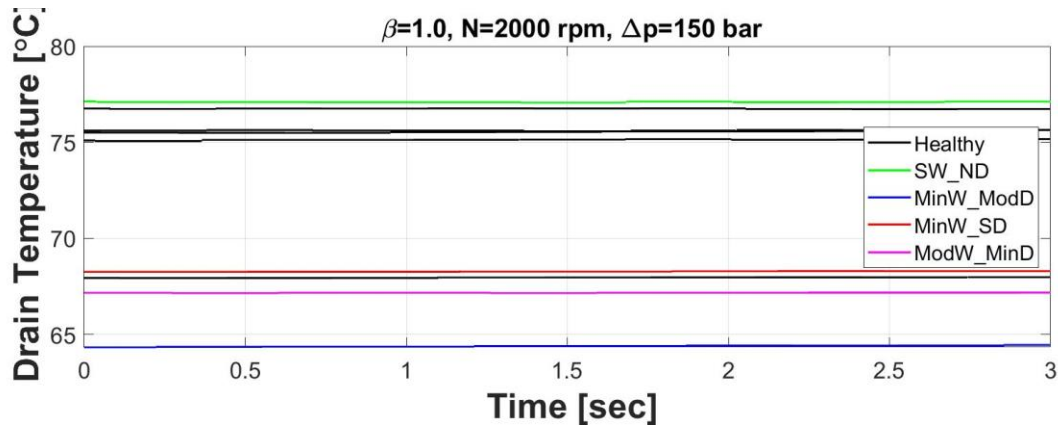


Figure 5.8: Drain temperature comparison between healthy and unhealthy valve plates operating under steady-state conditions.

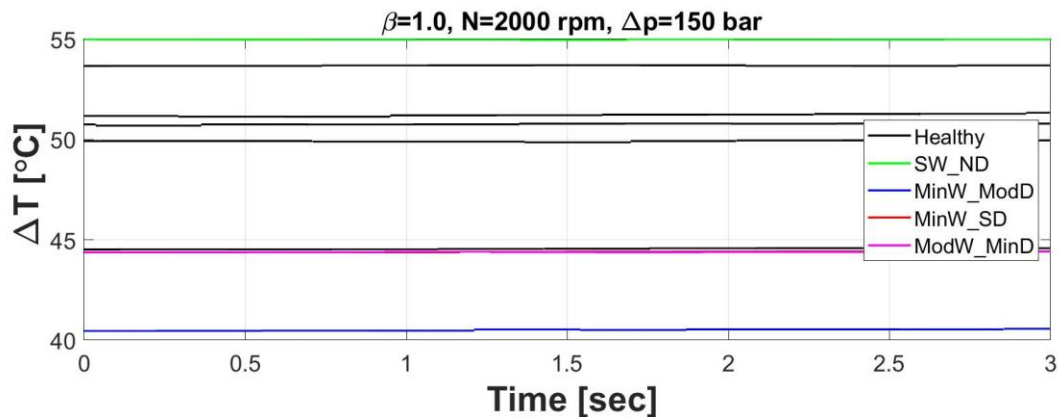


Figure 5.9: Difference between ambient and drain temperatures for comparing healthy and unhealthy valve plates operating under steady-state conditions.

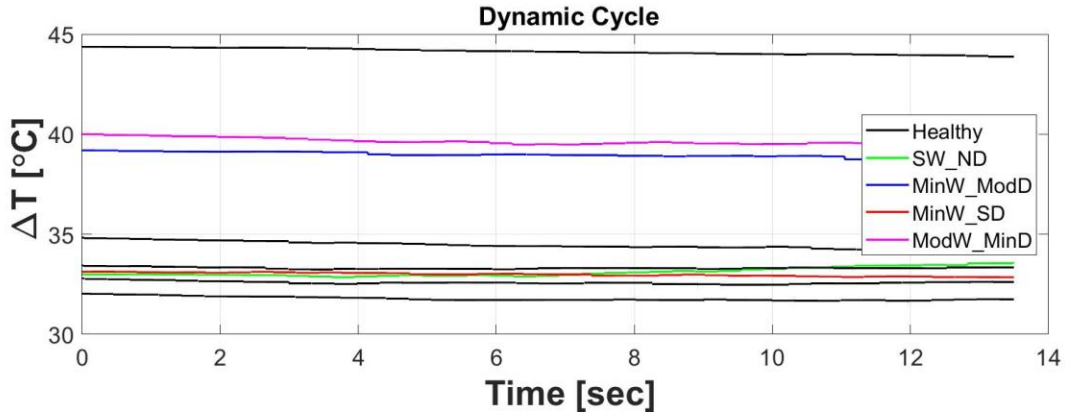


Figure 5.10: Difference between ambient and drain temperatures for comparing healthy and unhealthy valve plates operating under dynamic conditions.

5.2.2 Drain Flow

Logically, the drain flow is a natural place to compare between healthy and faulty valve plates. Figure 5.16 shows the differences between healthy and faulty conditions, excluding the extreme damaged valve plate. Notice only a single healthy measurement is used here for comparison purposes. Each of the faulty valve plate conditions exhibit more drain flow than any of the healthy measurements. There is an obvious increase in drain flow for each of the faulty valve plates.

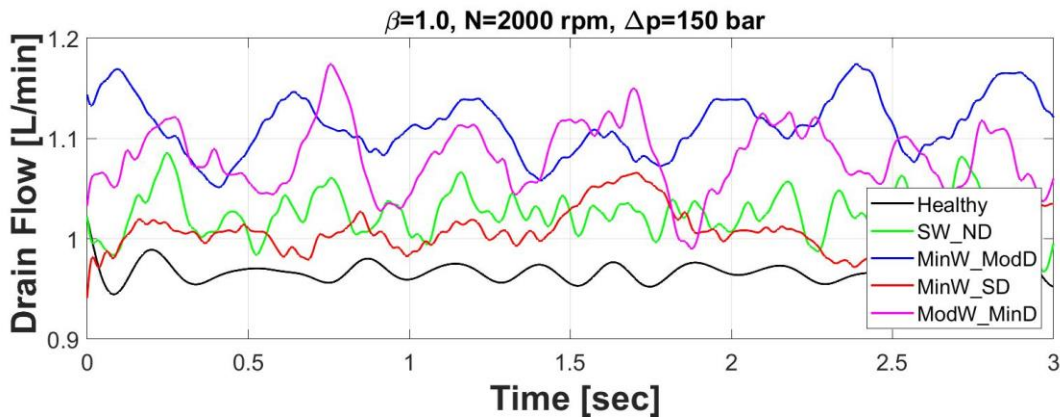


Figure 5.11: Drain flow comparison between healthy and unhealthy valve plates, excluding extreme damage.

Figure 5.12 demonstrates the impact a valve plate with extreme damage can have on the pump performance. The Extreme Damage (ED) valve plate experiences about 2.4 L/min of drain flow

while the other valve plates see around 1 or 1.1 L/min . This increase in drain flow will significantly decrease the volumetric efficiency of the pump, which will be shown later in this chapter. The extreme damage will not be included in a machine learning study on the stationary test-rig for the obvious discrepancy in pump performance. This study will focus on more subtle valve plate faults are detectable. However, the extreme damage valve plate will be used for machine learning studies on the excavator, as the minor damages may be more difficult to detect.

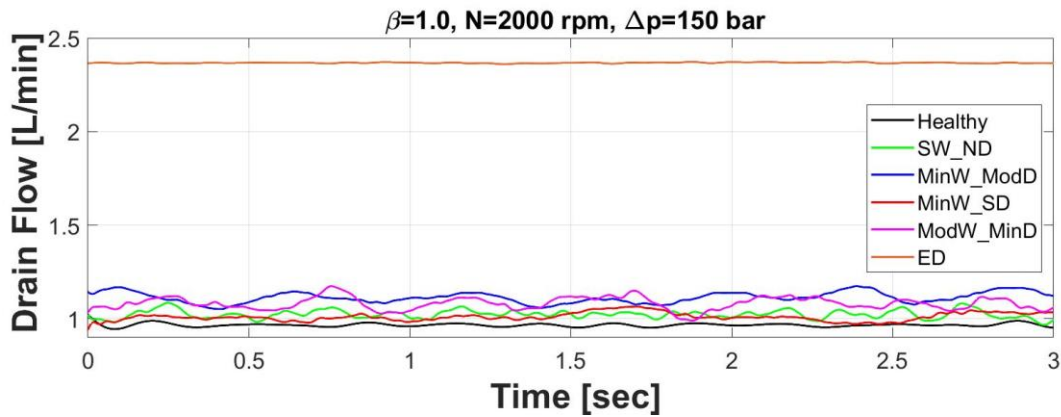


Figure 5.12: Drain flow comparison of healthy and unhealthy valve plates, including extreme damage.

5.2.3 Outlet Transient Pressure

The frequency domain of the transient pressures at the outlet port of each of the valve plate conditions can be seen in Figure 5.13. The repeatability between the healthy measurements showed nearly an exact match but differences can be seen between the healthy and faulty pump conditions. Looking at the 9th harmonic, see Figure 5.14 and Figure 5.15, a clear difference in shape and magnitude exist between the different pump conditions.

The shape of the healthy pump is significantly narrower than that of the other conditions. It is also interesting that the different faulty conditions each have a similar shape and magnitude. The reason for this result is not known at this time. However, if one is trying to observe a difference between a healthy pump and a pump with a faulty valve plate, then the frequency domain of the pressure transients successfully shows that difference.

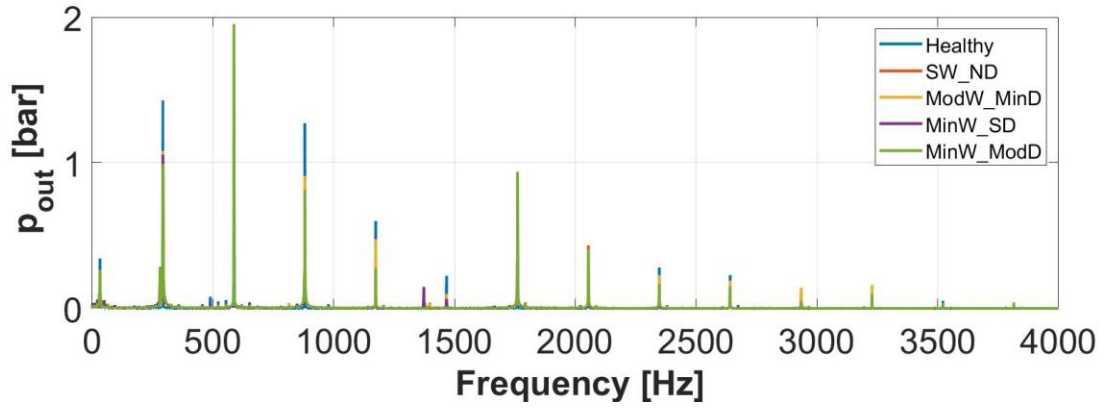


Figure 5.13: FFT of outlet transient pressure comparing faulty valve plates.

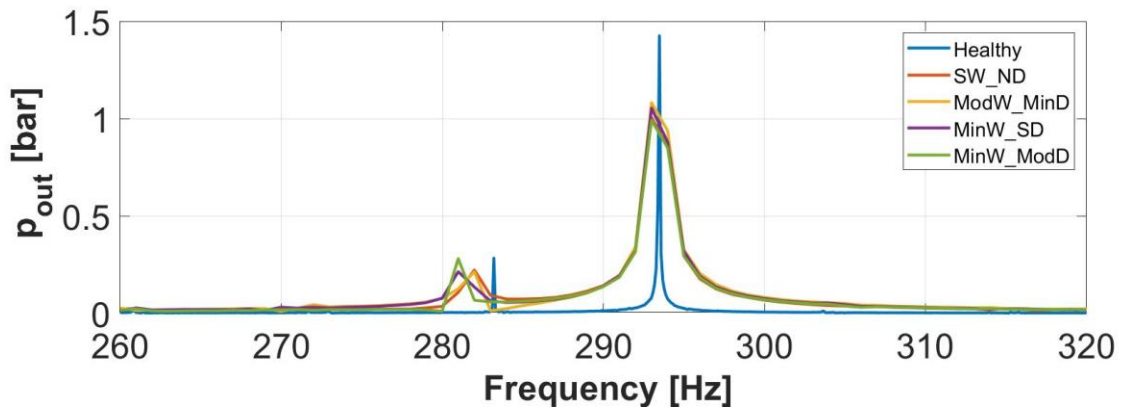


Figure 5.14: FFT of outlet pressure comparing faulty valve plates, zoomed between 260-320 Hz.

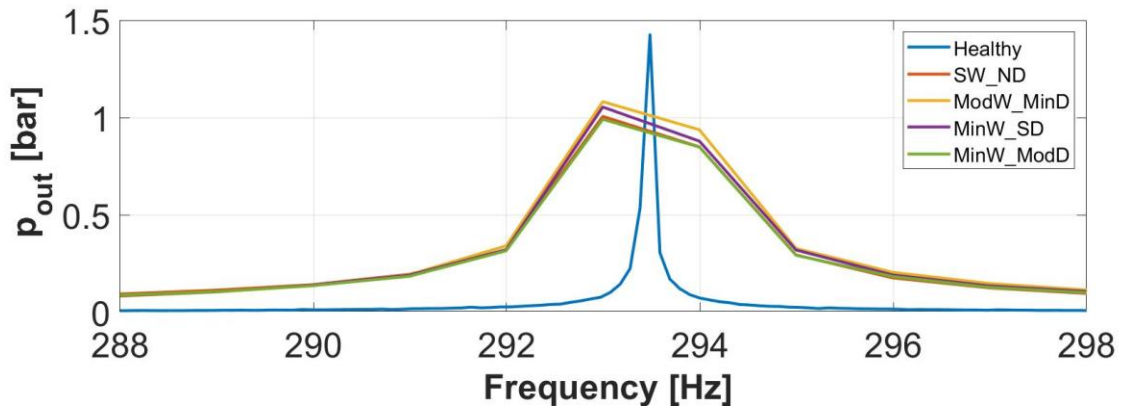


Figure 5.15: FFT of outlet pressure comparing faulty valve plates, zoomed at 9th harmonic.

5.2.4 Volumetric Efficiencies

It is to be expected that the faulty valve plates result in low volumetric efficiencies. Two different methods to observe volumetric efficiency are discussed. First, it can be beneficial to observe the outlet flow with respect to differential pressures. Figure 5.16 shows the outlet flow of each pump condition operating at the three differential pressures. From this plot the healthy pump has higher outlet flow rates, suggesting less leakage. This increased leakage from the faulty pumps is likely due to the worn or damaged valve plates. Figure 5.17 shows the significant difference in the outlet flow of the Extreme Damage (ED) valve plate compared to the other valve plate conditions. The outlet flow is lower because the ED valve plate exhibits higher case drain flows. Therefore, the outlet flow will be lower than the other valve plates.

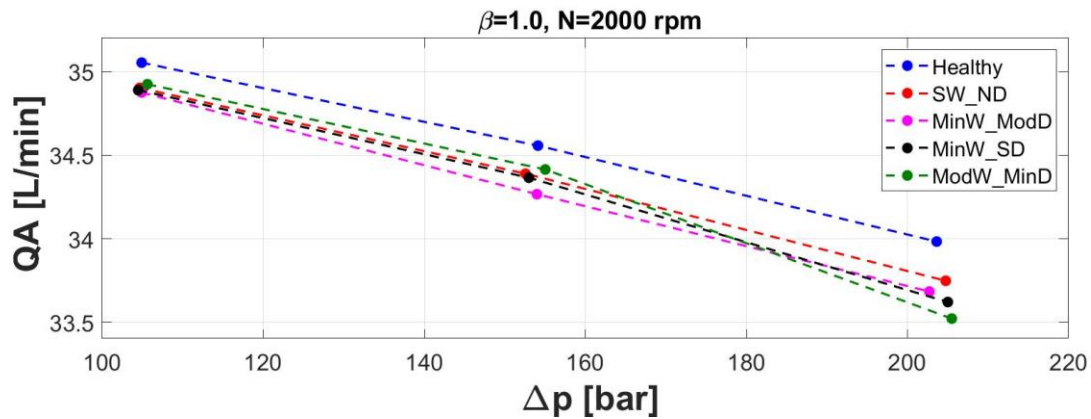


Figure 5.16: Outlet flow with respect to differential pressure at a fixed speed and displacement.

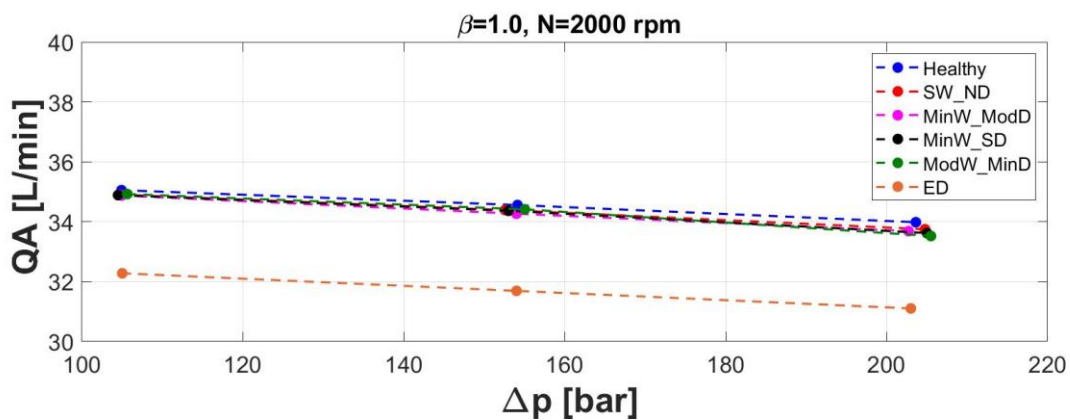


Figure 5.17: Outlet flow with respect to differential pressure at a fixed speed and displacement, including Extreme Damage.

Next, the measured volumetric efficiencies of the different pump conditions can be seen in Figure 5.18. The faulty valve plates lower volumetric efficiency, in these cases the volumetric efficiency is reduced by approximately 1%, from 96% to 95%. This slight decrease in efficiency may not be noticeable to the operator or detrimental to the functioning of the machine, but it does indicate wear is occurring. The level of volumetric efficiency at which a pump is rendered ineffective would need to be determined by pump and machine manufacturers.

Figure 5.19 compares the volumetric efficiencies of the healthy and each unhealthy valve plate, including the Extreme Damage (ED) case. The extreme damage valve plate significantly drops the pump volumetric performance by approximately 11%. The volumetric efficiency of the pump with the extreme damage valve plate is 84%. This difference is obvious to the naked eye and does not require a machine learning algorithm to determine if a fault is present in a stationary test-rig setting under steady-state operating conditions. However, it may be more difficult to detect faults on a mobile application. Therefore, the extreme damage case will be used on the mini excavator for condition monitoring purposes.

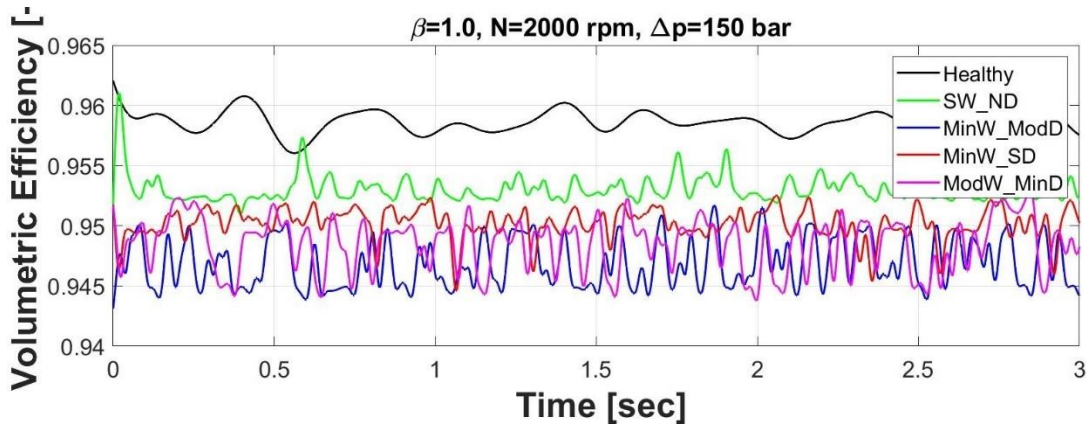


Figure 5.18: Volumetric efficiency comparison between healthy and unhealthy valve plates.

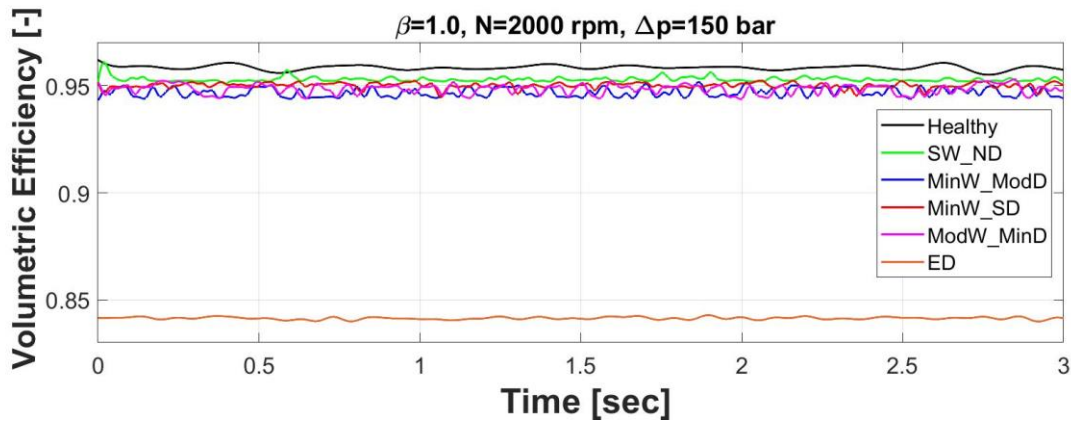


Figure 5.19: Volumetric efficiency comparison between healthy and unhealthy valve plates, including Extreme Damage.

5.3 Summary

The machine learning algorithms will see differences and make connections that the human brain cannot make. However, it is still beneficial to know that repeatability is achieved between measurements and that a clear difference between healthy and unhealthy pumps can be seen with the human eye.

This chapter has demonstrated the repeatability of the measurements in the drain pressure, drain flow, and outlet transient pressure measurements. It has been determined that measurement repeatability is agreeable, which means the healthy pump can be successfully compared to the pumps with the faulty valve plates. However, repeatability in oil temperatures was not achieved. This lack of repeatability is likely attributed to several factors, including human error. It is considerably difficult for oil temperatures to be the same.

Observable differences between the healthy and faulty pumps have been seen in the drain flow, outlet transient pressure, and volumetric efficiency. Also, a clear difference has been observed between the outlet flows of the different pump states, suggesting the healthy pump has less leakages. During the comparison observations, it was determined that temperatures would not be good candidates for a condition monitoring system for faulty valve plates because of the slow response time of the temperatures, and the inherent lack of repeatability. However, the goal has

been achieved to determine if a difference between the healthy and unhealthy pumps can be observed.

CHAPTER 6. FEATURE SELECTION/SENSOR REDUCTION

Dimensionality reduction, or feature selection in condition monitoring, is the process of reducing the number of features or dimensions of the data. This, in turn, can possibly reduce the number of sensors required for condition monitoring purposes.

This chapter focuses on the process of reducing the number of features, and in turn sensors, that are required for successful machine learning classification algorithms. First, an investigation on the accelerometer location is discussed to determine if redundant accelerometers are used. The chapter concludes with the backward elimination feature selection method utilizing a fine decision tree classifier and the justifications and reasoning behind which features are eliminated.(Bishop, 2006)

6.1 Feature Selection Background

The complexity of machine learning algorithms determines the number of input dimensions, or features, and the sample size, which determine computation costs and memory usage (Alpaydin, 2010). Dimensionality reduction not only reduces the computation costs and memory usage, but it also generate simpler models that are robust and more protected against overfitting (Webb, 2002; Alpaydin, 2010; Tang, Alelyani and Liu, 2014). Overfitting is when the model fits the data too closely and includes noise, which makes model generalization more difficult and less reliable (Kenton, 2019).

Dimensionality reduction can be summarized into two main categories: Feature extraction, and feature selection (Webb, 2002; Alpaydin, 2010; Tang, Alelyani and Liu, 2014). Feature extraction focuses on generating a new set of features by combining features from the original dataset. Common methods include: Principal Component Analysis (PCA) and Linear Discriminate Analysis (LDA). Detailed descriptions of PCA can be found from various sources, as it is a commonly understood dimensionality reduction method (Pearson, 1901; Belsley, 1991; Tipping and Bishop, 1999; Webb, 2002). The major disadvantage of the feature extraction methods is that it ignores the effects of the selected features on the performance of the algorithm (Kohavi and

John, 1997; Hall and Smith, 1999; Tang, Alelyani and Liu, 2014). This means feature extraction methods do not determine which original features are most influential based on the performance of the algorithm, which can lead to less predictive accuracy (Kohavi and John, 1997; Liu and Motoda, 2012; Tang, Alelyani and Liu, 2014).

Feature selection generates a new subset by selecting a certain number of features from the original dataset without combining features, unlike the feature extraction method. The goal is to select the relevant features and generate a small subset to reduce the complexity of the data. Irrelevant or redundant features add little to no benefit to the performance of the machine learning algorithm (Dash and Liu, 1997). Eliminating irrelevant or redundant features can mean a reduction in sensors required in the experimental measurements. However, feature selection can be computationally expensive since it requires several algorithm iterations to determine the “best” features. The two methods of feature selection are forward selection and backward elimination.

Forward selection begins with the machine learning algorithm starting with no features and adding features as the subset grows in complexity. During each step of feature addition, the performance of the algorithm is evaluated to see if the prediction accuracy of the machine learning algorithm has increased, decreased, or remained the same. If the prediction accuracy decreases or even remains the same, then the feature can be considered irrelevant.

Backward elimination is like the forward selection method but starts with the maximum number of features and eliminates one feature at a time until a simplified subset is generated that results in high accuracy and algorithm performance.

The backward elimination method is selected for the work presented in this dissertation because of its robustness against overfitting, ease of use, and wide acceptability (Tang, Alelyani and Liu, 2014). Many other feature selection methods exist that vary in complexity and reliability (Dash and Liu, 1997; Kwak and Choi, 2002; Webb, 2002; Alpaydin, 2010).

6.2 Accelerometer Location Comparison

Previous work has shown that only the amplitudes of the accelerations differ from one accelerometer location to another without a difference in the frequencies of the signals (Ramden, Weddfelt and Palmberg, 1993; Ramden, 1998). To compare the different accelerometers, the authors observed the spectrum and backstrum of the signals. The magnitude spectrum of the signal is found using the well-known fast Fourier transform or FFT. If the accelerometer location only affects the magnitude and not the frequency content of the signals, then it is possible to only have a single accelerometer for condition monitoring purposes. More details of the method used can be found in Chapter CHAPTER 2.

The first accelerometers that are compared are mounted on the pump case at the drain port, roller bearings, end case, or the swashplate pivot. For a reminder of the accelerometer locations see Figure 4.3. Figure 6.1 shows the different accelerometer signals in the frequency domain. The different accelerometers share the same frequency content but experience different acceleration magnitudes. The roller bearings dominate most of the frequencies among these sensor locations. A zoomed look in Figure 6.1(c) gives a better picture of how the frequency content of the signals remains the same despite the sensor location, but the magnitudes differ.

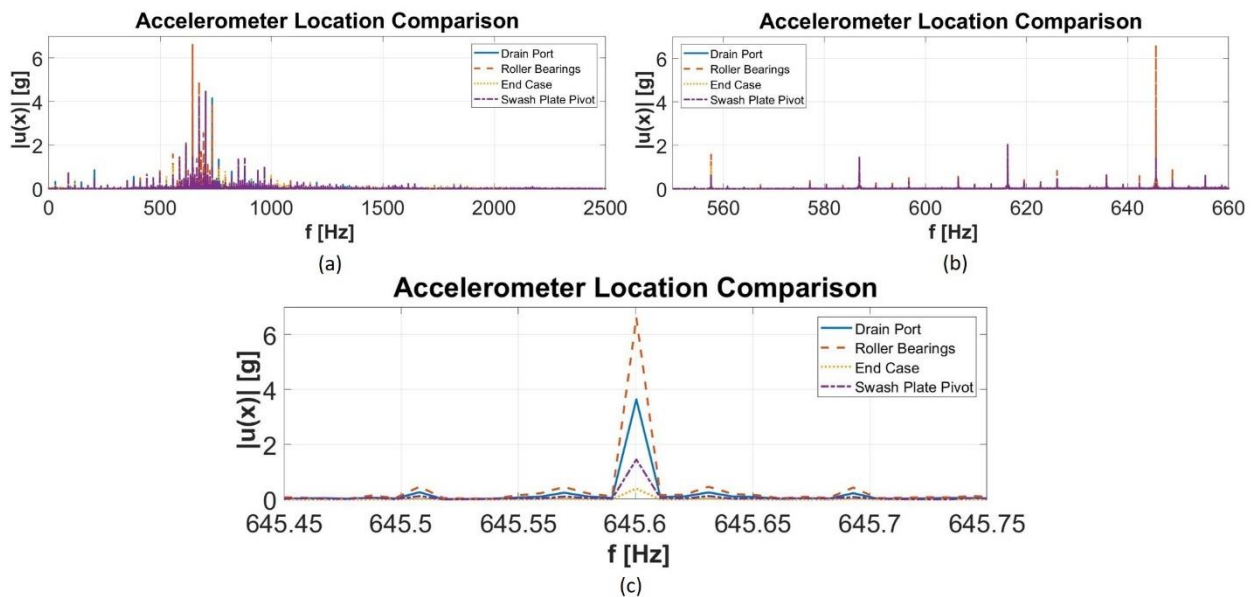


Figure 6.1: Accelerometer FFT location comparison of drain port, roller bearings, end case, and swashplate pivot.

The backstrum of the drain port, roller bearing, end case, and swashplate positions shows similar trends as in the frequency domain. It is clearly seen in Figure 6.2(b) and Figure 6.2(c) where the signals experience only a difference in magnitudes.

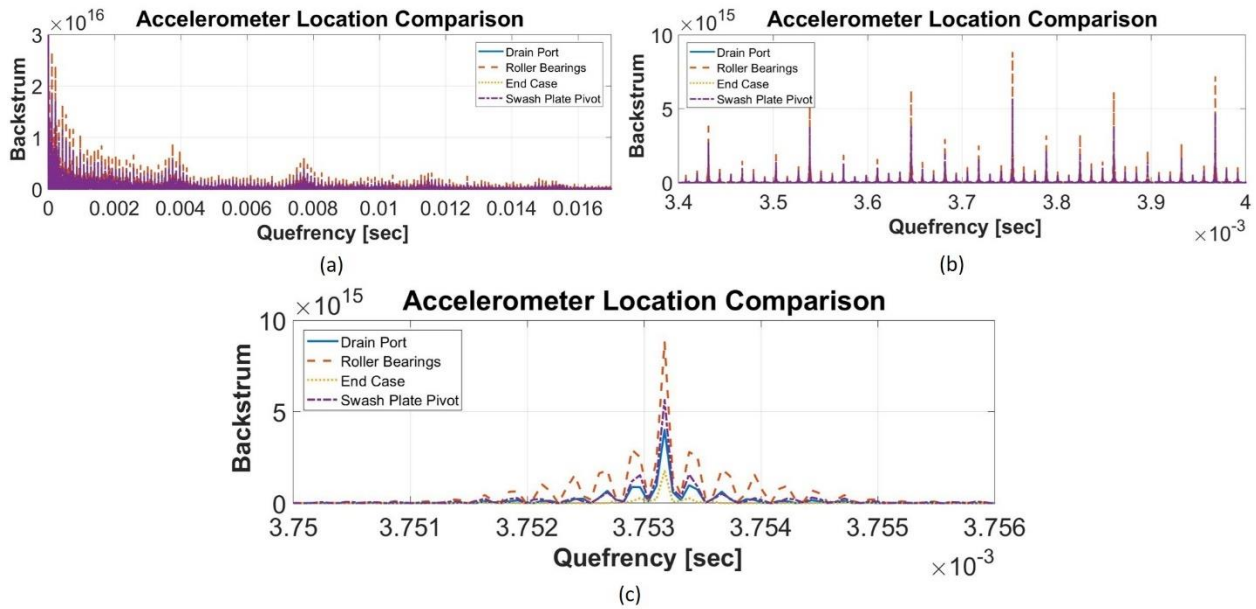


Figure 6.2: Accelerometer backstrum location comparison of drain port, roller bearings, end case, and swashplate pivot.

The roller bearings experienced the highest accelerations when comparing to the drain port, end case, and the swashplate pivot. Therefore, the roller bearing signal is kept as a reference for the remaining accelerometer locations. Figure 6.3 and Figure 6.4 show much of the same story but compare the roller bearings with the inlet port, outlet port, and the end case (near shaft) accelerometer locations. The roller bearings continue to dominate the majority of frequencies, especially around 600 Hz. However, the higher frequencies are dominated by the accelerations at the inlet and outlet ports. Although, it is interesting that the roller bearing always have higher magnitudes in the backstrum than the other locations, see Figure 6.4.

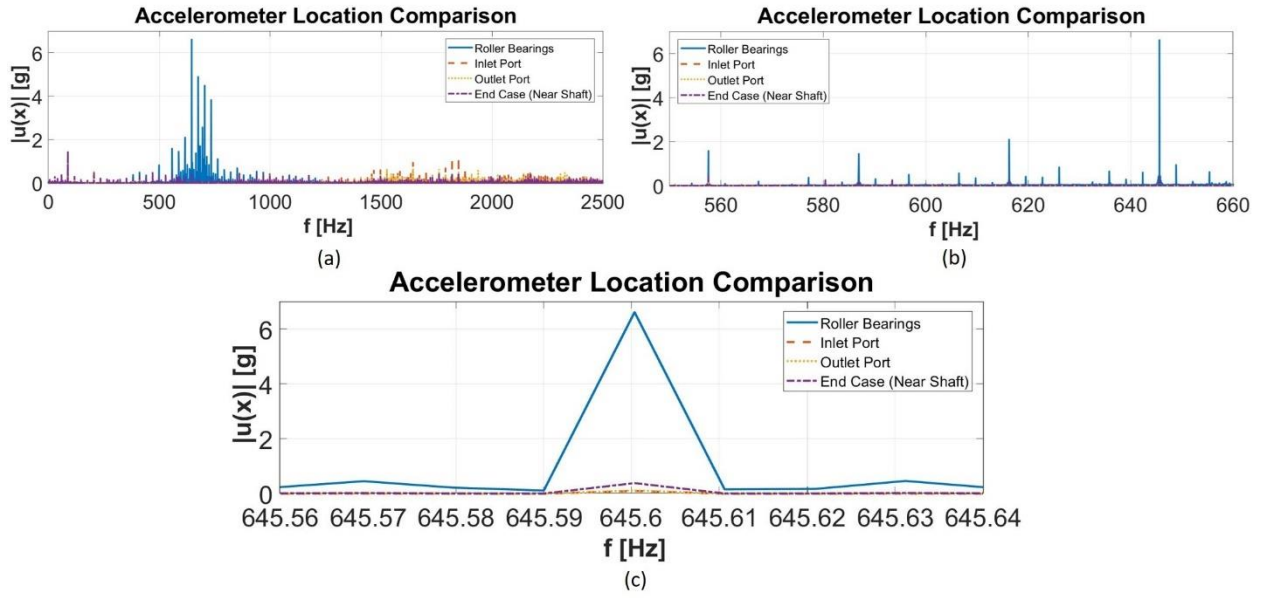


Figure 6.3: Accelerometer FFT location comparison of roller bearings, inlet port, outlet port, and the end case near the shaft.

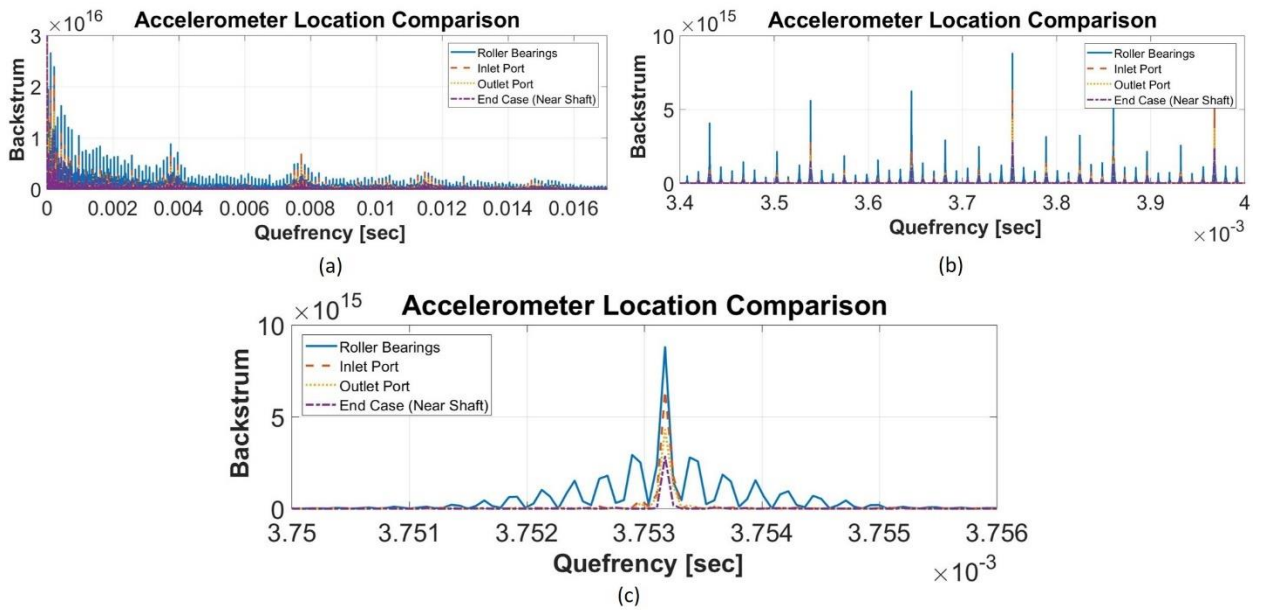


Figure 6.4: Accelerometer backstrum location comparison of roller bearings, inlet port, outlet port, and the end case near the shaft.

The final accelerometer location comparisons to make are those between the roller bearings, nameplate, and the control port. Among all the locations, the roller bearing, nameplate, and control

port have greater magnitudes and experience larger vibrations than the other locations, see Figure 6.5. The control port dominates at frequencies near 500 Hz. The roller bearings continue to dominate in accelerations near 600 Hz, and the control port dominates at frequencies between about 700 to 1000 Hz. However, it is clear that only the magnitudes of the signal change, Figure 6.5(b) and Figure 6.5(c). This is also confirmed in the backstrum signal, Figure 6.6.

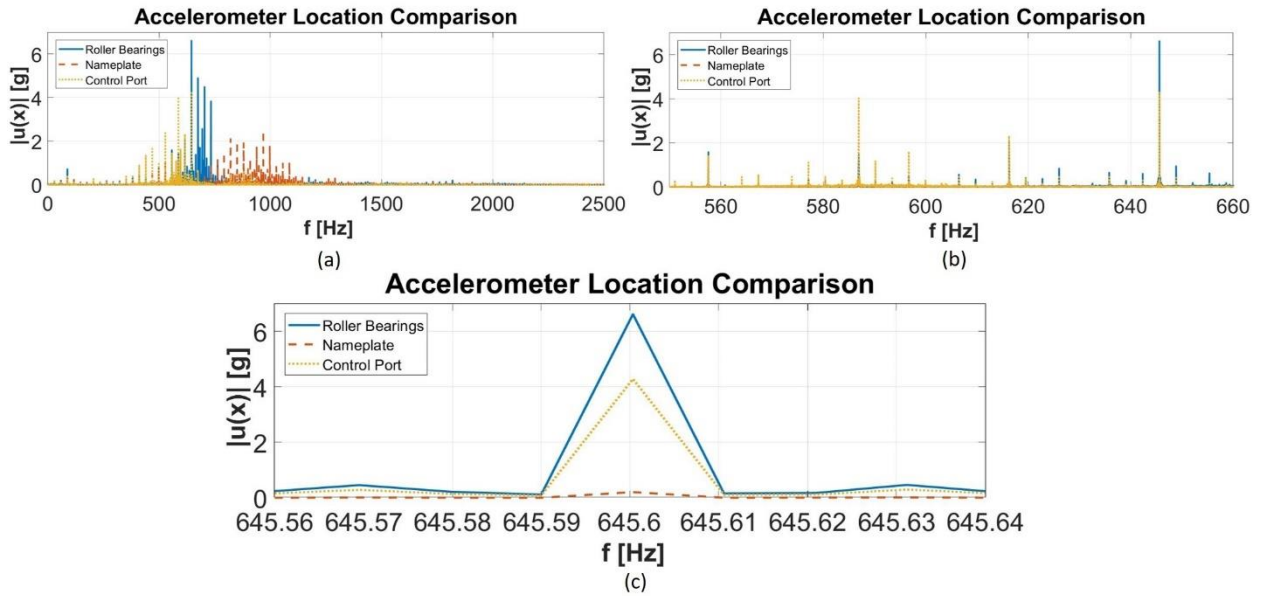


Figure 6.5: Accelerometer FFT location comparison of roller bearings, nameplate, and control port.

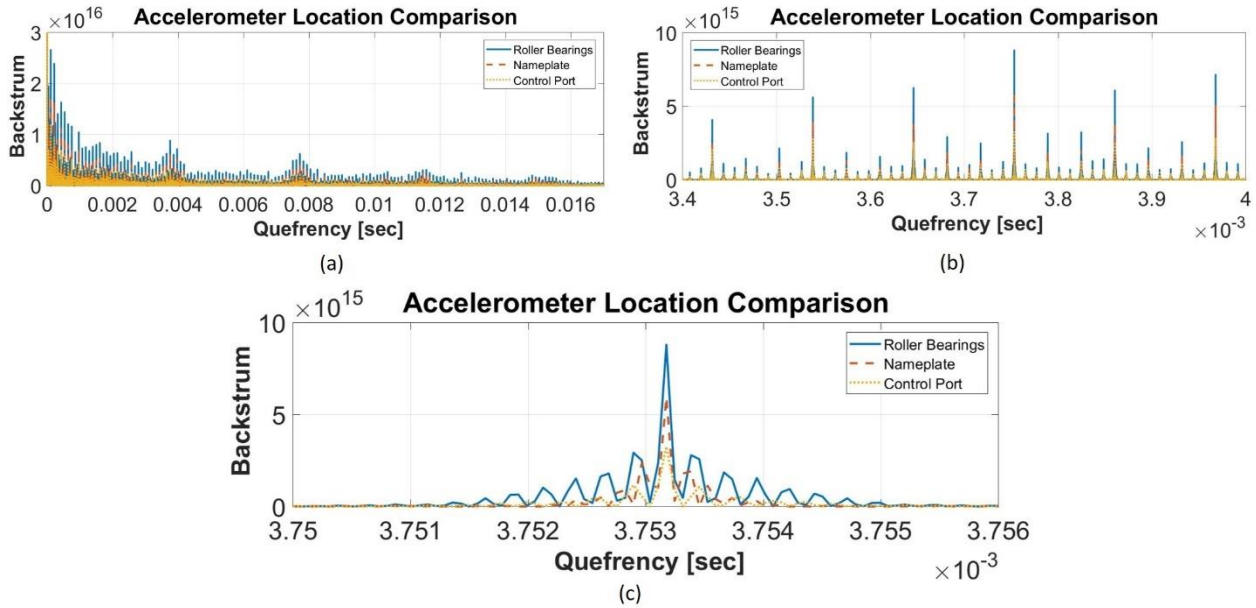


Figure 6.6: Accelerometer backstrum location comparison of roller bearings, nameplate, and control port.

6.3 Backward Feature Elimination Method Using a Fine Decision Tree

The backward elimination feature process that was discussed previously is used in conjunction with a fine decision tree classification algorithm included in the Statistics and Machine Learning Toolbox in MATLAB to reduce the dimensionality of the dataset (MathWorks, 2019e). More details about the classification algorithms will be discussed in a coming chapter, but the concept is to demonstrate how the feature selection process is implemented. It can be difficult to decide which feature to eliminate throughout the backward elimination process, but three main metrics are used to assist in the decision. A metric that is not discussed in detail is if the feature is viable under dynamic conditions. For example, the frequency spectrum or backstrum of the accelerometer signals are not valid over the course of a dynamic cycle. The first metric is performing a correlation study between the features. Next, the cost of the sensor is considered. Finally, observing the affects the feature has on the performance of the machine learning algorithm.

6.3.1 Correlation Study

A correlation study is the investigation of determining how closely related variables are to one another, and is a common practice in statistics (Kutner *et al.*, 2005; Navidi, 2008). Plotting two

variables against one another is a method to visualize the correlation between the two variables. Adding, a trendline to the plot and calculating the correlation coefficient, R , gives a better understanding of how closely the two variables are linearly correlated. An R value at zero indicates no linear correlation, but as R approaches -1 or 1 the linear correlation becomes stronger. A -1 or 1 indicates a perfect linear correlation. The sign on the correlation coefficient only indicates the slope of the trendline. Typically, variables with a correlation coefficient greater than 0.5 are considered to have a moderate linear correlation, but variables with a coefficient greater than 0.7 have a strong linear correlation.

It is useful to show the redundancy of implementing certain features in a condition monitoring algorithm. For instance, pump hydro-mechanical and volumetric efficiencies exhibit a strong linear correlation to torque and pump outlet flow, respectively. This is obvious as the hydro-mechanical, volumetric, and total efficiencies are calculated as shown below in Equations (6.1), (6.2, and (6.3.

$$\eta_{hm} = \frac{M_{th}}{M_e} \quad (6.1)$$

$$\eta_v = \frac{Q_e}{Q_{th}} \quad (6.2)$$

$$\eta_{tot} = \eta_{hm} * \eta_v \quad (6.3)$$

Other examples of redundancy of features are the differential pressure across the pump, Δp . The differential pressure and pump outlet pressure have a near perfect linear correlation with a coefficient of 0.998, see Figure 6.7. The lesson here is that machine learning algorithms do not necessarily require features that have been calculated from other features. This adds unnecessary complexity to the algorithm. Δp calculations are shown below in Equation (6.4.

$$\Delta p = p_{outlet} - p_{inlet} \quad (6.4)$$

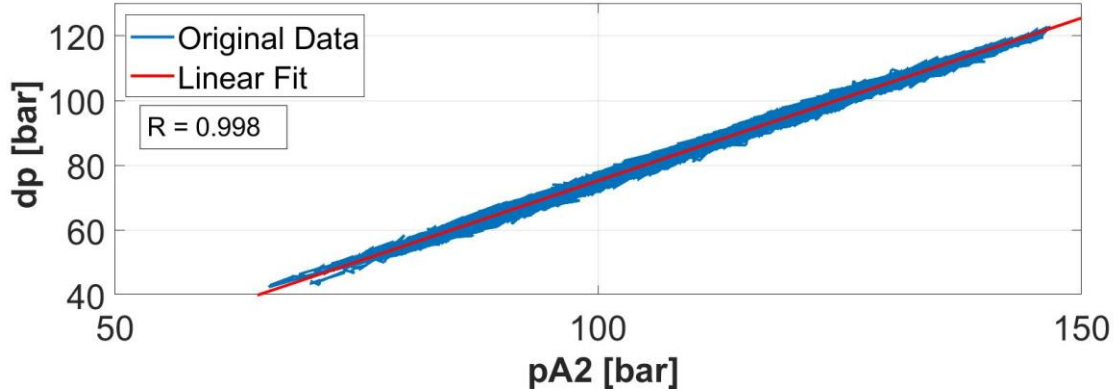


Figure 6.7: Correlation between differential pressure and outlet pressure.

Among the many features that are a result of the many sensors on the stationary test-rig that has been developed for this work, only two features are linearly correlated to one another. Those features are the pump displacement, β , and the pump outlet flow, Q_A . The correlation coefficient between these two features is 0.88. This correlation is logical since the pump outlet flow is determined by the pump displacement, as shown below in Equation (6.5).

$$Q_A = \beta * n * V \quad (6.5)$$

6.3.2 Cost of Sensor

Another metric to consider in feature selection is the cost of the sensors. The reason the cost of the sensors is taken into consideration is because the intent is for manufacturers to implement condition monitoring on mobile equipment. Adding expensive sensors ultimately adds to the cost of the machine. Table 6.1 contains the approximate cost for the sensors that are equipped on the stationary test-rig that has been discussed in Chapter CHAPTER 4 of this document. It would be best if the torque meter with the integrated speed sensor, piezoelectric pressure transducer, and flow meters can be eliminate. Eliminating these sensors would greatly reduce the cost of implementation on a mobile machine.

Sensor robustness and geometric footprint are additional considerations to make. Torque sensors and accurate gear type flow meters have a decent size geometric footprint. This is important to consider since space on mobile equipment is constrained. These two sensors are also not known for robustness, meaning they are sensitive to operating outside of the conditions they are designed for. Conditions on mobile equipment can be extreme and unpredictable.

Table 6.1: Approximate cost of sensors.

Sensor	Approx. Cost [\$]	Notes
Accelerometers	100	per axis (\$300 for triaxial)
Torque/Speed Sensor	> 5000	-
Piezoelectric Pressure Transducer	2500	-
Thermocouple	30	-
Flow Meter	> 2000	-
Piezoresistive Pressure Transducer	200	-

6.3.3 Increase Performance of Supervised Learning Algorithm

The final metric used to determine which features to eliminate is how the feature in question affects the performance of the machine learning algorithm. The performance of the algorithm/model can be evaluated by observing the model training time, prediction speed, and the model accuracy.

The model training time is the total time required to fully train the model with the specified machine learning algorithm. Longer training time results in greater computational requirements. Prediction speed is how many observations, or rows in the previously discussed data structure in Figure 4.11, the model can classify or predict in one second. The final performance metric observed is the overall classification model accuracy. The higher the accuracy then the lower the misclassified datapoints. A low accuracy indicates a high number of misclassifications.

6.3.4 Backward Elimination Results

To perform a feature selection using the backward elimination method, the Classification Learner App in MATLAB is used to input the data into a supervised learning Fine Decision Tree

classification algorithm (MathWorks, 2019a). The description of the different machine learning algorithms used in this work will be discussed in the next chapter. However, it is important to keep in mind that the same algorithm is used for each iteration of the feature selection process. Only the detailed results from the first operating condition (OpCon_1) will be shown, but a summary of the results for the other operating conditions will be given.

Table 6.2 contains the results from the backward elimination feature selection for OpCon_1, see Table 4.2 for reminder. Table 6.2 includes the number of features included in the model, the model training time, accuracy, features that were removed with the corresponding reasons for removing that feature, and a list of the selected features.

The feature selection began with training a model with 17 features, see Table 6.3 for descriptions of the feature abbreviations that are listed in Table 6.2. Temperatures have been eliminated due to the inconsistencies in repeatability, lack of dynamic response, and stratification inherent in temperature measurements. Other features not included are any efficiency calculations, due to correlation with measured parameters. Only two accelerometers are used for this study since it was determined only one or two accelerometers would be needed for condition monitoring purposes.

The model trained with 17 of 17 features have a training time of 101.73 seconds, a prediction speed of 1.7 million observations per second, and a 100% model prediction accuracy. This serves as the benchmark for the rest of the feature selection process.

The next features that are eliminated are sensors with high cost, such as flow meters, torque meters, and piezoelectric pressure transducers. Eliminating drain flow (QD), control flow (QC), outlet flow (QA), shaft torque (M), and the outlet transient pressure (pA1) slightly reduced the accuracy from 100% to 99.7%. This slight decrease in accuracy is almost negligible, but the training time dropped to 27.623 seconds while the prediction speed increased to 2.1 million observations per second. Eliminating these sensors would greatly reduce the cost of the condition monitoring system without sacrificing accuracy and performance.

Table 6.2: Results of the backward elimination feature selection method for OpCon_1.

Features	Training Time [sec]	Accuracy [%]	Prediction Speed [M obs/sec]	Features Removed	Selected Features	Reason for Removal
17/17	101.73	100	1.7	-	-	Temps not included (not feasible for dynamic cycles)
16/17	43.3777	100	1.8	QD	-	Sensor cost
15/17	31.03	99.9	2	QC	-	Sensor cost
14/17	29.532	99.9	2.2	QA	-	Sensor cost
13/17	28.212	99.7	2.1	M	-	Sensor cost
12/17	28.622	99.7	2.1	pA1	-	Sensor cost
11/17	27.623	99.7	2.1	FFT_pA1	-	Sensor cost
9/17	20.344	99.7	2.2	Back_684, Back_680	-	Not feasible for dynamic cycles
7/17	17.062	99.7	2.2	FFT_684, FFT_680	-	Not feasible for dynamic cycles
6/17	17.443	99.7	2.1	c_684	-	Possibly redundant sensor
5/17	15.156	99.6	2.2	N	pA2, pD, pS, Beta, c_680	-
4/17	12.366	99.6	2.2	c_680	pA2, pD, pS, Beta	-
3/17	12.144	99.5	2.3	pS	pA2, pD, Beta	-
2/17	16.327	91.7	2.2	-	pA2, pD	-
2/17	10.398	99.2	2.3	-	pD, Beta	-
2/17	11.111	95.9	2.3	-	pA2, Beta	-
1/17	10.417	93.7	2.1	-	Beta	-
1/17	13.058	79.3	2.2	-	pD	-
1/17	15.005	88.3	2.1	-	pA2	-
1/17	31.316	79.3	2.1	-	c_680	-
1/17	11.859	91.1	2.2	-	M	-
1/17	15.771	97.6	2	-	QD	-
1/17	21.712	79.5	2.1	-	QA	-
2/17	18.506	98.3	2.2	-	QD, pD	-
3/17	19.536	100	2.1	-	pD, QD, Beta	-
2/17	16.724	99.5	2	-	QD, Beta	-

Table 6.3: List of features with their corresponding abbreviations.

Abbreviation	Description
TA	Outlet temperature
TS	Supply or inlet temperature
TD	Drain temperature
TAMB	Ambient air temperature
pA2	Outlet pressure
pS	Supply or inlet pressure
pD	Drain pressure
QA	Outlet flow
QC	Control flow
QD	Drain flow
M	Shaft torque
N	Pump rotational speed
Beta	Pump displacement
Qs	Volumetric losses
dp	Differential pressure (pA2-pS)
eff_v	Volumetric efficiency
eff_hm	Hydro-mechanical efficiency
eff_tot	Total efficiency
c_684	Outlet port accelerations
c_680	Drain port accelerations
pA1	Outlet transient pressure
FFT_684	Spectrum of outlet accelerations
FFT_680	Spectrum of drain accelerations
FFT_pA1	Spectrum of transient pressures
Back_684	Backstrum of outlet accelerations
Back_680	Backstrum of drain accelerations

The backstrum and FFT signals of the accelerometers are eliminated because these signals are not feasible for dynamic cycles. Since the intent is to implement a condition monitoring system on a mobile device that primarily operates under dynamic conditions, it does not seem beneficial to include these signals. Eliminating these features did not affect the accuracy or prediction speed of the algorithm. The outlet port accelerometer (c_684) is also eliminated due to a sensor redundancy.

At this point, only six of the 17 features are being utilized. These features are the outlet port pressure (pA2), drain pressure (pD), inlet port pressure (pS), pump displacement (Beta), engine speed (N), and drain port accelerations (c_680). At this point it becomes a trial and error game to find the best combination of features to most accurately and quickly classify the data as healthy or unhealthy.

Table 6.2 shows several runs where only a single feature is selected to observe the contribution that feature gives to the accuracy of the algorithm. Several features that had previously been eliminated are run by themselves to see if the cost could possibly justify the use of the sensor. For example, observe the run that only contains the drain flow (QD). The drain flow is able to predict a faulty valve plate condition with an accuracy of 97.6%. This is exceptional accuracy for only a single sensor and logically makes sense that it can predict valve plate faults.

However, using two less expensive sensors can give better accuracy than the single flow meter, drain pressure (pD) and pump displacement (Beta). These two features can give an accuracy of 99.2% and a prediction speed of 2.3 million observations per second. These two sensors are also more robust than a flow meter and would likely be excellent candidates for a condition monitoring system mounted on a mobile machine.

It may seem like a machine learning algorithm is unnecessary when a single sensor or a few sensors can be used to detect the faulty condition of the valve plate, and a simpler method can be used. If a machine learning algorithm is not used, then a lookup table of data that includes the operating conditions of the pump and measured data of the parameter under observation must be constructed. It would likely take more computational expense to develop and use the lookup table than running

a simple machine learning algorithm to accomplish the same task. Therefore, a machine learning algorithm can still be the most efficient method for detecting faults on a machine.

Table 6.4 gives a summary of the feature combinations with the highest accuracies for each operating condition. Each of the steady-state operating conditions have similar results to one another and achieve accuracies of near 100%. However, the dynamic cycle accuracies are lower, which is to be expected. The accuracies of the dynamic cycle are in the upper 80%. It is still likely, however, that a different machine learning algorithm will give better results. This will be discussed in the next chapter, Algorithm Selection.

Table 6.4: Feature selection summary of each operating condition.

	Features/Sensors	Accuracy [%]
OpCon_1	pA2, pS, pD, Beta	99.6
	pA2, pD, Beta	99.5
	pD, QD, Beta	100
	pD, Beta	99.2
	QD, Beta	99.5
OpCon_2	pA2, pS, pD, Beta	99.2
	pA2, pD, Beta	98.8
	pD, Beta	98.8
	pD, QD, Beta	99.1
	QD, Beta	97
OpCon_3	pA2, pS, pD, Beta	98.6
	pA2, pD, Beta	98.2
	pD, Beta	97.9
	pD, QD, Beta	99.7
	pD, QD	97.7
	QD, Beta	99.4
Dynamic	pA2, pD, Beta, N	86.4
	pA2, pS, pD, Beta, N	88.5
	pA2, pD, N	84.3
	pA2, pS, pD, Beta	83.6
	pD, N	83.9

Considering the lengthy feature selection process for several operating conditions, the sensors that would be good to include on a mobile machine study would be the outlet, inlet and drain pressures. Additionally, pump displacement and engine speed would be beneficial.

A brief summary of the results of a feature selection that includes temperatures will be noted at this time to illustrate caution when developing a condition monitoring system. If temperatures are included in the feature selection, then it becomes possible to achieve a 100% accuracy using only a single temperature signal, such as drain temperature. However, using any single temperature signal gives the same results.

In Chapter CHAPTER 5, a concern was raised that the lack of temperature repeatability, inability for temperatures to react to transients, and the stratification of the data could potentially trick the machine learning system into producing false high accuracies. This has been made apparent when only a single thermocouple can detect valve plate faults with perfect accuracy when a drain flow meter is not capable of reaching the same level of accuracy. If any single signal can achieve near perfect accuracy, caution and further investigation must be utilized if that signal is to be used.

6.4 Summary

In summary, it was verified that accelerometer location does not change the frequency content but only the magnitudes of the spectrum and backstrum vary. Therefore, it is possible to include only a single accelerometer on the pump for condition monitoring purposes. Different feature selection methods were introduced, and the backward elimination method was selected and applied to reduce the dimensionality or sensors of the machine learning algorithm. It was determined that inlet pressure, outlet pressure, drain pressure, pump displacement, and pump speed would be excellent candidates to further an investigation on implementing a condition monitoring system on a mobile machine. Additionally, caution was given to using temperature signals or signals that can achieve near perfect prediction accuracy,

CHAPTER 7. ALGORITHM SELECTION

A condition monitoring system requires the best combination of sensors and machine learning algorithm to provide an accurate determination of the condition of the pump. The number of sensors required to accurately classify a healthy and unhealthy pump has been narrowed down to a few different combinations of sensors. With this reduced number of sensor combinations the algorithm selection process will require fewer iterations to find a suitable algorithm and sensor combination. This section discusses what software is used to perform the algorithm selection, as well as a brief background on a K-Nearest Neighbor and decision tree algorithms. Additionally, a supervised pattern recognition neural network and an unsupervised clustering neural network are introduced. Finally, the algorithm selection results from the steady-state and dynamic duty cycles will be presented.

Only a few classification algorithms will be discussed in this work because the presented algorithms showed the best results. The algorithms have been implemented using MATLAB's machine learning toolboxes and have not been developed by the author of this work.

7.1 K-Nearest Neighbor (KNN), Supervised Learning

K-Nearest Neighbor (KNN) is a non-parametric and one of the best-known classification and regression machine learning algorithms (Altman, 1992; Jain, 2010). The basic principle of KNN is that it assigns an unclassified data point to the classification of the nearest set of previously classified points. In other words, the unclassified data point takes on the classification of its “nearest neighbor.”

Figure 7.1 shows a binary classification scheme, a classification of blue circles and red “X.” The unclassified point is shown as a green triangle. This example compares the unclassified data point to the nearest of three classified points, corresponding to $k = 3$. The unclassified data point is closest to one blue circle and two red “X” and would then be classified as an “X” because majority rules.

Many techniques can be employed when developing KNN algorithms. However, a few considerations should be noted to achieve optimum performance when choosing the value of nearest neighbors, k . For a binary or two class problem, k should be an odd number to avoid ties that could arise in the algorithm (Duda, Hart and Stork, 2000). Additionally, k should not be a multiple of the number of classes to avoid ties. One of the most common techniques in determining the nearest neighbors is using the Euclidean distance method. This and other techniques are explained in more detail in other works (Grimson, Gutttag and Bell, 2016).

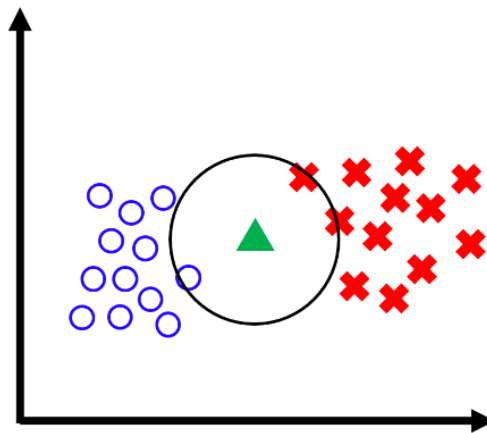


Figure 7.1: K-Nearest Neighbor (KNN) example (Keller *et al.*, 2019).

MATLAB's classification learner contains several different KNN classification algorithms and many have been used in the investigation of which machine learning algorithm is best to use for this work. Five different KNN algorithms have been investigated: Fine, medium, coarse, and weighted. These will be briefly discussed in the following subsections. Each of the algorithms involved a validation of 25% of the dataset, while the remaining 75% of the data is used for training the classification model. The results from the KNN algorithms are discussed in the results summary section of this chapter.

7.2 Decision Tree, Supervised Learning

Decision trees are another type of classification algorithm that can be used for nonlinear mapping from input variable to a set of output variables. A decision tree is a decision making method that provides each of the possible choices a probability according to a decision system (Magerman, 1995). Decision trees break up the complex decision-making process into several simpler and

smaller decisions. Trees are easy to interpret and can provided needed insight into the data (Webb, 2002).

The decision process starts at the root and continues through nodes and branches until the leaf node is reached, see Figure 7.2. The root is at the top of the tree, while the lead nodes are the bottom portions of the tree that do not continue to split. Leaf nodes represent the output (Alpaydin, 2010). A large tree is first constructed and then pruned to minimize the complexity and cost of the algorithm (Webb, 2002). Several stopping rules and pruning methods have been proposed in literature. In 1984, Breiman et al. proposed a method to successively grow and selectively prune the tree, using cross-validation to choose the subtree with the lowest estimate misclassification rate (Breiman *et al.*, 1984). More detailed explanations of decision trees can be found in literature (Webb, 2002; Alpaydin, 2010).

MATLAB contains three different decision tree algorithms in the Classification Learner toolbox: Fine, medium, and coarse decision trees. Decision trees in MATLAB’s classification learner are categorized by the maximum number of splits, or branches, the algorithm can contain. These three decision tree algorithms are used to investigate the “best” classification algorithm for the work that has been presented in this presentation. The results from the decision tree algorithms are discussed in the results summary section of this chapter.

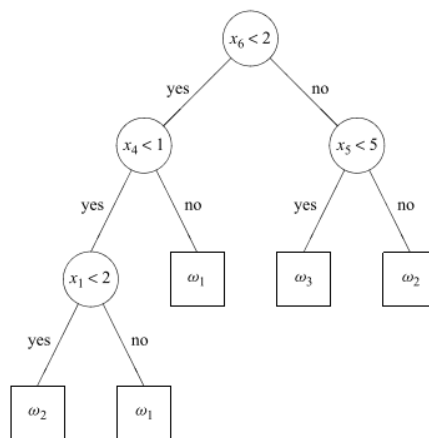


Figure 7.2: Simple or coarse decision tree (Webb, 2002).

7.3 Pattern Recognition Neural Network, Supervised Learning

MATLAB's pattern recognition neural network is considered a shallow neural network, meaning it only contains one hidden layer. This algorithm in MATLAB takes the input vectors, drain and ambient air temperature, and feeds them into a hidden layer of the neural network. The hidden layer contains 10 nodes. The outputs of the hidden layer then sent to a single output layer that has an s-shape sigmoid function to limit the output to the maximum and minimum values of the target data. The output is a single vector with each element being either a zero or one, healthy or unhealthy.

However, the pattern recognition neural network implemented in MATLAB contains an output layer that is also known as the Softmax layer. This layer adds insurance that each output from the hidden layer is between zero and one, and the components will add up to one. This is a redundant feature when doing a binary classification. However, when multi-class classification is used then the Softmax layer makes the output components normalized and must sum to one. The algorithm would not converge on a solution using the pattern recognition neural network. Therefore, this algorithm is eliminated from this investigation.

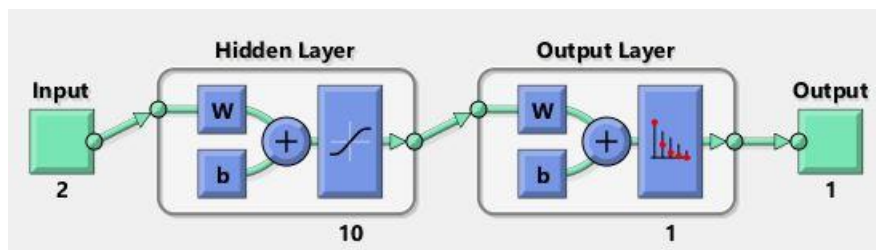


Figure 7.3: Neural pattern recognition network structure.

7.4 Clustering Neural Network, Unsupervised Learning

Clustering is supposed to group data by similarity based on how the neural network interprets the data without knowing the target outputs. Therefore, clustering is considered unsupervised learning. MATLAB's clustering neural network application uses a Self-Organizing MAP (SOM) as the clustering algorithm but arranged the neurons of the neural net into a 2D topology. This allows for a 2D approximation of the dataset, which is easier to interpret.

Figure 7.4 shows the neural network structure with drain temperature and ambient air temperature as inputs from OpCon_2 (Table 4.2). Previously, it was cautioned and advised not to use the temperatures as inputs to the machine learning system. However, the temperatures are used in this case to show that the clustering neural network is not suitable for this investigation. This neural network contains 4 neurons arranged in a 2 by 2 topographical structure. Therefore, four output vectors exist.

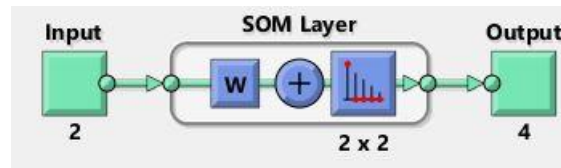


Figure 7.4: Clustering neural network structure

The clustering neural network has a training time of 166 seconds, and it is clear that the neural network believes two clusters exist because of the hits plotted on the SOM topology graph, Figure 7.5. The network believes 2,135,551 datapoints or samples belong to one group of data while 1,542,653 samples belong to another. However, the network finding two clusters does not mean it is accurate.

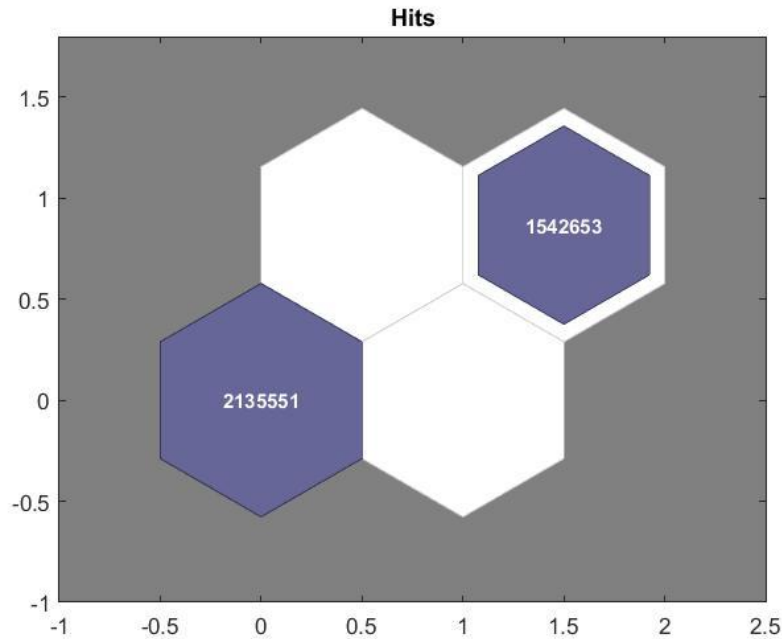


Figure 7.5: Sample hits from clustering algorithm.

The next step in determining the accuracy of the SOM is to observe the confusion matrix.

Table 7.1 is a generalized confusion matrix of the two categories of interest, healthy and unhealthy. The columns correspond to the algorithm’s clustering of the datapoints into healthy or unhealthy groups. The rows represent the true label for the data points, whether they are truly healthy or unhealthy.

A 4x4 confusion matrix consists of four categories: True Positive (TP), False Positive (FP), False Negative (FN), and True Negative (TN). True positive is when the algorithm predicts the datapoint, or sample, is from a healthy pump when the datapoint truly does belong to the healthy category. TN is when the algorithm predicts the datapoint to be from a faulty, or unhealthy, pump, and the datapoint truly belongs to the unhealthy category. FP is when the algorithm predicts the sample belongs to the healthy group but is a datapoint from an unhealthy pump condition. A false positive is known as a “Type I” error. FN is when the algorithm predicts the sample belongs to the unhealthy group, but really belongs to the healthy pump. A false negative is known as a “Type II” error.

Table 7.1: General confusion matrix.

		Predicted	
		Healthy	Unhealthy
Actual	Healthy	TP	FN
	Unhealthy	FP	TN

Table 7.2(a) is the confusion matrix that contains the number of samples or datapoints from the neural network clustering algorithm. The Healthy column sums to 2,135,551, which is the number of samples in the cluster on the bottom right of the topology graph in Figure 7.5. This column shows that only 54.4% of the 2,135,551 data points that have been predicted as healthy are correctly labeled by the SOM, see Table 7.2(b). The Unhealthy column sums to 1,542,653, but only 569,853, or 36.9%, of those datapoints are correctly labeled as unhealthy, see Table 7.2(b). The sum of all the values in Table 7.2(a) equal the total number of samples used as inputs to the neural network. In this case it is 3,678,204, which corresponds to an extremely large dataset.

Table 7.2: Clustering network confusion matrices.

		Predicted	
		Healthy	Unhealthy
Actual	Healthy	1162751	972800
	Unhealthy	972800	569853

(a)

		Predicted	
		Healthy	Unhealthy
Actual	Healthy	54.4%	63.1%
	Unhealthy	45.6%	36.9%

(b)

The information contained in the confusion matrix in Table 7.2(a) allows for the calculation of the overall accuracy of the clustering neural network. The accuracy is calculated by dividing the sum of TP and TN by the total number of samples in the dataset. This results in an algorithm accuracy of 47.1%. It is to be expected that an unsupervised learning algorithm is to have less accuracy than a supervised learning algorithm because it does not know what the correct outputs, or labels, to the data are during the training process. The calculation of accuracy and error rate are shown in Equations (7.1 and (7.2.

$$Accuracy = \frac{TP + TN}{Total} = \frac{1,162,751 + 569,853}{3,678,204} = 47.1\% \quad (7.1)$$

$$Error Rate = 1 - Accuracy = 1 - 0.471 = 52.9\% \quad (7.2)$$

Even using the temperature data that should be able to detect a faulty valve plate with 100% accuracy the unsupervised clustering network is incapable of achieving accuracies acceptable for a condition monitoring system. Therefore, the unsupervised clustering network is eliminated from this investigation and deemed unsuitable for this work.

7.5 Results Summary

In summary, several classification algorithms have been considered, and a brief investigation to an unsupervised clustering algorithm has been conducted which has proven unsuitable for this work. The types of algorithms that are best suited for this work are decision trees and KNN algorithms.

Table 7.3 shows a summary of the algorithm performances for the steady-state operating condition OpCon_2, and

Table 7.4 shows the algorithm selection results for the dynamic cycle. Each of the three steady-state conditions have similar algorithm selection results, so only the results from OpCon_1 will be shown and discussed.

Both

Table 7.3 and

Table 7.4 are composed of four separate tables that contain the algorithm selection results for four of the best performing feature combinations. These feature combinations are as follows: (a) pA2, pS, pD, and Beta; (b) pD, QD, and Beta; (c) pA2, pD, and N; and (d) pA2, pS, pD, N, and Beta.

Observing each of the conditions in

Table 7.3, it can be seen that the decision trees give slightly lower accuracies than those of the KNN algorithm class. However, the decision trees have significantly higher prediction speeds. For the steady-state conditions, the KNN algorithms would be recommended for use in a condition monitoring system, particularly the Fine KNN algorithm.

Table 7.3: Summary of results from classification algorithm comparison under the steady-state operating condition OpCon_2.

pA2, pS, pD, Beta, 25% Hold-Out Validation					pD, QD, Beta, 25% Hold-Out Validation				
Alorithm	Training Time [sec]	Accuracy [%]	Prediction Speed [obs/sec]	Algorithm Setting	Alorithm	Training Time [sec]	Accuracy [%]	Prediction Speed [obs/sec]	Algorithm Setting
Fine KNN	23.535	99.9	650 000	1 Neighbor	Fine KNN	20.494	99.4	800 000	1 Neighbor
Medium KNN	28.255	99.6	200 000	10 Neighbors	Medium KNN	25.186	99.4	270 000	10 Neighbors
Coarse KNN	56.381	99.3	48 000	100 Neighbors	Coarse KNN	44.701	99.3	68 000	100 Neighbors
Weighted KNN	28.483	99.8	190 000	10 Neighbors	Weighted KNN	24.404	99.5	260 000	10 Neighbors
Cubic KNN	60.126	99.6	45 000	10 Neighbors	Cubic KNN	37.398	99.4	99 000	10 Neighbors
Fine Tree	14.289	99.2	2 000 000	Max. 100 Splits	Fine Tree	12.714	99.1	2 200 000	Max. 100 Splits
Medium Tree	13.797	99	2 000 000	Max. 20 Splits	Medium Tree	11.483	98.9	2 200 000	Max. 20 Splits
Coarse Tree	13.042	98.4	2 000 000	Max. 4 Splits	Coarse Tree	10.602	98.2	2 300 000	Max. 4 Splits

(a) (b)

pA2, pD, N, Beta, 25% Hold-Out Validation					pA2, pS, pD, N, Beta, 25% Hold-Out Validation				
Alorithm	Training Time [sec]	Accuracy [%]	Prediction Speed [obs/sec]	Algorithm Setting	Alorithm	Training Time [sec]	Accuracy [%]	Prediction Speed [obs/sec]	Algorithm Setting
Fine KNN	20.148	99.9	780 000	1 Neighbor	Fine KNN	22.276	100	700 000	1 Neighbor
Medium KNN	25.651	99.8	240 000	10 Neighbors	Medium KNN	31.895	99.9	160 000	10 Neighbors
Coarse KNN	49.047	99.2	60 000	100 Neighbors	Coarse KNN	71.336	99.5	36 000	100 Neighbors
Weighted KNN	25.44	99.9	250 000	10 Neighbors	Weighted KNN	32.454	100	160 000	10 Neighbors
Cubic KNN	49.985	99.7	57 000	10 Neighbors	Cubic KNN	85.456	99.9	280 000	10 Neighbors
Fine Tree	13.835	98.9	2 100 000	Max. 100 Splits	Fine Tree	14.67	99.2	2 000 000	Max. 100 Splits
Medium Tree	12.529	98.6	2 300 000	Max. 20 Splits	Medium Tree	9.5372	99	2 100 000	Max. 20 Splits
Coarse Tree	11.611	98.2	2 100 000	Max. 4 Splits	Coarse Tree	7.6676	98.4	2 200 000	Max. 4 Splits

(c) (d)

The difference between decision trees and KNN algorithms is significantly more drastic when looking at the results from the dynamic cycle in

Table 7.4. The accuracy of the decision trees is at best 86.4%, when the KNN algorithms are capable of near 100% accuracies. Therefore, the KNN algorithms will likely be best suited for mobile applications.

Each of the four feature combinations perform similarly to one another when utilizing the same algorithm. This suggests that each of the four feature combinations are good candidates to use on a mobile machine investigation. However, based on the stationary measurements, the best feature and algorithm combination would be the Fine KNN algorithm utilizing data from the outlet pressure drain pressure pump speed, and pump displacement. This combination is the most robust and cost effective of the four different feature selection combinations.

Table 7.4: Summary of results from classification algorithm comparisons under the dynamic operating condition.

pA2, pS, pD, Beta, 25% Hold-Out Validation					pD, QD, Beta, 25% Hold-Out Validation				
Alorithm	Training Time [sec]	Accuracy [%]	Prediction Speed [obs/sec]	Algorithm Setting	Alorithm	Training Time [sec]	Accuracy [%]	Prediction Speed [obs/sec]	Algorithm Setting
Fine KNN	3.7291	99.6	1 000 000	1 Neighbor	Fine KNN	2.9196	100	1 600 000	1 Neighbor
Medium KNN	4.4552	98.6	270 000	10 Neighbors	Medium KNN	3.847	99.8	350 000	10 Neighbors
Coarse KNN	7.8557	94.7	67 000	100 Neighbors	Coarse KNN	6.5374	97.9	87 000	100 Neighbors
Weighted KNN	4.4223	99.3	270 000	10 Neighbors	Weighted KNN	3.5006	99.9	370 000	10 Neighbors
Cubic KNN	7.3638	98.3	76 000	10 Neighbors	Cubic KNN	4.3402	99.7	190 000	10 Neighbors
Fine Tree	3.9951	83.6	2 700 000	Max. 100 Splits	Fine Tree	3.5014	84.4	2 700 000	Max. 100 Splits
Medium Tree	2.1354	75.4	2 800 000	Max. 20 Splits	Medium Tree	1.843	77.6	2 800 000	Max. 20 Splits
Coarse Tree	1.5342	70.4	2 800 000	Max. 4 Splits	Coarse Tree	1.3791	72	2 900 000	Max. 4 Splits

(a) **(b)**

pA2, pD, N, Beta, 25% Hold-Out Validation					pA2, pS, pD, N, Beta, 25% Hold-Out Validation				
Alorithm	Training Time [sec]	Accuracy [%]	Prediction Speed [obs/sec]	Algorithm Setting	Alorithm	Training Time [sec]	Accuracy [%]	Prediction Speed [obs/sec]	Algorithm Setting
Fine KNN	3.4539	100	1 300 000	1 Neighbor	Fine KNN	3.9269	99.9	930 000	1 Neighbor
Medium KNN	3.9564	99.9	370 000	10 Neighbors	Medium KNN	4.7843	99.4	240 000	10 Neighbors
Coarse KNN	7.0514	98.9	76 000	100 Neighbors	Coarse KNN	8.8306	96.4	59 000	100 Neighbors
Weighted KNN	3.9355	100	360 000	10 Neighbors	Weighted KNN	4.4821	99.8	260 000	10 Neighbors
Cubic KNN	5.7172	99.9	120 000	10 Neighbors	Cubic KNN	8.553	99.2	60 000	10 Neighbors
Fine Tree	3.8132	86.4	2 800 000	Max. 100 Splits	Fine Tree	4.3835	85	2 800 000	Max. 100 Splits
Medium Tree	1.8666	76.3	2 800 000	Max. 20 Splits	Medium Tree	2.6081	75.4	2 600 000	Max. 20 Splits
Coarse Tree	1.371	68.9	3 000 000	Max. 4 Splits	Coarse Tree	1.9948	70.4	2 800 000	Max. 4 Splits

(c) **(d)**

CHAPTER 8. EXCAVATOR INSTRUMENTATION

8.1 Test-Rig Purpose

The main goal of instrumenting a mini excavator is to demonstrate a process for implementing a condition monitoring algorithm for an axial piston pump on mobile equipment. The sub-goals for this excavator are the same as the those for the stationary test-rig: perform fault detectability, sensor/dimensionality reduction, and machine learning algorithm development. The excavator test-rig can be seen in Figure 8.1



Figure 8.1: Maha Bobcat 435 DC prototype mini excavator.

The Bobcat 435 mini excavator at Maha Fluid Power Lab at Purdue University is a displacement controlled (DC) prototype machine, which concept was first conceived by (Rahmfeld and Ivantysynova, 1998). Several different efficiency and control studies have been performed on this machine in previous years (Williamson, 2010; Zimmerman, 2012; Busquets, 2016).

8.2 Schematic, Hardware, and Data Acquisition

This machine has already been instrumented with a data acquisition system and contains the same pumps, Parker P1, that have been used earlier in this work on the stationary test-rig. Therefore,

this machine makes an excellent testbed to perform condition monitoring on mobile equipment. Only minor additions, such as an accelerometer and drain line pressure, needed to be made to equip this test-rig for a condition monitoring investigation.

8.2.1 Hydraulic Schematic

The current hydraulic schematic of the excavator can be seen in Figure 8.2. This architecture is the novel pump switching design for DC systems. For more information, reference (Busquets, 2016). Only one of the pumps will be used for this investigation, Unit 3. Unit 3 provides flow to the swing and right track motors. The pumps in this excavator are 18 cc/rev Parker P1 units equipped with MOOG servo valves.

It is important to briefly describe the function of Unit 3 as it pertains to whether the machine is using the right track or utilizing the swing function to rotate the cab. If the right track is operating, then Unit 3 controls the speed of the right track motor through Displacement Control (DC) and behaves as a hydrostatic transmission. However, if the swing motor is activated to rotate the cabin of the machine, then the circuit incorporating Unit 3 changes from a DC circuit to a secondary controlled system. This means Unit 3 is no longer flow controlled but, instead, is pressure controlled. Unit 3's task is to maintain a pressure setting in the hydraulic hybrid accumulator. The duty cycles where measurements are made on this machine will be discussed later in this chapter, but Unit3 will not be running the right track motor. Unit 3 will exclusively be used to maintain the pressure in the hybrid swing drive system.

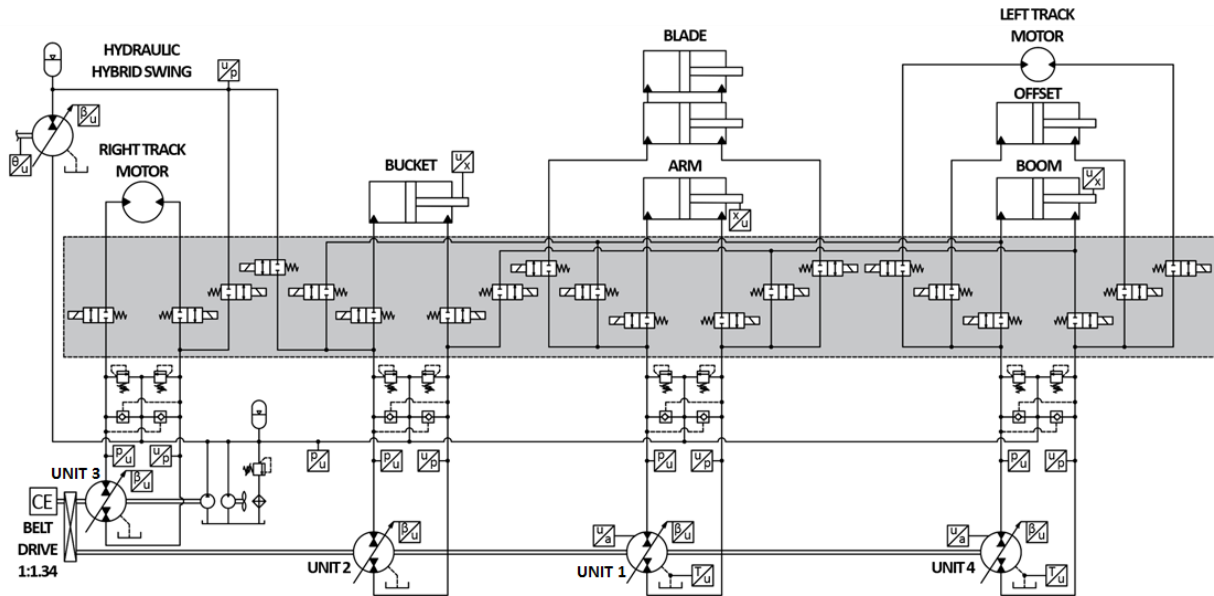


Figure 8.2: Hydraulic schematic of excavator (Busquets, 2016).

8.2.2 Sensors

The results of the stationary test-rig indicated that several sensors are not required for the successful detection of faulty pumps, such as thermocouples, torque sensors, and flow meters. However, many sensors will still be instrumented on the excavator to hopefully confirm what the stationary test-rig experiments determined.

The pump under investigation, Unit 3, is equipped with several different sensors. The pressure sensors monitor the pressure in the outlet, inlet, and drain ports. A single axis accelerometer is mounted on the case of the pump to measure case vibrations. Finally, the pump displacement, or swashplate angle, is measured using a Hall effect sensor. Additional parameters such as engine speed and oil temperatures are also measured. The different sensors mounted on the pump can be seen in

Table 8.1.

In total, 15 parameters are measured with respect to time on the excavator test-rig. Figure 8.3 shows a summary of what parameters are measured. It is noticeable that flow, torque, and pressure ripple are not parameters that are being measured. This is because the investigation on the stationary test-rig indicated the machine learning algorithms perform better without the use of

torque or flow, and the results using the pressure ripple is comparable to using a single accelerometer. Other reasons of not including these sensors is because of cost and the difficulty of implementation. Thermocouples are instrumented on this machine solely for the operator to view the temperatures. It was determined from the stationary test-rig experiments that oil temperatures may not be a reliable parameter to measure for condition monitoring purposes. The intent of the investigation is to keep in mind OEMs of mobile equipment and try to reduce cost and complexity as much as possible.

Table 8.1: Sensors equipped on pump.

Company	Model	Type	Full Scale	Accuracy
Parker	IQAN-SP500	Diaphragm Strain Gauge	0-500 bar	± 2.5 bar
Hydac	HDA 4475-B-0150	Diaphragm Strain Gauge	-1-10 bar	± 0.005 bar
PCB Piezotronics	352C03	Piezoelectric Accelerometer	±50g	10 mV/g or ± 1%
Parker	RS60	Hall Effect	47°	1.4°
Omega	KMQSS-062G-6	Thermocouple	0-1250 °C	2.2 °C or 0.75%

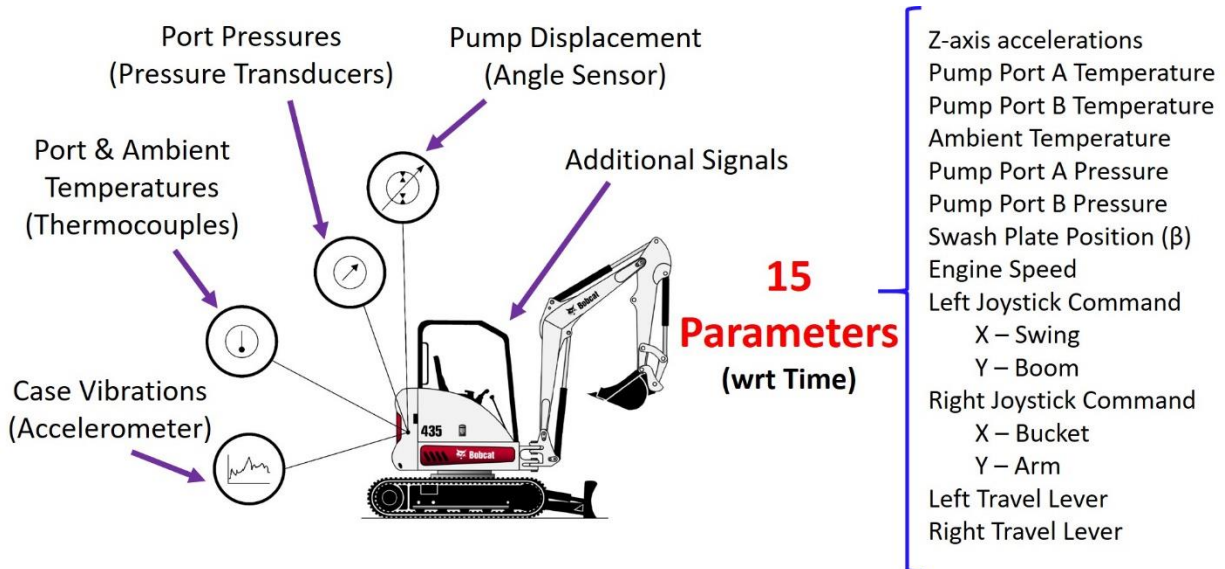


Figure 8.3: Measured parameters on excavator.

8.2.3 Data Acquisition

Only slight modifications have been made to the data acquisition system from the work done in (Busquets, 2016) to include accelerometer signals. All sensor signals are acquired on a National Instruments (NI) cRIO-9036 at a sampling frequency of 500 Hz, except for the accelerometers. The accelerometer needs to be sampled at a much faster frequency, so an NI USB-9162 is used to sample the accelerometer signals at 50 kHz.

Since the NI USB-9162 is separate from the cRIO-9036, a trigger signal is used to correctly align the accelerometer data with the data collected by the cRIO. A voltage signal is sent from the cRIO to the NI 9234 analog input Integrated Electronics Piezoelectric (IEPE) card mounted in the NI USB-9162 chassis. This voltage signal will be read by the USB-9162 to indicate when the measurement process begins. With the proper instrumentation of the excavator, experiments are ready to begin.

8.3 Duty Cycles

Machine learning algorithms are only reliable within the parameters they are trained, and this makes finding repetitive duty cycles crucial when developing condition monitoring systems. Some mobile equipment has a function or cycle that is performed each time it is used. As an example, folding cranes must unfold each time they are used, see Figure 8.4. This unfolding operation would be an ideal sequence to run diagnostics with a condition monitoring system since the loads and motion are consistent.

Finding these consistently repetitive cycles is more difficult for other mobile machines, such as an excavator. In fact, some machines do not have as repetitive and consistent of a cycle as the truck crane unfolding. Therefore, this means taking larger sums of data to train the algorithms or develop a cycle that can be easily repeatable.

This section discusses the duty cycles of the excavator that are employed for the training and testing of the machine learning algorithms. A controlled cycle is developed to check for algorithm efficacy under repeatable conditions, while a digging cycle is used to more accurately capture the

working conditions of the machine. Finally, the digging cycle is repeated but with a different operator to test the robustness of the condition monitoring system when a different operator is used.



Figure 8.4: Folding crane (Atlas GMBH, 2020).

8.3.1 Controlled

The controlled cycle is perhaps the most repeatable cycle for the excavator and is a great candidate to determine if the valve plate vaults are detectable on the mobile machine. The controlled cycle is an artificial cycle where only the cabin of the machine is rotated left approximately 90 degrees from center, swing back to the starting position, and then repeated. Figure 8.5 shows a simple illustration of the motion of the controlled cycle, and Figure 8.6 shows the speed of the cab during the progression of the cycle. No other functions (i.e. arm, boom, tracks, blade, bucket, etc.) are used throughout this controlled duty cycle, and the machine is placed in the same orientation and location for each test. The machine is running at a constant engine speed of approximately 2670 rpm.

This cycle eliminates operator variability by implementing a simple proportional controller to command a predetermined displacement setting for the swing motor, thus consistently rotating the cab of the swing in a repeatable and cyclical manner. Therefore, this cycle is automated. As

mentioned previously, Unit 3 is used to maintain a set pressure level in the hybrid accumulator when the swing is under operation. As the swing rotates, Unit 3's displacement varies to attempt to maintain a set pressure setting for the swing drive. This pressure setting is about 225 bar.

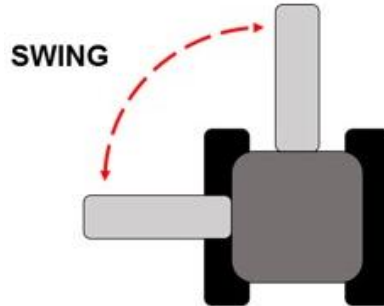


Figure 8.5: Controlled duty cycle illustration.

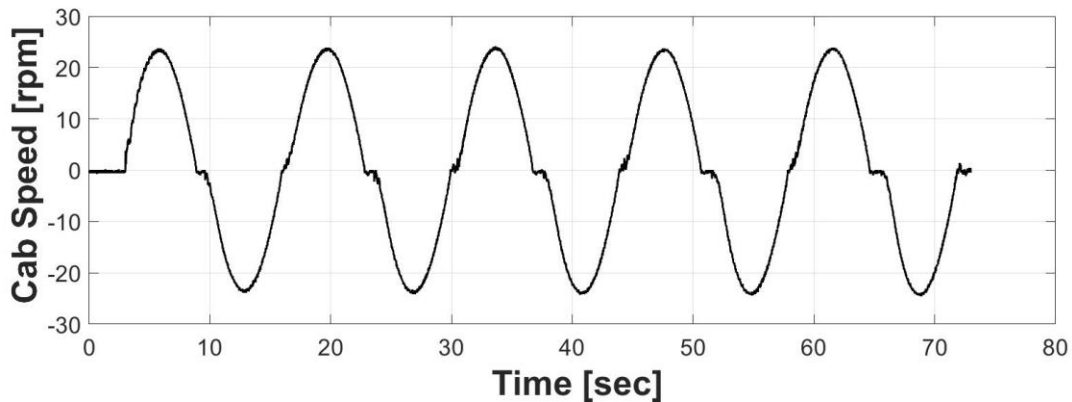


Figure 8.6: Cabin speed for the controlled duty cycle.

8.3.2 Digging

The next chosen duty cycle is that of an excavator digging in a pile of dirt and rotating approximately 180 degrees to unload the bucket, see Figure 8.7. This cycle introduces a real operator and realistic working conditions. The pile of soil has a consistency of loose and dry clay for better repeatability among measurements. The reason a pile of loose soil is selected is to avoid the variability that is inherent when actively digging into the earth.

It may be possible to detect damaged valve plates using a condition monitoring system that is trained under the controlled duty cycle. However, if this is not the case, then a machine learning

algorithm will be trained using the data collected from the digging cycle to determine fault detectability.

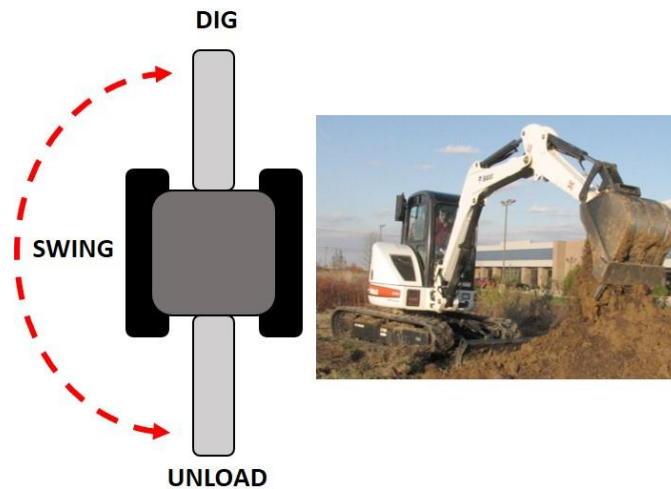


Figure 8.7: Digging cycle illustration.

8.3.3 Different Operator

The final duty cycle is that same as the digging cycle, Figure 8.7, but implements a different operator. The purpose of this cycle is to determine if operator variability influences the validity of the condition monitoring system. It is possible that a condition monitoring system that is trained under one operator will give different results with a different operator. This duty cycle is for comparison purposes, and the data obtained in this cycle will not be used to train any machine learning model. However, the data will be used to test and compare results from models trained under the controlled and digging duty cycles.

CHAPTER 9. EXCAVATOR MEASUREMENT OBSERVATIONS

As done with data taken on the stationary test-rig, it is important to observe the data to see ensure data fed into the machine learning algorithms is acceptable. To ensure acceptability, one must observe the repeatability of the measurements and see if trends exist between the different levels of pump health. This chapter will focus on the observations of the data from the controlled cycle on the excavator. First, repeatability of the healthy measurements will be observed, and then the healthy measurements will be compared to the different states of pump health. Signals such as the cab speed, engine speed, and port pressures are examined.

A few important caveats need to be addressed at this time. First, the observations plots shown in this chapter show filtered data only for the purpose to examine trends within the data. The filtered or smoothed data is not used in the algorithm training because of the inherent information lost in the filtering. Second, the mini excavator is a functioning mobile machine with an internal combustion diesel engine. Some variation in operating conditions and parameters are to be expected as it is a real-world experimental setup.

9.1 Excavator Repeatability Observations

As discussed during the stationary test-rig observations, it is important to examine the data for repeatability. If repeatability is achieved, then the data is valid and can be used for machine learning purposes with higher levels of confidence.

9.1.1 Cab Speed

The first parameter to observe is the rotational speed of the cabin. Only slight deviation between the five separate healthy measurements can be seen in Figure 9.1, and this deviation is caused by the proportional controller that controls the hybrid swing motor. Figure 9.2 shows only a single cycle of the cab rotation and some deviation can be seen. However, repeatability of the cab speed is achieved.

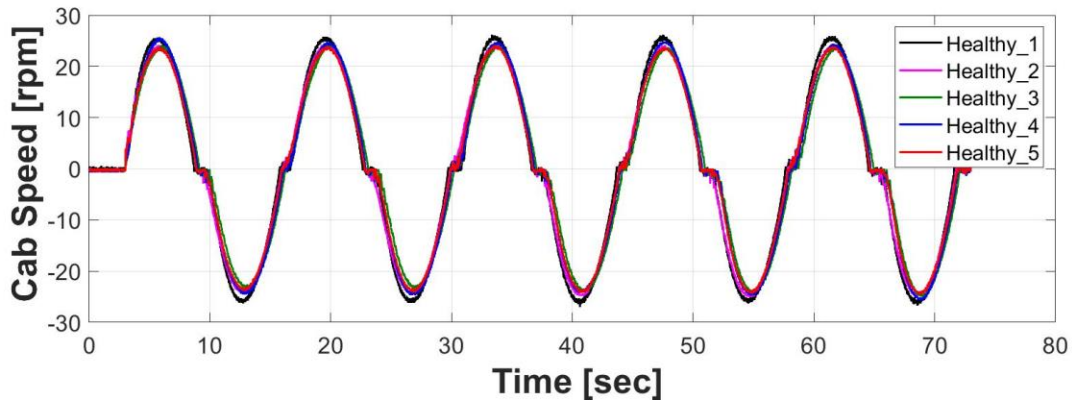


Figure 9.1: Excavator cab rotation speed of repeatability analysis of the controlled cycle.

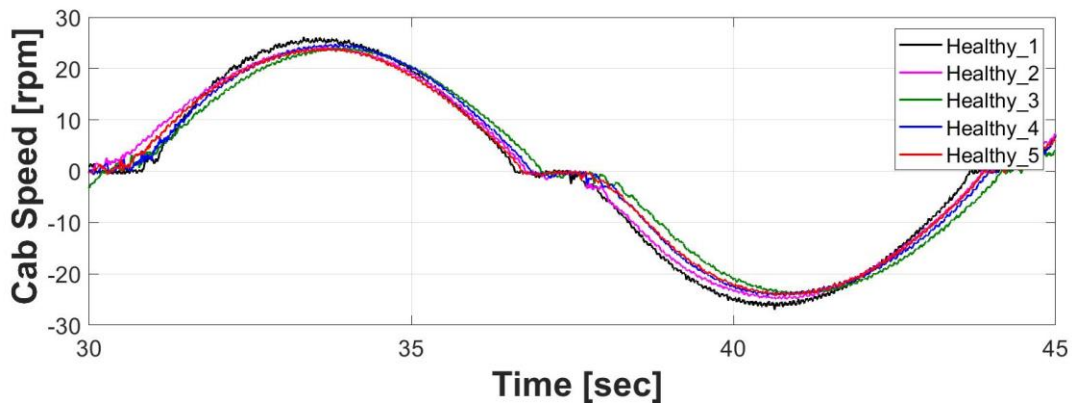


Figure 9.2: Zoomed view of cab speed rotation repeatability.

9.1.2 Engine Speed

The engine speed of the different healthy measurements can be seen in Figure 9.3. The most the engine speed varying from one measurement to the next is approximately 15 RPM. The engine is set to maintain a constant maximum speed and the controller does a fairly repeatable job reaching the same engine speed.

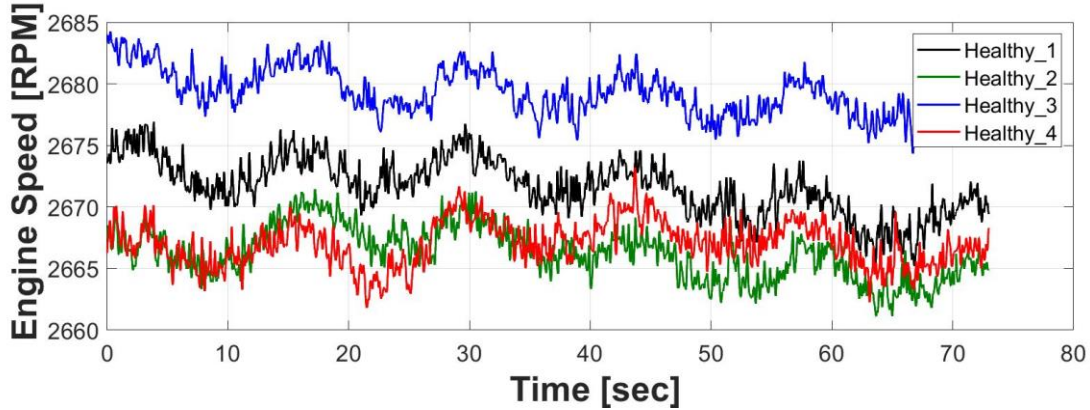


Figure 9.3: Engine speed of repeatability analysis of the controlled cycle.

9.2 Pressure Ports

Since the right track and only the swing is operating, Unit 3 is tasked with maintaining a set pressure in the hybrid swing accumulator, as discussed in a previous chapter. This means the pressure port, Port A, is always the low-pressure port the swing is under operation. Here, Figure 9.4, the low-pressure in the system is very consistent and repeatable. The low-pressure is maintained around 29 bar.

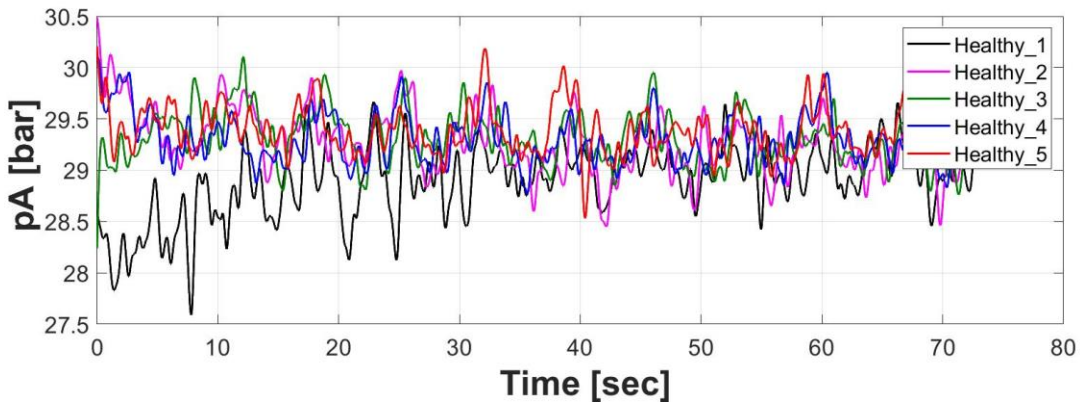


Figure 9.4: Port A pressure of repeatability analysis of the controlled cycle.

The pressure port, Port B, is the outlet to Unit 3 and is connected to the hybrid accumulator and swing motor. The controller of Unit 3 is set to maintain a pressure around 225 bar. It can be seen in Figure 9.5 that some variation does exist, but it is important to remember that this plot is highly filtered to observe trends. The variation comes from the gains used in the controller. This variation

will be address more when compared to the other measurement cycles where damaged pumps were tested but is not significant enough to be considered unrepeatable.

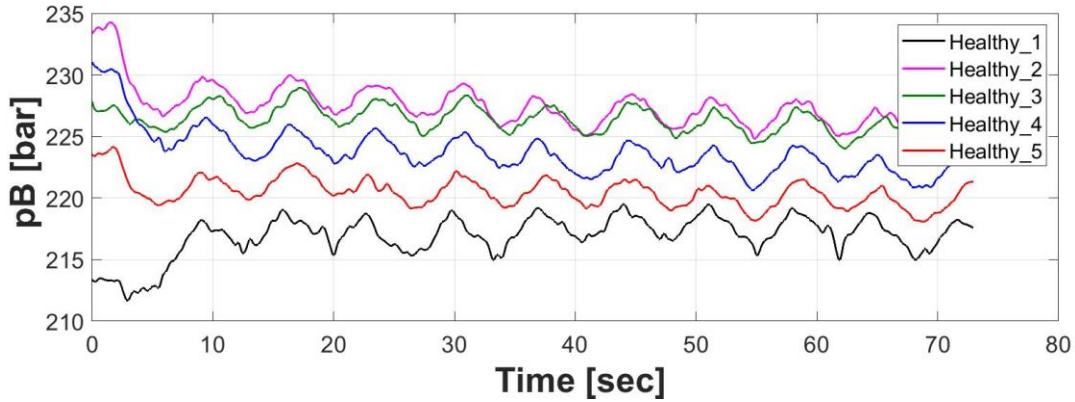


Figure 9.5: Port B pressure of repeatability analysis of the controlled cycle.

9.2.1 Drain Line Pressure

Figure 9.6 shows the high repeatability of the drain pressure between the different healthy measurements. To further explain that the variation of pB, Figure 9.5, is not critical consider the magenta line, Healthy_2. This has the highest pB pressure but is one of the lowest drain pressures; while the blue, Healthy_4, pressure port pB has the third highest pressure and the highest drain pressure. This shows that the slight variation in the high-pressure port does not necessarily greatly influence the drain pressure. It is true that the as the pressure port, pB, increases then the leakages would increase. This would, in turn, increase the pressure in the drain line. However, the minor variation in the high-pressure port does not translate into a significant enough variation in the drain pressure, especially since the unfiltered data is fed into the machine learning algorithm.

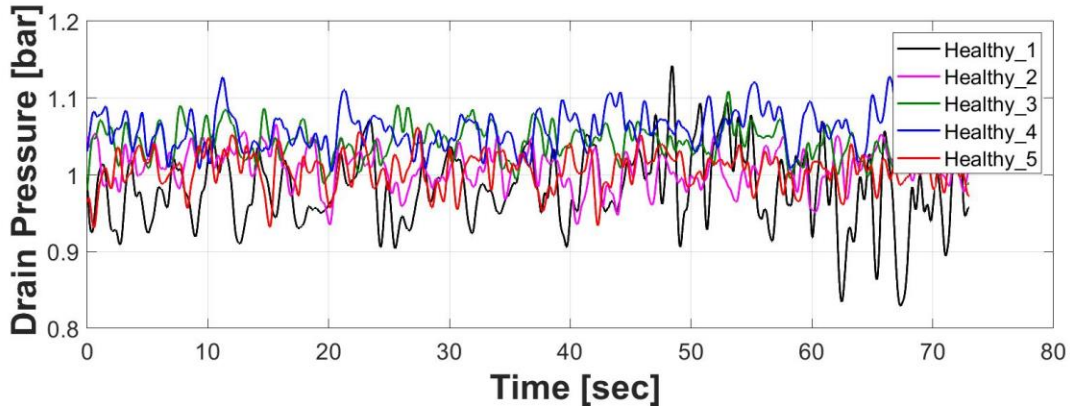


Figure 9.6: Drain port pressure of repeatability analysis of the controlled cycle.

9.3 Observable Wear/Damage

In addition to repeatability, it is important to examine the differences between the different states of pump health. This section will show the healthy pump measurements in black and the unhealthy measurement in color.

9.3.1 Cab Speed

As shown in Figure 9.7, the cab speed for the healthy and unhealthy pumps are nearly identical. Only a single healthy measurement is used to compare the various unhealthy pump conditions since it has been previously established that the cab speed under the different healthy conditions is repeatable. If the pump can provide sufficient flow to maintain a set pressure in the accumulator, then the cab speed can be met with the secondary controlled implemented on the excavator for the swing drive.

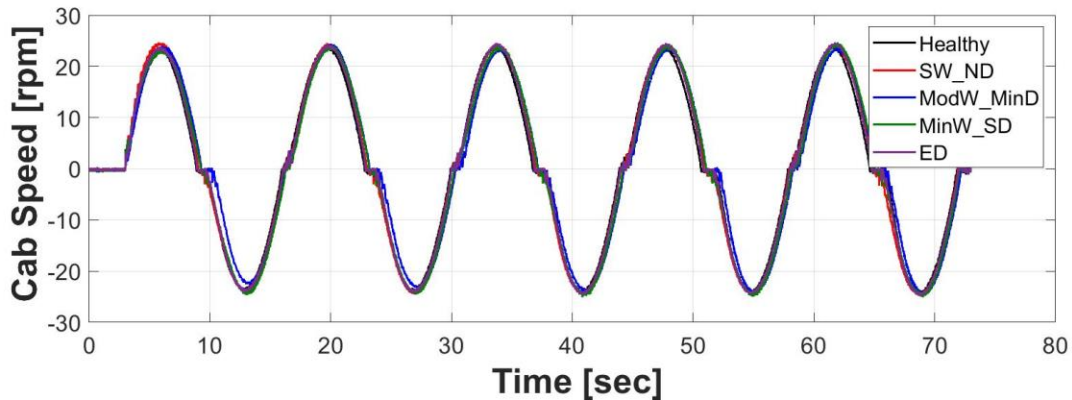


Figure 9.7: Comparison of cab speed between healthy and unhealthy pump states.

9.3.2 Engine Speed

The range of the engine speed is a little more varied among the different unhealthy pumps when compared to the healthy measurement, see Figure 9.8. This could lead to a clear bias in the machine learning algorithms. The machine learning algorithm could see these stratifications of engine speed and solely use those to classify the pump as healthy or unhealthy. If the machine learning algorithms see data from a new measurement set, then it could incorrectly classify the pump as healthy or vice versa. However, it is key to capture the operating conditions of the pump to correctly classify the health of the pump. Therefore, it may be possible to keep the engine speed as a viable parameter in the machine learning algorithm, but caution must be taken.

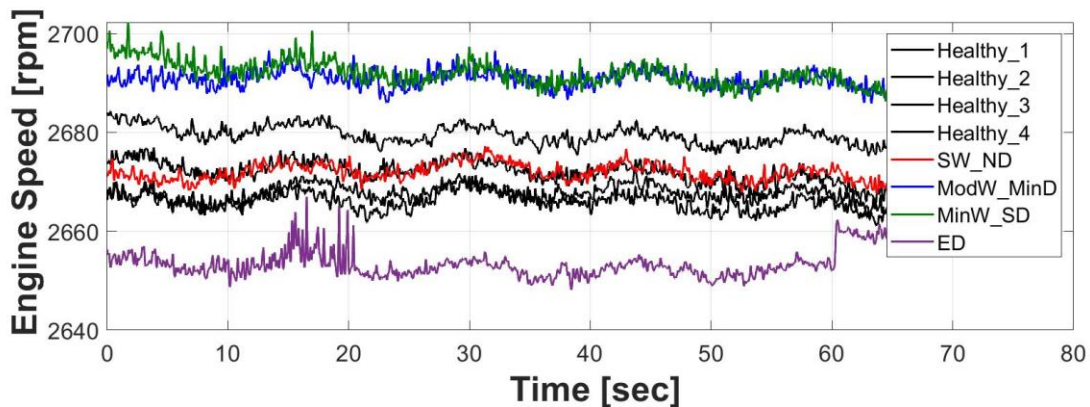


Figure 9.8: Comparison of engine speed between healthy and unhealthy pump states.

9.3.3 Pressure Ports

The low-pressure setting is maintained around 29 bar regardless of the state of the pump, Figure 9.9. The low-pressure setting is not expected to noticeably vary from the different valve plate conditions.

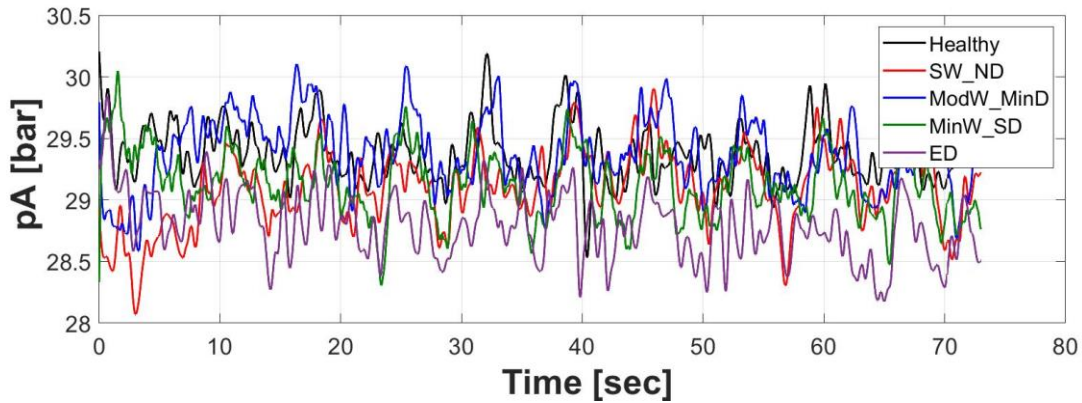


Figure 9.9: Comparison of pA between healthy and unhealthy pump states.

The high-pressure port, pB, is another parameter that defines the operating condition of the pump, similar to engine speed. Figure 9.10 shows the Port B pressure of the different measurements of the pump under the controlled cycle on the excavator. It can be seen that the pressure settings vary from about 215-235 bar. This variation is caused by the controller that sets and maintains a constant pressure setting for the swing accumulator. However, all the healthy cycles cover the majority of the variation range. pB is likely a viable parameter to help define the operating condition of the pump if the data is trained with all healthy sets of measurements.

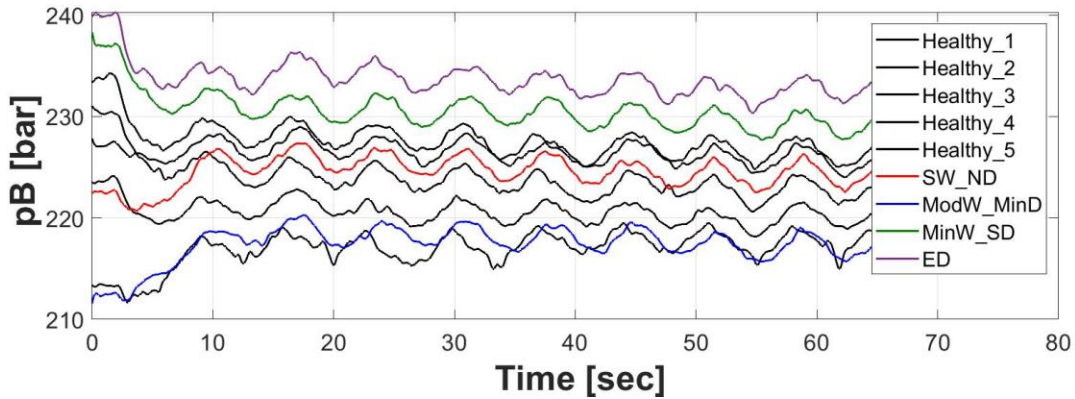


Figure 9.10: Comparison of pB between healthy and unhealthy pump states.

9.3.4 Drain Pressure

Perhaps the clearest differences between the unhealthy and healthy valve plates can be observed in the drain pressure, Figure 9.11. The Minor Wear Severe Damage (MinW_SD) case has very similar drain pressure as the healthy cases. However, more pressure oscillations are present. The Moderate Wear Minor Damage (ModW_MinD) and Severe Wear No Damage (SW_ND) cases have noticeably higher drain pressure levels than the healthy condition. Finally, the Extreme Damage (ED) valve plate case exhibits the highest drain pressure with a pressure near 1.4 bar. The drain pressure seems to be a good indicator of valve plate condition and pump health.

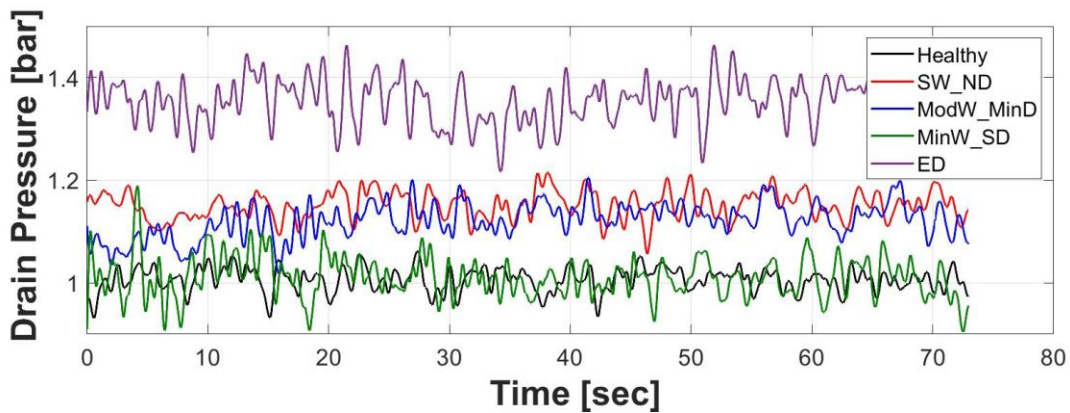


Figure 9.11: Comparison of drain pressures between healthy and unhealthy pump states.

CHAPTER 10. EXCAVATOR MACHINE LEARNING RESULTS

While some trends can be observed by the human eye, others need to be interpreted by machine learning algorithms. This chapter focuses on the results from implementing the data gathered from the different duty cycles previously mentioned into several machine learning algorithms and selecting which sensors contribute the most to a successful condition monitoring system. First, the feature selection results will be discussed with models trained using the controlled and digging duty cycles. Next, the results from the investigation on algorithm selection will be discussed. Finally, it is necessary to see how a model trained from a certain duty cycle behaves when the model is fed with data from another cycle.

10.1 Feature Selection

The purpose of the feature selection is to determine the minimum number of sensors required to accurately and effectively detect valve plate faults for condition monitoring systems. The feature selection method employed on the excavator is different than what was used on the stationary test-rig. First, each of the features under investigation is used singly to determine the magnitude that feature contributes to the accuracy of the machine learning algorithm. Next, a forward selection process is used because of the few numbers of features/sensors under consideration. The features under investigation are inlet pressure (pA), outlet pressure (pB), drain pressure (pD), pump displacement (Beta), pump case vibrations (Accel), and engine speed (N). Feature selection results will be shared of both the controlled and digging cycles.

10.1.1 Controlled Cycle

First, each of the six features is used as the sole input to the Fine Decision Tree machine learning algorithm to examine how each feature influences the algorithm training time, accuracy, and prediction speed. Table 10.1 shows the entirety of the feature selection results for the controlled cycle. It can be observed that the engine speed (N) does indeed give the highest accuracy of determining if the data is classified as healthy or unhealthy, 96.8%. As noted in the observations of the excavator measurements, the engine speed could provide a false accuracy number due to the stratification of the data seen in Figure 9.8. While it may be possible the machine learning

algorithm is using this stratified data to make its predictions, the engine speed may still be necessary to define the operating conditions for the condition monitoring system to best classify the data as healthy or unhealthy.

Other parameters, such as the case accelerations (Accel), 58.1%, and the pump inlet pressure (pA), 64% show to produce the least accurate results of the six features that have been evaluated individually. Pump displacement (Beta) and outlet pressure (pB) give comparable accuracies of 72.7% and 73.3%, respectively. The drain pressure (pD) shows to be a promising parameter to monitor for the detection of valve plate wear with an accuracy of 83.2%.

Table 10.1: Feature selection results of the controlled cycle using a fine decision tree algorithm.

Features	Training Time [sec]	Accuracy [%]	Prediciton Speed [M obs/sec]	Selected Features
1/6	83.578	64	3.6	pA
1/6	49.786	73.3	3.7	pB
1/6	63.51	83.2	3.8	pD
1/6	46.475	72.7	3.8	Beta
1/6	36.516	96.8	3.7	N
1/6	137.93	58.1	3.2	Accel
2/6	66.216	89.5	3.7	pB, pD
3/6	64.545	99.8	3.6	pB, pD, N
2/6	55.889	99.3	3.7	pD, N
2/6	62.362	88.4	3.7	pD, Beta
6/6	118	99.9	3.7	pA, pB, pD, Beta, N, Accel

When combining features together the accuracy greatly increases. For example, combining outlet pressure (pB) and drain pressure (pD) the accuracy increases to nearly 90%. Engine speed (N), outlet pressure (pB) and drain pressure (pD) give an accuracy of 99.8%, while using all six features give a marginal improved accuracy of 99.9%. Considering only the controlled cycle indicates that drain pressure, outlet pressure, and engine speed are among the most important signals for determining valve plate fault. The case accelerations seem to not contribute additional information that the other signals do not contain. Therefore, it could be determined that accelerometers are not necessary to detect valve plate wear.

10.1.2 Digging Cycle

Unsurprisingly, the accuracies from the feature selection process using the digging cycle data are significantly lower than those from the controlled cycle. Table 10.2 shows the results from the feature selection process utilizing data from the digging cycle. It is to be noted that accelerations are not included with this data because they were deemed negligible under controlled conditions. It is interesting to see the engine speed (N) does not contribute nearly as significantly to the accuracy of the classification algorithm as it does with the controlled cycle, 55.8% to 96.8%. This discrepancy in accuracy is likely because the stratification of the engine speed for the controlled cycle. The engine speed is not stratified in the digging cycle, which is more realistic. This confirms that the engine speed does not significantly contribute to the identification of valve plate fault on the excavator pump. However, it could still be useful in defining the operating condition of the pump.

Outlet pressure (pB), drain pressure (pD) and pump displacement (Beta) give a result of 69.6%, which is second best to using all five features which gives an accuracy of 71.8%. This shows that it would be best to include all five sensors when running a condition monitoring system on an excavator during a digging cycle.

Table 10.2: Feature selection results of the digging cycle using a fine decision tree algorithm.

Features	Training Time [sec]	Accuracy [%]	Prediction Speed [M obs/sec]	Selected Features
1/5	2.3211	53.1	3	pA
1/5	1.8833	61.7	3.2	pB
1/5	1.8675	60.9	3.6	pD
1/5	1.8899	62.9	3.7	Beta
1/5	1.9358	55.8	3.6	N
2/5	2.2774	66.9	3.6	pB, pD
3/5	2.5882	67.6	3.3	pB, pD, N
2/5	2.2801	63	3.7	pD, N
2/5	2.2574	67.7	3.6	pD, Beta
3/5	2.4922	69.6	3.6	pB, pD, Beta
5/5	3.4512	71.8	3.5	pA, pB, pD, Beta, N

10.2 Algorithm Selection

The feature selection process gives the condition monitoring system designer an idea of which sensors contribute the most to accurately detecting faults, and the algorithm selection process takes those key features and selects machine learning algorithms that are best suited for the application. The algorithms investigated have already been discussed in this dissertation. However, the two primary algorithms used are decision trees and K-Nearest Neighbors (KNNs). Variations of these two primary algorithms will be used in this work. The results from the algorithm selection will be discussed from both the controlled and digging duty cycles.

10.2.1 Controlled Cycle

A summary of the best results from the algorithm selection for the controlled data can be seen in Figure 10.1. Here several combinations of features work well for the accurate detection of valve plate faults, but only two algorithms give the best results, Fine Tree and Fine KNN. Notice that any feature combination that contains engine speed gives near perfect accuracies, but this could be due to the stratification of the engine speeds. However, looking at the two feature combinations of outlet pressure with drain pressure and drain pressure with pump displacement, they give high accuracies of 96.2% and 96.3%, respectively. These two could potentially be more reliable than the feature combinations with engine speed. Between the two, the outlet pressure and drain pressure feature combination could be the better option as the outlet pressure helps define the operating condition of the pump. For a complete view of the algorithm selection results please see Figure 12.1 in the Appendix.

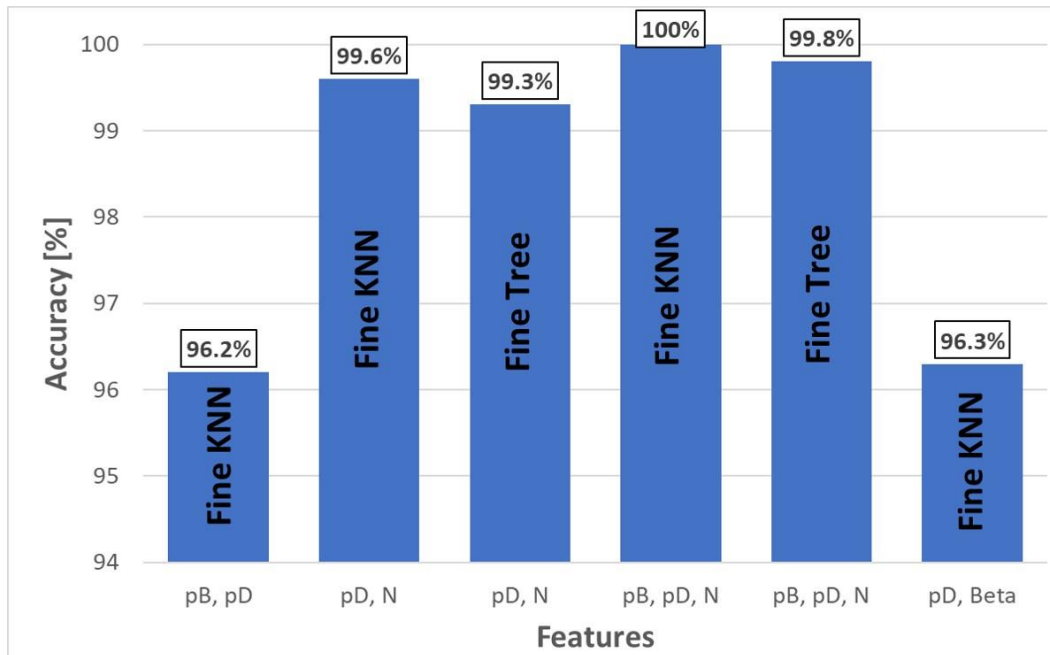


Figure 10.1: Algorithm selection summary for controlled cycle.

10.2.2 Digging Cycle

The Fine Decision Tree is not the best algorithm for the digging cycle, but it is the KNN algorithms that prove to be decent at classifying the healthy and unhealthy pump conditions. Figure 10.2 shows the summary of the algorithm selection for the digging duty cycle. As discussed in the feature selection section, all five features give the best results. The best algorithm with the combined five features is the Fine KNN algorithm and gives an accuracy of 93.6%. If only the outlet pressure (pB), drain pressure (pD), and the engine speed (N) are used, then the best algorithm to use is the Weighted KNN. However, this only gives an accuracy of 75%, which is not reliable enough to detect valve plate faults. It is, therefore, recommended to use the five features and a Fine KNN algorithm for the digging cycle. For the complete set of results for the algorithm selection process of the digging cycle see Figure 12.2 in the Appendix.

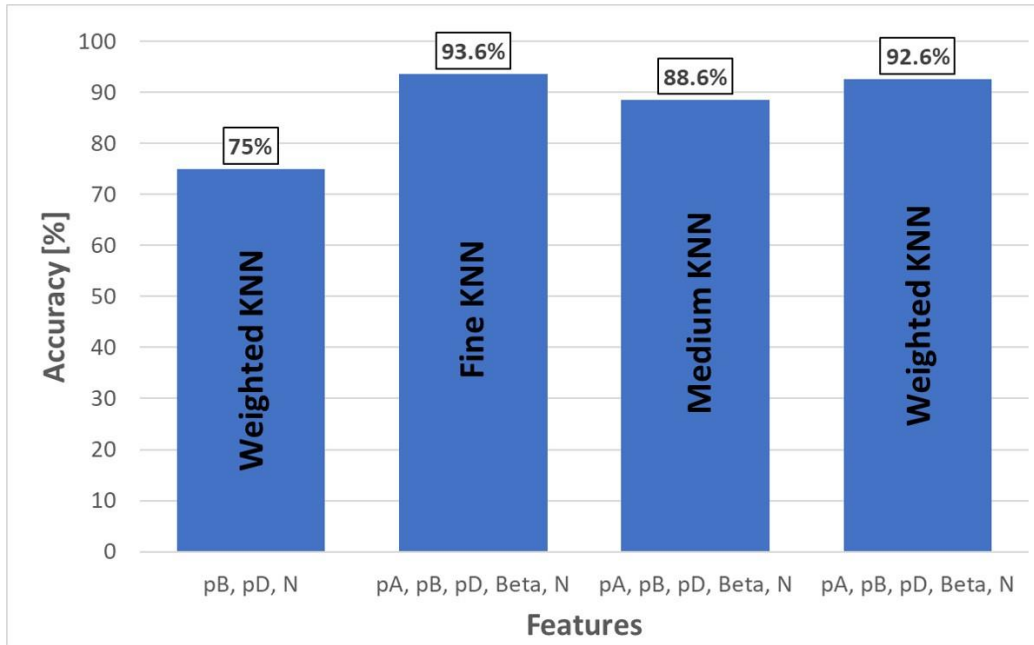


Figure 10.2: Algorithm selection summary for digging cycle.

10.3 Trained Model Results

While observing how different features and algorithms behave under a single operating condition is important, it is also critical to see how using a model trained under the controlled duty cycle behaves using data from the digging and different operator cycles. The Fine KNN algorithm proved to be best suited for the controlled duty cycle and is, therefore, selected as the algorithm to use for the remainder of this study. However, different feature combinations are still used for comparison.

Table 10.3 shows the results from using data from the digging and different operator cycles that have been entered a classification model that has been trained using a Fine KNN algorithm under the controlled cycle. Using data from either of the other two cycles does not give strong accuracy results when using a model trained on the controlled cycle data. At best, the digging cycle has an accuracy of 59.2% to detect valve plate faults.

Table 10.3: Trained Fine KNN model of controlled cycle using data from different operating conditions.

Features	Cycle	Accuracy [%]
pB, pD	Digging	54.4
	Different Operator	58.9
pB, pD, N	Digging	56.5
	Different Operator	66.5
pD, N	Digging	59.2
	Different Operator	54.6

The controlled cycle is quite different from the digging and different operator cycles. Therefore, this leads to the investigation of the cross-compatibility between the digging and different operator cycles, since these two cycles are very similar. Table 10.4 shows the results from using data from the controlled and different operator cycles that have been entered a classification model that has been trained using a Fine KNN algorithm under the digging duty cycle. Notice the lack of detectability in the different operator cycle, 58%, even though the two cycles are very similar. These results glaringly tell of the importance of a repeatable cycle to accurately and reliably perform a condition monitoring function for the system.

Table 10.4: Trained Fine KNN model of digging cycle using data from different operating conditions.

Features	Cycle	Accuracy [%]
pA, pB, pD,	Controlled	62.2
Beta, N	Different Operator	58.0

At this point it has become apparent to see how each of the levels of valve plate faults influenced the detection accuracy using data from a different cycle. The different levels of valve plate fault have been discussed in previous chapters, but as a review they are: Healthy, Minor Wear Severe Damage (MinW_SD), Moderate Wear Minor Damage (ModW_MinD), Severe Wear No Damage (SW_ND), and Extreme Damage (ED). It is interesting how well the model can detect the various levels of valve plate health. The model trained with outlet pressure (pB), drain pressure (pD), and engine speed (N) under the controlled cycle is used for this investigation.

Figure 10.3 gives the breakdown of each valve plate condition under the digging operation using a trained Fine KNN model of the controlled cycle, a cross-compatibility condition. All conditions combined give an accuracy of 56.5%, which can also be seen in

Table 10.3. A likely reason as to why the accuracy for the healthy condition is so low is because most the faulty valve plate conditions are too similar one another. Meaning, the Minor Wear Severe Damage, Moderate Wear Minor Damage, and Severe Wear No Damage cases have similar pump performance characteristics that the machine learning algorithm has difficulty detecting the faults on a mobile machine under cross-compatibility conditions. However, the algorithm can more accurately classify the Extreme Damage (ED) case with an accuracy of 86.1% than the other cases. Although the accuracy of 86.1% is not exceptional, it does suggest that the more severe the damage or wear of the valve plate becomes then the detectability accuracy increases for cross-compatibility scenarios. Therefore, cross-compatibility of condition monitoring model may be possible if only extreme cases are to be detected.

Although cross-compatibility does not give significantly positive results in this work, it does not mean condition monitoring cannot be implemented on a machine like an excavator. These results glaringly illustrate the importance of a repeatable cycle to accurately and reliably perform a condition monitoring function for the system. Therefore, repeatable and controlled conditions must be used for condition monitoring of incremental faults on a mobile machine. However, if only severe damage cases where pump performance is severely impacted, then cross-compatibility between different operating conditions may be possible.

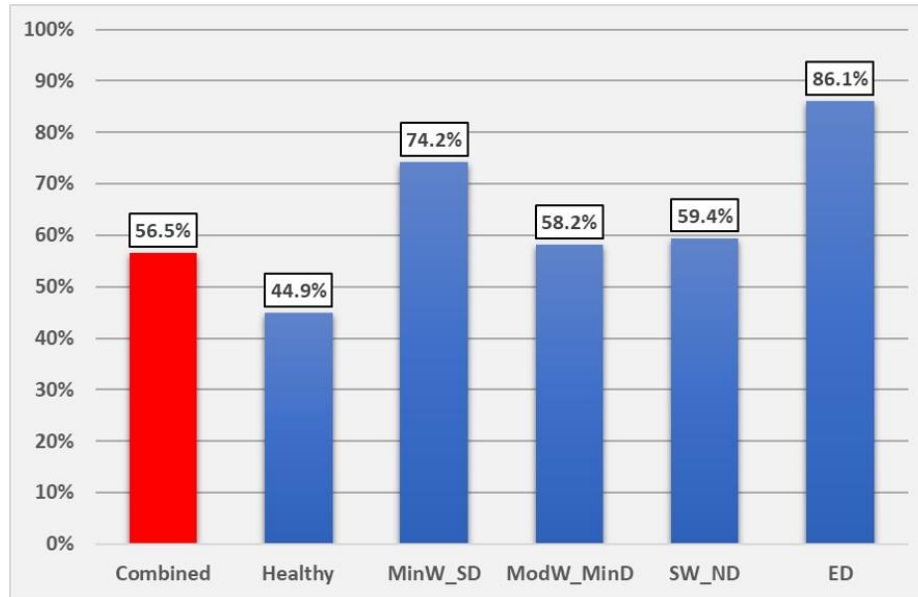


Figure 10.3: Breakdown of each valve plate condition under the digging operation using a trained Fine KNN model of the controlled cycle.

10.4 Summary

In summary, a feature selection process to determine the most critical sensors for faulty valve plates was performed for both the controlled and digging duty cycles. This process discovered that accelerometers are not necessary for valve plate fault detection, but other signals such as drain pressure, outlet pressure, and engine speed are important to achieve higher fault detectability. A potential issue with using the engine speed was addressed for the controlled condition because of obvious stratifications found in the measurements. However, it was determined that keeping engine speed would be beneficial to defining the pump operating condition that the machine learning algorithm can then use. The feature selection process for the digging duty cycle showed that using outlet pressure, inlet pressure, drain pressure, engine speed, and pump displacement are useful.

Next, the algorithm selection was discussed and showed that the Fine K-Nearest Neighbor (KNN) seems to give the best results for both the controlled and digging duty cycles. Using the Fine KNN algorithm results in detection accuracies near 100% in the controlled cycle if engine speed is included. Without engine speed, fault detection accuracy falls slightly to about 96%, which could still be acceptable for a condition monitoring system. Fault detection accuracy during the digging

cycle significantly increased using a Fine KNN algorithm that includes inlet pressure, outlet pressure, drain pressure, engine speed, and pump displacement. The fault detection accuracy increased from 71.8% using a Fine Decision Tree to 93.6% implementing the Fine KNN machine learning algorithm.

Finally, an investigation was completed which explored the cross-compatibility between a model trained under one cycle and using data from another cycle as an input into the model. This study showed that a model trained under the controlled duty cycle does not give reliable and accurate fault detectability for data run in a digging cycle, below 60% accuracies. The same is true for a model trained using the digging cycle with data run in a controlled cycle, even if the machine is in similar operating conditions but with a different operator.

The investigation in this work has shown the importance of controlled and repeatable conditions for a successful and effective condition monitoring system on mobile hydraulics. It is incomprehensible and unrealistic to design a condition monitoring system that can successfully detect incremental faults for every conceivable operating condition for mobile machines. For this reason, it is recommended to have a program built into the machine to perform a diagnostic check or only be interested in faults where pump performance is severely impacted, i.e. pump drain pressure increases significantly to 3 bar. An example of a diagnostic check on a mobile machine is when an operator would press a button to perform a series of motions on an excavator to do a system check. The data collected in this system check would then be fed into an algorithm that has been trained on that exact cycle, such as the controlled cycle performed in this work.

CHAPTER 11. CONCLUSION

The aim of this work was to develop a process of implementing a condition monitoring system for a swashplate type axial piston pump on a mobile machine that could determine if the pump is healthy or unhealthy. The output of the condition monitoring system was to be binary, healthy or unhealthy, and the goal was not to determine which component is faulty or give the Remaining Useful Life (RUL) of the pump.

A successful step-by-step process was developed to show how to implement a condition monitoring strategy onto a mobile machine. Firstly, it was the axial piston pump was shown and how each of the components interact with one another. This activity and an extensive literature review led to the selection of the valve plate as a good case study for pump failure. Varying degrees of valve plate wear and damage were obtained and documented using an optical profilometer.

Second, an experimental stationary test-rig was developed. This test-rig was used to test condition monitoring methods in a controlled and stable environment before it was to be implemented on a mobile machine. The following list states the purposes/achievements of the stationary test-rig:

1. Performed fault detectability under steady-state and dynamic operating conditions.
 - a. A difference in drain flow, outlet pressure transients, and volumetric efficiencies were observed between the healthy and unhealthy conditions of the pump.
2. Tested for repeatability under measurements.
 - a. Excellent repeatability between measurements was demonstrated and proved.
3. Performed a dimensionality/sensor reduction to minimize the number of sensors required for successful condition monitoring of axial piston pumps.
 - a. It was determined that pump outlet pressure, drain pressure, speed, and displacement were enough to efficiently and accurately detect the faulty pump conditions.
4. Compared and selected several different machine learning algorithms that accurately detected faulty pumps with minimum computational expenses.

- a. Supervised learning K-Nearest Neighbor (KNN) algorithms were found to be the “best” machine learning algorithms investigated and gave excellent results.

Next, a Bobcat 435 mini excavator was instrumented to perform experiments for implementing a condition monitoring system on a mobile machine. This machine has been instrumented with fewer sensors than the stationary test-rig because of the results and observations made from the stationary test-rig data. The excavator does not have flow meters, torque meters, or transient pressure transducers because of the sensor cost, difficulty of implementing the sensor on a mobile machine, and because the sensors do not add relevant information to the machine learning algorithm to successfully detect a faulty pump.

Three relevant duty cycles were developed to conduct condition monitoring measurements on the mini excavator. A controlled duty cycle was developed to eliminate any operator and load variability to give as repeatable of a cycle as possible. Next, cycle where the excavator is digging in a loose pile of soil and unloading was used to represent realistic operating conditions. The final cycle was the same as the digging cycle but with a different operator.

A similar process that was performed on the stationary test-rig was then implemented on the excavator to develop a condition monitoring system. Measurement repeatability was demonstrated and noticeable observations in the drain pressure were seen between the different valve plate faults under the controlled duty cycle.

The feature selection process that determined the most critical sensors for faulty valve plate detection and algorithm selection process were then performed. The feature selection process discovered that accelerometers were not necessary for valve plate fault detection, but other signals such as outlet pressure, inlet pressure, drain pressure, engine speed, and pump displacement are important to achieve higher fault detectability. The algorithm selection was discussed and showed that the Fine K-Nearest Neighbor (KNN) seems to give the best results for both the controlled and digging duty cycles.

Finally, an investigation in the cross-compatibility between a model trained under one cycle and using data from another cycle as an input into the model. The investigation showed that a model trained under the controlled duty cycle does not accurately detect valve plate faults when data from the digging cycle is used. Also, a model trained with the digging cycle data does not give acceptable results when a different operator is used. However, positive results are shown that the cross-compatibility of condition monitoring models may be possible if the faults are more extreme and severe.

In conclusion, the research done in this work has shown how vast amounts of experimental measurements must be conducted to develop accurate condition monitoring systems for mobile hydraulics. This investigation has also shown the importance of controlled and repeatable conditions for a successful and effective condition monitoring system on mobile hydraulics. It is incomprehensible and unrealistic to design a condition monitoring system that can successfully detect faults for every conceivable operating condition for mobile machines, which would need to be done to ensure reliable detectability. Therefore, it is recommended to have a program built into the machine to perform a diagnostic check. However, this work is only a step into the future of condition monitoring of mobile hydraulic machines.

CHAPTER 12. FUTURE WORK

The work for condition monitoring of hydraulic systems on mobile equipment is far from complete with the conclusion of this work. Ultimately, an accurate prediction of RUL on a machine and specify which component is failing is the end goal. However, current machines on the market do not even have a monitoring system that indicates the pump is in the process of failing, a binary health condition.

The high nonlinearity and randomness involved with the wear of hydraulic systems makes predicting RUL extremely difficult without large amounts of machine data recorded by the manufacturers. Something industry is working on is gathering and collecting more data from their machines. With this data, a better understanding of how the hydraulic systems fail can be turned into practice in developing condition monitoring systems.

Additional work can be conducted on determining the specific components within the pump that are failing. This could be done by observing distinct signal characteristics of the different faulty components. This has been done on roller bearings for rotating machinery.

The process in this work can also be implemented to gather more wear information and how the wear of different components affects the performance of hydraulic systems. Varying degrees of wear and many more components can be investigated and analyzed to build the knowledge base of how hydraulic systems wear and how that wear can be detected.

If a condition monitoring system aimed at detecting valve plate failure is desired for an axial piston pump on mobile machines, then it is recommended to measure the engine speed, pump displacement, inlet pressure, and the outlet pressure of the pump. These measurements will give the machine learning algorithm knowledge on the operating conditions of the pump. Finally, the drain pressure should be monitored to detect changes to leakage due to valve plate fault.

REFERENCES

- Alpaydin, E. (2010) *Introduction to Machine Learning Second Edition*. 2nd edn, *Introduction to Machine Learning*. 2nd edn. Massachusetts Institute of Technology.
- Altman, N. S. (1992) ‘An Introduction to Kernel and Nearest-Neighbor Nonparametric Regression’, *The American Statistician*, 46(3), pp. 175–185.
- Argo-Hytos (2019) *Lubrication Condition Sensor*. Available at: <https://www.argo-hytos.com/en/products/sensors-measurement/lubrication-condition-sensors/lubcos-h2o-ii.html>.
- Atlas GMBH (2020) *Atlas Cranes & Excavators*. Available at: [https://www.atlasgmbh.com/en/products.aspx?p=10420&pn=ATLAS 240.2 LM+ / 240.2 E&pg=61c80b53-96ad-4819-a558-37d877c822b2](https://www.atlasgmbh.com/en/products.aspx?p=10420&pn=ATLAS%20240.2%20LM+/240.2%20E&pg=61c80b53-96ad-4819-a558-37d877c822b2).
- Babbillion, L. and Poirson, A. (1920) ‘Sur une méthode thermométrique de mesure du rendement des turbines hydrauliques’, *La Houille Blanche*, 6, pp. 217–221.
- Backe, W. and Schwarz, T. (1989) ‘Condition monitoring on hydraulic displacement units’, in *Proc. 2nd Bath International fluid power workshop*. Bath, UK.
- Belsley, D. A. (1991) *Conditioning Diagnostics: Collinearity and Weak Data in Regression*. New York: John Wiley & Sons.
- Bishop, C. (2006) *Pattern Recognition and Machine Learning*. Springer Science+Business Media, LLC.
- Bogert, B. P. (1963) ‘The quefreny alanysis of time series for echoes; Cepstrum, pseudo-autocovariance, cross-cepstrum and saphe cracking’, *Time series analysis*, pp. 209–243.
- Bosch-Rexroth (2019) *Oil measurement technology*. Available at: <https://www.boschrexroth.com/en/xc/products/product-groups/mobile-hydraulics/oil-measurement-technology>.
- Breiman, L. *et al.* (1984) *Classification and regression trees*. Wadsworth International Group.
- Busquets, A. (2018) *An Investigation of Micro-Surface Shaping on the Piston/Cylinder Interface of Axial Piston Machines*. Purdue University.
- Busquets, E. (2016) *Advanced Control Algorithms for Compact and Highly Efficient Displacement-Controlled Multi-Actuator and Hydraulic Hybrid Systems*. Purdue University.
- Casoli, P., Bedotti, A., *et al.* (2018) ‘A methodology based on cyclostationary analysis for fault detection of hydraulic axial piston pumps’, *Energies*, 11(7), p. 1874.

- Casoli, P., Campanini, F., *et al.* (2018) ‘Overall efficiency evaluation of a hydraulic pump with external drainage through temperature measurements’, *Journal of Dynamic Systems, Measurement, and Control*, 140(8).
- Cooley, J. W. and Tukey, J. W. (1965) ‘An Algorithm for the Machine Calculation of Complex Fourier Series’, *Mathematics of Computation*, 19(90), pp. 297–301.
- Crowther, W. . *et al.* (1998) ‘Fault diagnosis of a hydraulic actuator circuit using neural networks - An output vector space classification approach’, *Proceedings of the Institution of Mechanical Engineers. Part I: Journal of Systems and Control Engineering*, 212(1), pp. 57–68.
- Dalla Lana, Eduardo and De Negri, V. J. (2006) ‘A New Evaluation Method for Hydraulic Gear Pump Efficiency Through Temperature Measurements’, *SAE Technical Paper*, 1.
- Dash, M. and Liu, H. (1997) ‘Feature Selection for classification’, *Intelligent Data Analysis*, 1(1–4), pp. 131–156.
- Drozdor, N. Y. (1985) ‘Tribological Problems in Reliability of Machines’, *Soviet Engineering Journal*, 5, pp. 5–8.
- Du, J., Wang, S. and Zhang, H. (2013) ‘Layered clustering multi-fault diagnosis for hydraulic piston pump’, *Mechanical Systems and Signal Processing*. Elsevier, 36(2), pp. 487–504. Available at: <http://dx.doi.org/10.1016/j.ymssp.2012.10.020>.
- Duda, R., Hart, P. and Stork, D. (2000) *Pattern Classification*. 2nd edn. Wiley-Interscience.
- Edlund, R. (1979) ‘An Agriculture Equipment Manufacturer’s Approach to Assure a Clean Hydraulic System’, *SAE Transactions*, 88, pp. 2987–2994.
- Esposito, A. (2009) *Fluid Power with Applications*. Upper Saddle River, New Jersey: Prentice Hall.
- Eyre, T. S. (1976) ‘Wear Characteristics of Metals’, *Tibology International*, 10, pp. 203–212.
- Fatima, S. *et al.* (2013) ‘Technique for optimal placement of transducers for fault detection in rotating machines’, *Proceedings of the Institution of Mechanical Engineers, Part O: Journal of Risk and Reliability*, 227(2), pp. 119–131.
- Feicht, F. (1976) ‘Factors Influencing Service Life and Failure of Hydraulic Components’, *Olhydraulik and Pnuematik*, 20, pp. 804–806.
- Fey, C. G. *et al.* (2000) ‘Analysis of Common Failure Modes of Axial Piston Pumps’, *Sae Technical Paper Series*, (724).
- Foster, K. R., Koprowski, R. and Skufca, J. (2014) ‘Machine learning, medical diagnosis, and biomedical engineering research - commentary’, *BioMedical Enerineering Online*, 13.

- Grimson, E., Guttag, J. and Bell, A. (2016) ‘6.0002 Introduction to Computational Thinking and Data Science’. Massachusetts Institute of Technology: MIT OpenCourseWare. Available at: <https://ocw.mit.edu>.
- Hall, M. and Smith, L. (1999) ‘Feature selection for machine learning: comparing a correlation-based filter approach to the wrapper’, in *FLAIRS conference*, pp. 235–239.
- Hertz, J. *et al.* (1991) ‘Introduction to the Theory of Neural Computation’, *Physics Today*, 44(12), pp. 70–70. Available at: <http://physicstoday.scitation.org/doi/10.1063/1.2810360>.
- Huang, Z. *et al.* (2010) ‘A fault diagnosis method of rolling bearing through wear particle and vibration analyses’, *2010 International Conference on Advanced Mechanical Engineering, AME 2010*, 26–28, pp. 676–681. Available at: <http://www.scopus.com/inward/record.url?eid=2-s2.0-78650888636&partnerID=40&md5=d8234973f259f21d63d97c46406e336f>.
- Hunt (1985) ‘Contamination and Viscosity Monitoring of Automobile and Motor Cycle Oils Using a Portable Contamination Meter’, in *Proceedings of the International Conference on Vehicle Monitoring and Fault Diagnosis*. London, UK, pp. 41–48.
- Hydac (2019) *Contamination Sensors*. Available at: <https://www.hydac.com/de-en/products/sensors/contamination-sensors.html>.
- Ivantysyn, J. and Ivantysynova, M. (2003) *Hydrostatic Pumps and Motors*. First Engl. Tech Books International.
- Jain, A. K. (2010) ‘Data clustering: 50 years beyond K-means’, *Pattern Recognition Letters*. Elsevier B.V., 31(8), pp. 651–666. Available at: <http://dx.doi.org/10.1016/j.patrec.2009.09.011>.
- Kazama, T. and Yamaguchi, A. (1993) ‘Application of a Mixed Lubrication Model for Hydrostatic Thrust Bearings of Hydraulic Equipment’, *Journal of Tribology*, 115(4), p. 686.
- Kazama, T. and Yamaguchi, A. (1995) ‘Experiment on Mixed Lubrication of Hydrostatic Thrust Bearings for Hydraulic Equipment’, *Journal of Tribology*, 117(3), p. 399.
- Keller, N. J. *et al.* (2019) ‘Classification of Machine Functions: A Hydraulic Excavator Case Study’, in *The Sixteenth Sandinavian International Conference of Fluid Power*. Tampere, Finland.
- Kenton, W. (2019) *Overfitting*, *Investopedia*. Available at: <https://www.investopedia.com/terms/o/overfitting.asp>.
- Kjølle, A. (1993) ‘The thermodynamic method applied to hydraulic transmissions’, in *Proceedings of the JFPS International Symposium on Fluid Power*. The Japan Fluid Power System Society.
- Kohavi, R. and John, G. H. (1997) ‘Wrappers for feature subset selection’, *Artificial Intelligence*.

- Krogerus, T. *et al.* (2007) ‘Fault classification based on self-organizing maps in water hydraulic forklift’, in *Proceedings of the Tenth Scandinavian International Conference on Fluid Power, SICFP’07*.
- Kutner, M. *et al.* (2005) *Applied linear statistical models*. 5th edn. Boston: McGraw-Hill Irwin.
- Kwak, N. and Choi, C.-H. (2002) ‘Input feature selection for classification problems’, *IEEE Transactions on Neural Networks*, 13(1), pp. 143–159.
- Lan, Y. *et al.* (2018) ‘Fault diagnosis on slipper abrasion of axial piston pump based on Extreme Learning Machine’, *Measurement: Journal of the International Measurement Confederation*. Elsevier, 124(October 2017), pp. 378–385. Available at: <https://doi.org/10.1016/j.measurement.2018.03.050>.
- Li, Z. (2005) ‘Condition Monitoring of Axial Piston Pump’, (November), p. 134. Available at: <http://ecommons.usask.ca/bitstream/handle/10388/etd-11252005-202705/EricLithesis2005NovA.pdf>.
- Liu, H. and Motoda, H. (2012) *Feature selection for knowledge discovery and data mining*. Springer Science+Business Media, LLC.
- Lu, C., Ma, N. and Wang, S. (2011) ‘Fault detection for hydraulic pump based on chaotic parallel RBF network’, *EURASIP Journal on Advances in Signal Processing 2011*, (1), p. 49.
- Lu, F., Burton, R. and Schoenau, G. (1994) ‘Feasibility study on the use of a neural network to detect and locate excess piston wear in an axial piston pump’, in *Innovations in Fluid Power, 7th Bath International Fluid Power Workshop*.
- Lu, F., Burton, T. and Schoenau, G. (1995) ‘A Neural Network Based Incipient Fault Detection System for an Axial Piston Hydraulic Pump’, in *Proceedings of 1995 IASTED International Conference, SIP-95*.
- Lybeck, N., Marble, S. and Morton, B. (2007) ‘Validating prognostic algorithms: A case study using comprehensive bearing fault data’, *IEEE Aerospace Conference Proceedings*.
- Magerman, D. M. (1995) *Statistical Decision-Tree Models for Parsing*.
- MathWorks (2019a) *Classification Learner*. Available at: <https://www.mathworks.com/help/stats/classificationlearner-app.html>.
- MathWorks (2019b) *Cross-Validation*. Available at: <https://www.mathworks.com/discovery/cross-validation.html>.
- MathWorks (2019c) *Neural Net Clustering*. Available at: <https://www.mathworks.com/help/deeplearning/ref/neuralnetclustering-app.html>.
- MathWorks (2019d) *Neural Net Pattern Recognition*. Available at: <https://www.mathworks.com/help/deeplearning/ref/neuralnetpatternrecognition-app.html>.

- MathWorks (2019e) *Statistics and Machine Learning Toolbox*. Available at: <https://www.mathworks.com/products/statistics.html>.
- Mizell, D. (2018) *A STUDY OF THE PISTON CYLINDER INTERFACE OF AXIAL PISTON MACHINES*. Purdue University.
- MP Filtri (2019) *In-Line Contamination Monitors*. Available at: <https://www.mpfiltri.co.uk/particle-counters/icu/>.
- Navidi, W. (2008) *Statistics for engineers and scientists*. New York, NY, USA: Mcgraw-Hill Higher Education.
- Neale, M. J. (1985) 'Experience with condition monitoring in other industries', in *Proceedings of the International Conference on Vehicle Monitoring and Fault Diagnosis*. London.
- Opperman, M. (2007) *A new approach for failure prediction in mobile hydraulic systems*. Germany.
- Pearson, K. (1901) 'On lines and planes of closest fit to systems of points in space', *The London, Edinburgh, and Dublin Philosophical Magazine and Journal of Science*, 2(11), pp. 559–572.
- Pomierski, W. (2001) 'Condition monitoring thermodynamic method for testing hydrostatic transmissions in non-steady state of working conditions', in *The Seventh Scandinavian International Conference on Fluid Power, SICFP*. Linköping, Sweden, pp. 229–241.
- Rahmfeld, R. and Ivantysynova, M. (1998) 'Energy Saving Hydraulic Actuators for Mobile Machines', in *1st Bratislav Fluid Power Symposium*. Casta-Pila, Slovakia.
- Ramden, T. (1998) *Condition Monitoring and Fault Diagnosis of Fluid Power Systems: Approaches with Neural Networks and Parameter Identification*. Linköping University.
- Ramdén, T., Krus, P. and Palmberg, J. (1995) 'Condition monitoring of fluid power pumps using vibration measurements and neural networks trained with complex optimisation', in *Vibration and Noise 95*.
- Ramdén, T., Krus, P. and Palmberg, J. (1995) 'Fault diagnosis of complex fluid power systems using neural networks', in *Proceedings of the Fourth Scandinavian International Conference on Fluid Power*. Tampere, Finland.
- Ramden, T., Weddfelt, K. and Palmberg, J. (1993) 'Condition monitoring of fluid power pumps by vibration measurement', in *10th International Conference on Fluid Power-the Future for Hydraulics*, pp. 263–276.
- Rowe, W. B. (2012) *Hydrostatic, aerostatic and hybrid bearing design*. Elsevier.

- Schoenau, G. J., Stecki, J. S. and Burton, R. T. (2000) 'Utilization of artificial neural networks in the control, identification and condition monitoring of hydraulic systems - An overview', *SAE Technical Papers*, 109(2000), pp. 205–212. Available at: <https://www.scopus.com/inward/record.uri?eid=2-s2.0-84877449243&doi=10.4271%2F2000-01-2591&partnerID=40&md5=be29ec1a6148566c11001ba0f16e3b2d>.
- Silva Gabriel (1990) 'Wear Generation in Hydraulic Pump', *SAE Technical Paper Series*, (901679), p. 18.
- Stecki, J. S. (1998) *Total contamination control*. Edited by J. S. Stecki. Melbourne, Australia: Fluid Power Net International.
- Tang, J., Alelyani, S. and Liu, H. (2014) 'Feature Selection for Classification: A Review', *Data Classification: Algorithms and Applications*, 37.
- TIBCO Software (2019) *k-Nearest Neighbors*. Available at: <http://www.statsoft.com/Textbook/k-Nearest-Neighbors#distancemetric>.
- Tipping, M. E. and Bishop, C. M. (1999) 'Probabilistic principal component analysis', *Journal of the Royal Statistical Society: Series B (Statistical Methodology)*, 61(3), pp. 611–622.
- Wang, S. and Wang, Z. (1993) 'The fault diagnosis of bearing failure to hydraulic pump', *Beijing University of Aeronautics and Astronautics, Journal*, 4, pp. 26–31.
- Wang, X. *et al.* (2016) 'Remaining useful life prediction based on the Wiener process for an aviation axial piston pump', *Chinese Journal of Aeronautics*.
- Watton, J. (2007) *Modelling, Monitoring and Diagnostic Techniques for Fluid Power Systems*. London: Springer.
- Webb, A. R. (2002) *Statistical Pattern Recognition*. 2nd edn. John Wiley & Sons Ltd.
- Williamson, C. (2010) *Power Management for Multi-Actuator Mobile Machines with Displacement Controlled Hydraulic Actuators*. Purdue University.
- Witt, K. (1974) 'Druckflüssigkeiten und thermodynamisches Messen', *Ingenieur Digest Verlag-Ges.*
- Yamaguchi, A. and Matsuoka, H. (1992) 'A mixed lubrication model applicable to bearing/seal parts of hydraulic equipment', *Journal of Tribology*, 114(1), pp. 116–121.
- Ye, S.-G. and Xu, B. (2018) 'Noise Reduction of an Axial Piston Pump by Valve Plate Optimization', *Chinese Journal of Mechanical Engineering*, 31.
- Zecchi, M. (2013) *A novel fluid structure interaction and thermal model to predict the cylinder block/valve plate interface performance in swash plate type axial piston machines*. Purdue University.

Zhao-neng, C. and Wang, J. (1989) 'Reliability Research on Hydraulic Axial Piston Pump', in *Proceedings of the JFPS International Symposium on Fluid Power*, pp. 119–123.

Zimmerman, J. (2012) *Toward Optimal Multi-Actuator Displacement Controlled Mobile Hydraulic Systems*. Purdue University.

APPENDIX

Algorithm	Training Time [sec]	Accuracy [%]	Prediction Speed [obs/sec]	Algorithm Setting
Fine KNN	63.168	75.1	870 000	1 Neighbor
Medium KNN	90.584	81.7	300 000	10 Neighbors
Coarse KNN	176.8	83.1	75 000	100 Neighbors
Weighted KNN	95.432	76.6	280 000	10 Neighbors
Cubic KNN	105.79	81.7	210 000	10 Neighbors
Fine Tree	66.717	83.2	3 300 000	Max. 100 Splits
Medium Tree	55.958	83.2	3 500 000	Max. 20 Splits
Coarse Tree	44.365	83	3 800 000	Max. 4 Splits

(a)

Algorithm	Training Time [sec]	Accuracy [%]	Prediction Speed [obs/sec]	Algorithm Setting
Fine KNN	75.53	96.2	1 300 000	1 Neighbor
Medium KNN	94.722	95.4	360 000	10 Neighbors
Coarse KNN	186.36	92.5	80 000	100 Neighbors
Weighted KNN	97.378	96.1	360 000	10 Neighbors
Cubic KNN	116.86	95.3	190 000	10 Neighbors
Fine Tree	68.834	89.5	3 800 000	Max. 100 Splits
Medium Tree	45.262	88.7	3 700 000	Max. 20 Splits
Coarse Tree	35.41	87.3	4 200 000	Max. 4 Splits

(b)

Algorithm	Training Time [sec]	Accuracy [%]	Prediction Speed [obs/sec]	Algorithm Setting
Fine KNN	77.063	99.6	1 300 000	1 Neighbor
Medium KNN	95.435	99.6	340 000	10 Neighbors
Coarse KNN	183.41	99.5	86 000	100 Neighbors
Weighted KNN	98.06	99.6	340 000	10 Neighbors
Cubic KNN	119.64	99.6	180 000	10 Neighbors
Fine Tree	54.657	99.3	3 700 000	Max. 100 Splits
Medium Tree	43.457	99.1	3 700 000	Max. 20 Splits
Coarse Tree	32.735	96	4 200 000	Max. 4 Splits

(c)

Algorithm	Training Time [sec]	Accuracy [%]	Prediction Speed [obs/sec]	Algorithm Setting
Fine KNN	87.692	100	1 200 000	1 Neighbor
Medium KNN	104.3	100	350 000	10 Neighbors
Coarse KNN	201.03	100	75 000	100 Neighbors
Weighted KNN	108.07	100	350 000	10 Neighbors
Cubic KNN	140.45	100	150 000	10 Neighbors
Fine Tree	61.266	99.8	3 700 000	Max. 100 Splits
Medium Tree	50.462	99.1	3 900 000	Max. 20 Splits
Coarse Tree	34.832	96	4 300 000	Max. 4 Splits

(d)

Algorithm	Training Time [sec]	Accuracy [%]	Prediction Speed [obs/sec]	Algorithm Setting
Fine KNN	78.406	96.3	1 300 000	1 Neighbor
Medium KNN	99.552	95.5	340 000	10 Neighbors
Coarse KNN	197.59	92.6	77 000	100 Neighbors
Weighted KNN	103.95	96.2	340 000	10 Neighbors
Cubic KNN	123.52	95.2	180 000	10 Neighbors
Fine Tree	65.384	88.4	3 200 000	Max. 100 Splits
Medium Tree	48.895	87.7	3 800 000	Max. 20 Splits
Coarse Tree	41.479	85.9	4 000 000	Max. 4 Splits

(e)

Figure 12.1: Algorithm selection results of controlled cycle using a 25% hold-out validation with the following features: **(a)** pD only, **(b)** pB and pD, **(c)** pD and N, **(d)** pB, pD, and N, **(e)** pD and Beta.

Algorithm	Training Time [sec]	Accuracy [%]	Prediction Speed [obs/sec]	Algorithm Setting
Fine KNN	1.6445	53.9	2 100 000	1 Neighbor
Medium KNN	1.9611	56.2	420 000	10 Neighbors
Coarse KNN	3.441	60.1	100 000	100 Neighbors
Weighted KNN	1.9541	54.4	420 000	10 Neighbors
Cubic KNN	2.2188	56.2	330 000	10 Neighbors
Fine Tree	1.7153	60.8	3 700 000	Max. 100 Splits
Medium Tree	0.97686	60.9	4 200 000	Max. 20 Splits
Coarse Tree	0.80645	60.7	3 700 000	Max. 4 Splits

(a)

Algorithm	Training Time [sec]	Accuracy [%]	Prediction Speed [obs/sec]	Algorithm Setting
Fine KNN	1.9605	59.4	1 300 000	1 Neighbor
Medium KNN	2.4056	63.7	350 000	10 Neighbors
Coarse KNN	4.1854	67.2	860 000	100 Neighbors
Weighted KNN	2.3899	61.7	350 000	10 Neighbors
Cubic KNN	3.0548	63.7	180 000	10 Neighbors
Fine Tree	2.4076	66.6	3 600 000	Max. 100 Splits
Medium Tree	1.1769	65.8	3 700 000	Max. 20 Splits
Coarse Tree	0.91457	65.5	4 100 000	Max. 4 Splits

(b)

Algorithm	Training Time [sec]	Accuracy [%]	Prediction Speed [obs/sec]	Algorithm Setting
Fine KNN	1.9647	57.9	1 500 000	1 Neighbor
Medium KNN	2.4268	61.9	3 600 000	10 Neighbors
Coarse KNN	4.2142	64.8	87 000	100 Neighbors
Weighted KNN	2.4323	61.1	330 000	10 Neighbors
Cubic KNN	2.9559	62	190 000	10 Neighbors
Fine Tree	2.223	63.6	3 500 000	Max. 100 Splits
Medium Tree	1.2198	61.4	3 900 000	Max. 20 Splits
Coarse Tree	0.91918	60.9	4 000 000	Max. 4 Splits

(c)

Algorithm	Training Time [sec]	Accuracy [%]	Prediction Speed [obs/sec]	Algorithm Setting
Fine KNN	2.1485	72	1 000 000	1 Neighbor
Medium KNN	2.6525	74.6	2 800 000	10 Neighbors
Coarse KNN	4.7841	72.9	73 000	100 Neighbors
Weighted KNN	2.682	75	270 000	10 Neighbors
Cubic KNN	4.1125	74.3	100 000	10 Neighbors
Fine Tree	2.7537	67.3	3 200 000	Max. 100 Splits
Medium Tree	1.4461	66.1	3 300 000	Max. 20 Splits
Coarse Tree	1.0139	65.4	3 800 000	Max. 4 Splits

(d)

Algorithm	Training Time [sec]	Accuracy [%]	Prediction Speed [obs/sec]	Algorithm Setting
Fine KNN	1.9478	60.8	1 300 000	1 Neighbor
Medium KNN	2.433	65.3	310 000	10 Neighbors
Coarse KNN	4.2387	68.5	84 000	100 Neighbors
Weighted KNN	2.4314	63.3	350 000	10 Neighbors
Cubic KNN	3.0024	65.3	190 000	10 Neighbors
Fine Tree	2.3215	67.6	3 500 000	Max. 100 Splits
Medium Tree	1.2457	67.3	3 700 000	Max. 20 Splits
Coarse Tree	0.88685	66.7	4 100 000	Max. 4 Splits

(e)

Algorithm	Training Time [sec]	Accuracy [%]	Prediction Speed [obs/sec]	Algorithm Setting
Fine KNN	2.1884	69.6	980 000	1 Neighbor
Medium KNN	2.6749	73.9	280 000	10 Neighbors
Coarse KNN	4.8073	74.5	71 000	100 Neighbors
Weighted KNN	2.6706	73.2	270 000	10 Neighbors
Cubic KNN	4.184	73.9	97 000	10 Neighbors
Fine Tree	2.4834	69.9	3 500 000	Max. 100 Splits
Medium Tree	1.4065	67.2	3 700 000	Max. 20 Splits
Coarse Tree	0.97194	66.9	3 800 000	Max. 4 Splits

(f)

Algorithm	Training Time [sec]	Accuracy [%]	Prediction Speed [obs/sec]	Algorithm Setting
Fine KNN	2.8197	93.6	510 000	1 Neighbor
Medium KNN	2.7132	88.6	150 000	10 Neighbors
Coarse KNN	7.3035	81.5	42 000	100 Neighbors
Weighted KNN	3.7297	92.6	150 000	10 Neighbors
Cubic KNN	9.7611	88	280 000	10 Neighbors
Fine Tree	3.6023	71.8	3 100 000	Max. 100 Splits
Medium Tree	2.0779	67.1	3 700 000	Max. 20 Splits
Coarse Tree	1.4571	66.8	3 600 000	Max. 4 Splits

(g)

Figure 12.2: Algorithm selection results of digging cycle using a 25% hold-out validation with the following features: (a) pD only, (b) pB and pD, (c) pD and N, (d) pB, pD, and N, (e) pD and Beta, (f) pB, pD, Beta, (g) pA, pB, pD, Beta, N.

PUBLICATIONS

- Keller, N. Vacca, A. (2020). Condition Monitoring of an Axial Piston Pump on a Mini Excavator. *International Journal of Fluid Power*. **UNDER REVIEW**
- Keller, N. Vacca, A. (2020). Demonstrating a Condition Monitoring Process for Axial Piston Pumps with Damaged Valve Plates on a Stationary Test-Rig. *International Journal of Fluid Power*. **UNDER REVIEW**
- Stump, P. Keller, N. Vacca, A. (2019). Energy Management of Low-Pressure Systems Utilizing Pump- Unloading Valve and Accumulator. *Energies*.
- Keller, N. Ivantysynova, M, Vacca, A. et al. (2019). Classification of Machine Functions: A Hydraulic Excavator Case Study. *The Fourteenth Scandinavian International Conference on Fluid Power*.
- Kwon, H. Keller, N. Ivanysysnova, M. (2018). Thermal Management of Open and Closed Circuit Hydraulic Hybrids – A Comparison Study. *The 11th International Fluid Power Conference (IFK)*, Aachen, Germany.
- Keller, Nathan J. (2017). A New Approach to Sizing Low Pressure Systems. *ASME/BATH 2017 Symposium on Fluid Power and Motion Control*. American Society of Mechanical Engineers.
- Keller, Nathan J. (2017). A 21st Century Approach to Hydraulic Actuation Technology. M.S. Thesis. School of Mechanical Engineering, Purdue University, West Lafayette, IN, USA.